FUNCTIONAL INSIGHTS INTO RAD51 REGULATORY PROTEINS IN HOMOLOGOUS RECOMBINATION

by

Meghan Rose Sullivan

B.S., University of Rochester, 2013

Submitted to the Graduate Faculty of

School of Medicine in partial fulfillment

of the requirements for the degree of

Doctor of Philosophy

University of Pittsburgh

2018

UNIVERSITY OF PITTSBURGH

SCHOOL OF MEDICINE

This dissertation was presented

by

Meghan Rose Sullivan

It was defended on

November 29, 2018

and approved by

Patricia Opresko, Professor, Department of Environmental and Occupational Health

Roderick O'Sullivan, Assistant Professor, Department of Pharmacology and Chemical Biology

Gary Thomas, Professor, Department of Microbiology and Molecular Genetics

Judith Yanowitz, Associate Professor, Department of Obstetrics, Gynecology, and Reproductive Sciences

Dissertation Director: Kara Bernstein, Associate Professor, Department of Microbiology and Molecular Genetics

FUNCTIONAL INSIGHTS INTO RAD51 REGULATORY PROTEINS IN HOMOLOGOUS RECOMBINATION

Meghan Rose Sullivan, PhD

University of Pittsburgh, 2018

Accurate repair of DNA is critical for genome stability and cancer prevention. DNA double-strand breaks are one of the most toxic lesions and can be repaired using the high-fidelity homologous recombination (HR) pathway. HR is highly conserved and uses a homologous template for repair. One central HR step is RAD51 nucleoprotein filament formation on the single-stranded DNA ends. RAD51 filament formation is required for the homology search and strand invasion steps of HR. RAD51 activity is tightly controlled by many positive and negative regulators, collectively termed the RAD51 mediators. The human RAD51 paralogs (RAD51B, RAD51C, RAD51D, XRCC2, XRCC3, and SWSAP1) are RAD51 mediator proteins that are highly conserved throughout eukaryotes and structurally resemble RAD51. They assemble into subcomplexes, BCDX2, CX3, and the Shu complex, to promote the HR activity of RAD51. The RAD51 mediators function to nucleate, elongate, stabilize, and disassemble RAD51 during repair. RAD51 paralog mutations are found in many breast and ovarian cancers as well as other cancer types. Despite their discovery three decades ago, few advances have been made in understanding their function. This work identified that the *C. elegans* Shu complex is functionally conserved from yeast and is composed of two RAD-51 paralogs, RFS-1 and RIP-1, which bind SWS-1. Disruption of the worm Shu complex results in DNA damage sensitivity and reduced RAD-51 foci showing for the first time

that the Shu complex promotes HR in higher eukaryotes. In subsequent studies in human cell lines, this work demonstrated that disruption of the human RAD51 paralog, RAD51C, through cancer-associated point mutations can also cause DNA damage sensitivity and reduced HR. The conserved Walker A motif of human RAD51C is particularly important for maintaining protein-protein interactions of the BCDX2 and CX3 complexes and maintaining HR proficiency that we propose is critical for prevention of breast and ovarian cancers. Together, this work sheds light onto the function of the RAD51 regulators and their role in maintaining genome stability.

TABLE OF CONTENTS

LIST OF TABLES

LIST OF FIGURES

LIST OF SUPPLEMENTAL TABLES

LIST OF SUPPLEMENTAL FIGURES

LIST OF ABBREVIATIONS

BCDX2 Complex- RAD51B-RAD51C-RAD51D-XRCC2 complex

BER- Base excision repair

BIR- Break-induced replication

CHO- Chinese hamster ovary

CO- Crossover

CX3- RAD51C-XRCC3 complex

DDR- DNA damage response

dHJ- Double Holliday junction

DSB- Double-strand break

dsDNA- Double-stranded DNA

D-loop- Displacement loop

FA- Fanconi anemia

FANCD1- BRCA2

FANCN- PALB2

FANCO- RAD51C

FANCR- RAD51

FANCU- XRCC2

HR- Homologous recombination

ICL- Inter-strand crosslink

IR- Ionizing radiation

LOH- Loss-of-heterozygosity

MEF- Mouse embryonic fibroblast

MMC- Mitomycin C

MMS- Methyl methanesulfonate

MRN- MRE11-RAD51-NBS1

NCO- Non-crossover

NHEJ- Non-homologous end joining

PARP- Poly (ADP-ribose) polymerase

PARPi- Poly (ADP-ribose) polymerase inhibitor

SCEs- Sister chromatid exchanges

SDSA- Synthesis dependent strand annealing

ssDNA- Single-stranded DNA

TIRF- Total internal reflection fluorescence

PREFACE

To everyone who has guided and supported me:

To my graduate thesis advisor, Kara Bernstein, for mentoring and encouraging me in my development as a scientist

To the Bernstein lab, past and present, for creating such a positive atmosphere, especially to Stefanie Böhm, Stephen Godin, and Juli Martino, my patient mentors

To my thesis committee, Roddy, Patty, Judy, and Gary for their advice and input throughout my graduate education

To my collaborators in the Yanowitz lab, especially to Brooke my coauthor on Chapter 2

To my collaborators in the Jasin lab, to Maria Jasin for generously hosting me at Memorial Sloan Kettering and to Rohit Prakash for our ongoing RAD51C studies in Chapter 3

To Elaine Sia, my undergraduate advisor, who fostered in me a love for genetics

To the graduate program in Molecular Genetics and Developmental Biology and the Genome Stability group who have supported my training

To the women who participated in the ARIEL2 study and to the families who participated in RAD51C epidemiology studies without whom this work could not have been completed

To Eric for his continued support through the writing of this dissertation

and finally, To my parents who tirelessly supported me through my entire education

Thank you

1.0 INTRODUCTION

1.1 DOUBLE-STRAND BREAK REPAIR

Exogenous and endogenous DNA damage is constantly challenging our genomic integrity. Exogenous DNA damaging agents, such as radiation, ultraviolet light, and chemicals, or endogenously generated DNA damage, such as errors in replication or cellular processes that generate reactive oxygen species (ROS), create a wide-variety of DNA lesions (Bhattacharjee and Nandi 2017). Maintaining genome stability requires many coordinated processes within the cell to ensure conservation of our genetic material through each cell division (Shibata and Jeggo 2014). Collectively, these processes are referred to as the DNA damage response (DDR) (Ciccia and Elledge 2010). Accurate DNA repair is a key part of the DDR and is critical as a loss of genome stability is a common theme in cancer development (Hanahan and Weinberg 2011). The most deleterious type of DNA damage is a double-strand break (DSB) as even a single unrepaired DSB results in cell death (Bennett et al. 1993) and misrepair of DSBs is associated with increased genomic instability and consequently tumorigenesis (Shibata and Jeggo 2014). Therefore, cells have evolved highly specialized responses to recognize and repair DSBs.

Non-homologous end joining (NHEJ) and homologous recombination (HR) are the two predominant pathways to repair DSBs (Symington and Gautier 2011). Once a DSB is recognized and the DDR is initiated, the cell must determine the appropriate repair pathway based on the

nature of the break and the availability of a potential repair template. A major factor governing repair pathway choice is cell cycle phase. NHEJ is the predominant DSB repair pathway in human cells and can be used throughout the cell cycle, especially in G1 phase (Symington and Gautier 2011). Conversely, HR is primarily restricted to S and G2 phases when a sister chromatid is available as a repair template. NHEJ does not rely on a homologous template but rather employs minimal processing around the break-site and ligation of the ends (Rodgers and McVey 2016). Therefore NHEJ more frequently results in a loss of genetic material through micro-insertions and deletions (INDELs) (Rodgers and McVey 2016). In contrast, HR is a tightly regulated and faithful template-guided repair process that replaces the lost or resected nucleic acids around the damage using the information provided by the intact homologous sequence. This increased fidelity ensures the preservation of the genome through each cell division. Commitment to HR requires DSB end resection and formation of RAD51 nucleoprotein filaments.

1.1.1 Commitment to HR through DSB end resection and RAD51 filament formation

Use of the HR pathway requires 5' to 3' end resection at the break site exposing single-stranded DNA (ssDNA) overhangs that ultimately prevent canonical NHEJ from repairing the break (Figure 1) (Symington and Gautier 2011). DNA end resection is initiated by MRE11-RAD50-NBS1 (MRN) binding to the DNA ends, which subsequently recruits CtIP to generate 3' ssDNA overhangs (Sartori et al. 2007; Symington and Gautier 2011). In addition to the resection activity of MRE11, repair pathway choice is also directed by the opposing actions of 53BP1 and BRCA1 (Bouwman et al. 2010; Bunting et al. 2010). Once a break is detected, 53BP1 and BRCA1 compete for directing the cell to commit to NHEJ or HR, respectively (Figure 1A) (Bunting et al. 2010; Chapman et al. 2012). 53BP1 promotes NHEJ by inhibiting DNA end resection while

simultaneously tethering two double-stranded DNA (dsDNA) ends together enabling their subsequent ligation (Chapman et al. 2012). How BRCA1 inhibits 53BP1 activity remains unclear. However, when BRCA1 binds BARD1, it can ubiquitinate the endonuclease, CtIP, increasing CtIP affinity for DNA thus promoting resection (Yu et al. 2006; Chapman et al. 2012; Densham et al. 2016). At the same time, the DNA ends are shielded from resection through the 53BP1-interacting partners, RIF1 and the newly identified "shieldin" complex (REV7-SHLD1-SHLD2-SHLD3) (Ghezraoui et al. 2018; Gupta et al. 2018; Mirman et al. 2018; Noordermeer et al. 2018). Loss of 53BP1 or the shieldin complex, impairs NHEJ resulting in increased HR (Figure 1A) (Bouwman et al. 2010; Bunting et al. 2010; Ghezraoui et al. 2018; Gupta et al. 2018; Mirman et al. 2018; Noordermeer et al. 2018). Alternatively, engagement of BRCA1 in cell cycle phase G1 similarly allows HR to occur outside of S/G2 phases. During cell cycle phase G1, BRCA1 activity is normally suppressed as the ubiquitylation of PALB2 prevents their interaction and the recruitment of PALB2-BRCA2 (Orthwein et al 2015). However, if the BRCA1-PALB2 interaction is restored, BRCA2 can be recruited to the DSB promoting HR (Orthwein et al 2015). Ultimately, preventing extensive end resection is important for limiting hyper-recombination by HR and preventing loss of genetic material. Extensive resection can result in loss-of-heterozygosity by alternative deleterious repair pathways such as single-strand annealing (SSA; Figure 1B) or break induced replication (BIR; not pictured) (Verma and Greenberg 2016).

Figure 1.

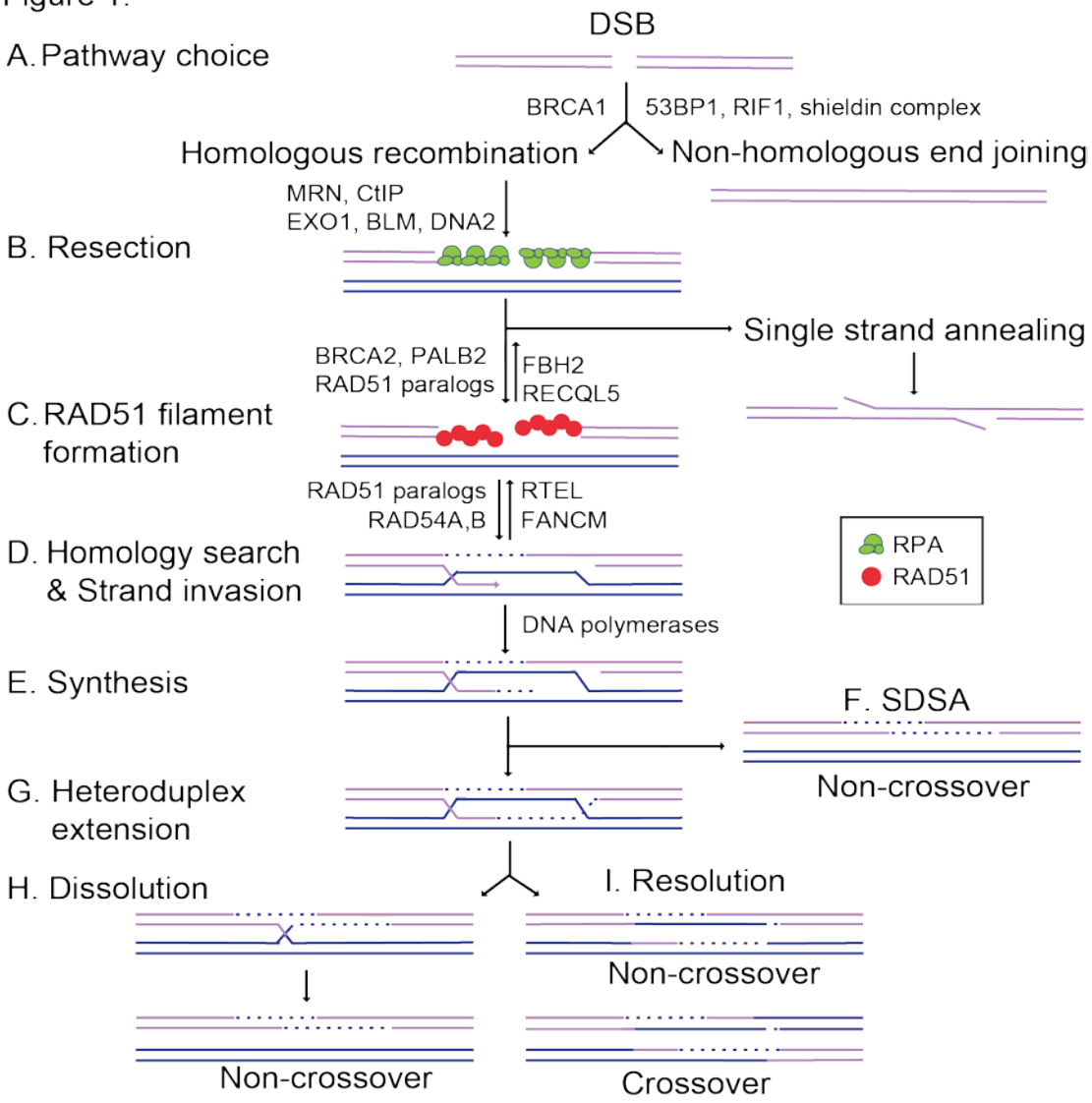

Figure 1. Schematic of DNA double-strand break repair pathways.

After formation of a double-strand break (DSB; purple lines), cells can repair the damage through two primary mechanisms, homologous recombination (HR) using a homologous template (blue lines) or non-homologous end joining (NHEJ). A. Pathway choice between HR or NHEJ is mediated by BRCA1 which promotes HR whereas 53BP1, RIF1, and the shieldin complex promote NHEJ. B. Resection by the MRN (MRE11, RAD51, NBS1) complex, CtIP, EXO1, BLM, and DNA2 creates 3' ssDNA overhangs which are coated by the trimeric replication protein A (RPA) complex (green circles). During canonical HR, RPA is displaced by RAD51 (red circles). Alternatively, RAD51-independent repair can occur through single-strand annealing where complementary DNA sequences anneal and flap endonuclease cleave the overhangs and the DNA ends are

ligated together. C. RAD51 filament formation is regulated by the positive RAD51 regulators, BRCA2, PALB2, and the RAD51 paralogs. At the same time, RAD51 is negatively regulated by FBH2 and RECQL5. D. RAD51-mediated homology search and strand invasion then occurs and is regulated by the RAD51 paralogs and RAD54A,B. At the same time, RAD51-mediated D-loops are negatively regulated by RTEL and FANCM. E. The DNA polymerases then copy the missing information from the homologous template (shown in blue, a sister chromatid or a homologous chromosome). F. During Synthesis Dependent Strand Annealing (SDSA) the D-loop is displaced, and the DNA is resolved into a non-crossover product. G. If there is heteroduplex extension and a double Holliday junction forms by second-end capture then these DNA intermediates can be resolved by dissolution or resolution. H. Dissolution results in non-crossover products. I. Resolution results in both crossover and non-crossover products.

Once DNA end resection occurs, the HR pathway can be utilized. Increasing evidence suggests that the primary role of HR is actually to repair DNA damage that occurs during replication (Shibata and Jeggo 2014). While canonical HR repairs a direct DSB, this pathway can also repair lesions produced by stalled or collapsed replication forks (Shibata and Jeggo 2014). Cells commit to a homology-directed mechanism of repair when extensive resection is performed by the action of multiple nucleases. BRCA1 interacts with MRN and CtIP to promote SSA and HR (Stark et al 2004). The binding of HR factors also compete with Ku70/80 binding to further suppress NHEJ (Jasin and Rothstein 2013). Short- and long-term resection is mediated by MRN/CtIP in conjunction with EXO1 or BLM and DNA2 (Figure 1B) (Bernstein and Rothstein 2009). EXO1 is a 5' to 3' exonuclease, whereas BLM helicase does not have nuclease activity itself and therefore relies on DNA2 nuclease for resection of the 5' end (Bernstein and Rothstein 2009). This resection reveals 3' ssDNA ends which are quickly coated by replication protein A complex (RPA) (Bernstein and Rothstein 2009). RPA-coated filaments ensure that the ssDNA overhangs are not degraded and prevent secondary structures from forming (Bernstein and Rothstein 2009).

RAD51 then displaces RPA to form the pre-synaptic filament, and this requires the activity of several so-called "RAD51 mediator" proteins (Figure 1C) (Godin et al. 2016a). RAD51 nucleoprotein filaments search for homologous sequence to invade and displace one strand of the homologous template to form a displacement-loop (D-loop; Figure 1D) (Jasin and Rothstein 2013). In canonical HR, this structure allows for the pairing of the broken strand with the displaced strand to form a heteroduplex (Figure 1D) and DNA synthesis restores any missing nucleotides at the breaksite (Figure 1E). Subsequently second end capture results in the formation of a double Holliday junction (dHJ) (Figure 1G). This intermediate is resolved through either a dissolution or resolution mechanism, yielding non-crossover (NCO) or a crossover (CO) (Figure 1H,I) (Jasin and Rothstein 2013). Alternatively, during synthesis dependent strand annealing (SDSA), only one-end invasion occurs thus forming a single Holliday junction, and this intermediate is dissolved into a NCO product (Figure 1F) (Jasin and Rothstein 2013). In this introduction, we will focus on mechanisms that regulate commitment to HR through the RAD51 mediators.

1.1.2 Overview of RAD51 structure, function, and activity

RAD51 filament formation is key for the cellular commitment to perform HR and is a highly conserved step (Godin et al. 2016a). The centrality of RAD51 to HR is underscored by its evolutionary conservation from bacterial RecA to human RAD51 as well as the amino acid level similarity to its meiotic counterpart, DMC1, and its paralogs (described below) (Lin et al. 2006).

RAD51 plays a critical role during the DNA homology search and strand invasion. RAD51 assembles into a heptamer that encircles the DNA forming a helical nucleoprotein filament in which one RAD51 molecule binds to three nucleotides (Lee et al. 2015; Qi et al. 2015). This nucleoprotein filament is termed the presynaptic filament (Smith and Rothstein 2017). Recently,

single molecule experiments visualized by total internal reflection fluorescence (TIRF) microscopy enabled Eric Greene's laboratory to resolve the details of the homology search (Qi et al. 2015). DNA in a flow cell measured binding dynamics. Individual ssDNA curtains pre-coated in RAD51 were mixed with dsDNA of varying lengths of homology to measure binding to the presynaptic filament. This revealed homology search by the presynaptic filament efficiently samples dsDNA in at least eight nucleotide increments discounting matches of seven or less nucleotides (Qi et al. 2015). Single molecule studies further revealed that after finding eight nucleotide microhomology, RAD51-mediated strand exchange occurs in three nucleotide steps with proper Watson-Crick base pairing and is conserved from bacterial RecA to human RAD51 (Lee et al. 2015). The homology search has been modeled *in vivo* in budding yeast using fluorescent microscopy and endonuclease-induced DSBs (Smith and Rothstein 2017). Upon DNA damage, both the broken ends and undamaged chromosomes increase in local mobility to enable the search for homology in both haploid and diploid yeast cells (Dion et al. 2012; Mine-Hattab and Rothstein 2012). *In vivo,* the homology search and movement of the DNA ends require yeast Rad51, DNA end resection proteins such as Sae2/CtIP, and the DNA damage checkpoint (Mec1, Rad9, and Rad53) (Dion et al. 2012; Mine-Hattab and Rothstein 2012). In human cells, movement of the DSB ends during the homology search is controversial. DSBs at telomeres also exhibit increased mobility, which results in telomere-telomere recombination (Cho et al. 2014). In some cases, DSB mobility was not observed when monitoring both ends of a breaksite in live cells at an I-SceI cut site visualized by flanking LacO and TetO arrays (Soutoglou et al. 2007). This immobility was dependent on Ku proteins is thought to be important for preserving genome stability by preventing illegitimate fusions (Soutoglou and Misteli 2007). In other instances, movement of DSB ends was observed in live cells through clustering of chromosome domains

(Aten et al. 2004; Krawczyk et al. 2012). RAD51 has proved challenging to study in mammalian systems because, unlike yeast, loss of functional RAD51 is not tolerated in mouse models and $RAD51^{-/-}$ cells cannot be propagated (Lim and Hasty 1996; Tsuzuki et al. 1996). Therefore, much of what we know about the homology search is based upon work done in model organisms such as yeast.

1.1.3 Overview of key RAD51 regulators

Although RAD51 nucleoprotein filament is required for the homology search and strand invasion steps of HR, a rate limiting step to RAD51 filament formation is the displacement of RPA from ssDNA (Jasin and Rothstein 2013). Since RPA binds with higher affinity to ssDNA than RAD51 (Chen and Wold 2014; Ma et al. 2017), RAD51 mediator proteins are required to regulate RAD51 filament formation. RAD51 mediators primarily function to nucleate, elongate, and stabilize the RAD51 nucleoprotein filament. In addition, new roles for these proteins have been identified in RAD51 filament flexibility and even end capping which is thought to stimulate strand exchange (Taylor et al. 2015; Taylor et al. 2016).

In mammalian cells, RAD51 filament nucleation is mediated by the RAD51 loader, BRCA2, and this function is carried out in other eukaryotes, such as budding yeast, by the Rad52 protein (Sung 1997a; Jensen et al. 2010; Prakash et al. 2015). In humans, RAD51 binds BRCA2 through the BRC repeats and the C terminal domain of BRCA2 (Wong et al. 1997; Pellegrini et al. 2002; Esashi et al. 2007; Jensen et al. 2010). BRCA2 regulation of RAD51 is complex but in part is regulated through the BRC repeats in BRCA2 which bind RAD51 by mimicing the oligomerization interface of RAD51 (Pellegrini et al. 2002; Sanchez et al. 2017). BRCA2 delivers RAD51 monomers to the ssDNA rather than dsDNA allowing filament formation and ultimately

promoting RAD51 strand-exchange activity (Carreira et al. 2009; Jensen et al. 2010; Sanchez et al. 2017). Underscoring the importance of the coordination of RAD51 activity by BRCA2, *BRCA2* mutations in the BRC repeats have been found in cancers (Gayther et al. 1997). Furthermore, mice with deletion of exon containing the BRC repeat of BRCA2 are inviable (Chen et al. 1998; Jonkers et al. 2001). BRCA2 also binds and coordinates the activity of several other recombination factors including DSS1 and PALB2 to promote RAD51 loading and activity (Prakash et al. 2015).

In addition to BRCA2, other RAD51 mediators include the RAD51 paralogs, which are proteins that structurally resemble RAD51 itself, and the Shu complex, a RAD51 paralog-containing complex (Tao et al 2012; Sasanuma et al 2013). RAD51 paralogs arose from a gene duplication of the ancestral RADA protein in Archaea and have maintained their structural similarity to RAD51 (Thacker 1999; Miller et al 2004). In humans, there are six RAD51 paralogs including RAD51B, RAD51C, RAD51D, XRCC2, XRCC3, and SWSAP1. Once RAD51 filaments are nucleated, the RAD51 paralogs are thought to aid in several aspects of RAD51 regulation such as stabilization and elongation of the RAD51 filament itself and in filament remodeling to facilitate the homology search. However, the precise function of the individual RAD51 paralogs remains largely enigmatic and why so many RAD51 paralogs are needed is unknown.

In addition to the RAD51 paralogs, other positive RAD51 regulators also aid in downstream recombination steps after RAD51 filaments have formed. The DNA translocase paralogs RAD54A and RAD54B are chromatin remodelers that enable strand exchange through their dsDNA-dependent ATPase activities (Alexeev et al. 2003; Wesoly et al. 2006; Lisby and Rothstein 2015). In addition to the positive regulators, negative regulators also aid in disassembly of RAD51 filaments. FBH2 and RECQL5, act as antirecombinases to dissociate RAD51 from

ssDNA, whereas FANCM and RTEL specifically function during D-loop disassembly (Karpenshif and Bernstein 2012; Simandlova et al. 2013; Lisby and Rothstein 2015; Sarek et al 2015). These negative regulators are equally important as they modulate recombination by limiting RAD51 activity at illegitimate recombination sites (Figure 1) (Lisby and Rothstein 2015).

1.2 RAD51 REGULATION IN MAMMALIAN MODELS

1.2.1 The RAD51 paralogs

The mammalian RAD51 paralogs were first identified 30 years ago (Jones et al. 1987). Five of the six RAD51 paralogs are considered canonical RAD51 paralogs (include RAD51B, RAD51C, RAD51D, XRCC2, XRCC3) and share 20-30% amino acid sequence identity with RAD51 itself, particularly around the Walker A and B motifs (Cartwright et al. 1998; Thacker 1999; Thompson and Schild 1999; Lin et al. 2006). The more recently identified SWSAP1 protein is a highly divergent RAD51 paralog that shares closest sequence homology with RadA (~24%), an archaeal RecA family member and also contains Walker A and B motifs (Liu et al. 2011). Walker A and B motifs are sequences that bind ATP and in the case of RAD51 also hydrolyzes ATP (Sung and Stratton 1996). The RAD51 paralogs assemble into sub-complexes *in vivo* as the heterotetramer BCDX2 (RAD51B, RAD51C, RAD51D, and XRCC2), the heterodimer CX3 (RAD51C and XRCC3), and the Shu complex (SWSAP1 and SWS1) (Figure 2) (Masson et al. 2001a; Masson et al. 2001b; Martin et al. 2006; Liu et al. 2011). RAD51C is also a member of an additional complex which consists of BRCA2, PALB2, and RAD51 itself (Figure 2). Unlike the canonical RAD51 paralog subcomplexes, the Shu complex consists of a Shu2/SWS1 protein family member that is

characterized by the SWIM domain, a conserved zinc-finger like binding motif, CXC…X_n…CXHXXA, where X is any amino acid (Godin et al. 2015). In all organisms where the Shu complex has been analyzed, the Shu2/SWS1 protein family member interacts with the RAD51 paralogs to regulate RAD51 function (Martino and Bernstein 2016; McClendon et al. 2016). All of the RAD51 paralog containing complexes are thought to promote RAD51 mediated activities, although their precise composition and function in this process is largely unknown.

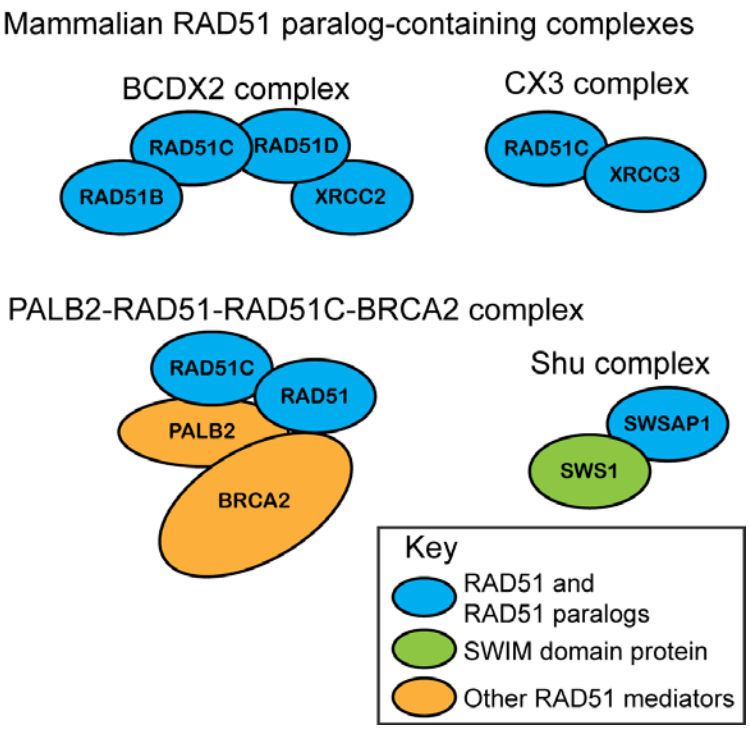

Figure 2. Mammalian RAD51 paralog-containing complexes.

The BCDX2 complex is a RAD51 paralog heterotetramer consisting of RAD51B, RAD51C, RAD51D, and XRCC2. The CX3 complex is a RAD51 paralog heterodimer consisting of RAD51C and XRCC3. The PALB2-RAD51-RAD51C-BRCA2 complex consists of the RAD51 paralog, RAD51C, RAD51 itself, and two additional RAD51 mediator proteins, BRCA2 and PALB2. PALB2 acts as a scaffold in this complex by interacting with RAD51, RAD51C, and BRCA2. The Shu complex consists of a highly divergent RAD51 paralog, SWSAP1, and its binding partner SWS1. SWS1 is a member of the evolutionarily conserved Shu2/SWS1 family, which contains a SWIM domain, and interacts with RAD51 paralogs throughout eukaryotes. Blue circles indicate RAD51 or a RAD51 paralog, a green circle indicates a SWIM domain containing Shu2/SWS1 protein family member, and an orange circle indicates an additional RAD51 mediator protein.

Initial determination of RAD51 paralog sub-complex assembly was determined using yeast-two-hybrid and yeast-three-hybrid systems due to the insolubility of recombinantly expressed RAD51 paralogs (Schild et al. 2000; Masson et al. 2001b; Miller et al. 2002; Wiese et al. 2002; Liu et al. 2011). Although biochemical investigation of the mammalian RAD51 paralogs

has lagged significantly behind cellular studies, the protein-protein interactions of the RAD51 paralog sub-complexes, BCDX2 and CX3, were later confirmed using recombinant proteins purified from *Escherichia coli* and Sf9 insect cells (Masson et al. 2001a; Masson et al. 2001b). The RAD51 paralogs are thought to be incorporated into their respective subcomplexes in a 1:1 stoichiometry. For example, recombinant CX3 and BCDX2 assemble into a 1:1 and 1:1:1:1 stoichiometry, respectively, when purified from either insect Sf9 cells or human HeLa cells (Kurumizaka et al. 2001; Masson et al. 2001a; Masson et al. 2001b). *In vitro,* the BCDX2 complex can also assemble into stable heterodimers, which include BC (RAD51B and RAD51C) and DX2 (RAD51D and XRCC2) (Braybrooke et al. 2000; Sigurdsson et al. 2001). Unlike RAD51 which interacts with additional RAD51 monomers to form a filament, the RAD51 paralogs do not, but rather assemble into heterodimers and these protein-protein interactions are critical for their stability (Liu et al. 2011; Chun et al. 2013). Within the BCDX2 complex, RAD51C and RAD51D interact with each other and also with RAD51B or XRCC2, respectively (Figure 2) (Schild et al. 2000; Masson et al. 2001b; Sigurdsson et al. 2001; Miller et al. 2004). This is similar to the yeast Shu complex, which forms a horseshoe shape as revealed by X-ray crystallography (Zhang et al. 2017b). Much of our current understanding of the RAD51 paralogs is based on biochemical studies in other model organisms, particularly yeast and worms. The mammalian paralogs may play a number of roles in aiding RAD51 throughout repair.

Recently, RAD51C was found to act in a third complex distinct from the other RAD51 paralog sub-complexes. Mass spectrometry revealed that RAD51C interacts directly with PALB2 which acts as a scaffold to simultaneously bind RAD51, RAD51C, and BRCA2 in HeLa S3 cells (Park et al. 2014). PALB2, as the "partner-and-localizer of BRCA2," is necessary to recruit BRCA2 to sites of DNA damage (Xia et al. 2006). PALB2 mutants that disrupt RAD51C

interaction show increased BRCA2 foci but decreased RAD51 foci (Park et al. 2014). Therefore, the PALB2-RAD51-RAD51C-BRCA2 complex may facilitate BRCA2 removal after RAD51 filament nucleation (Park et al. 2014).

1.2.2 *In vitro* characterization of RAD51 paralog function in RAD51 pre- and post-synaptic filament assembly

Initiation of RAD51 filament assembly on ssDNA over hangs may be facilitated, in part, by both the CX3 and BCDX2 complexes. Consistent with this notion, CX3 exhibits ATP-independent DNA binding affinity for ssDNA (Kurumizaka et al. 2001; Masson et al. 2001a). CX3 also binds to other DNA substrates such as 5' or 3' tailed DNA but with reduced affinity (Kurumizaka et al. 2001; Masson et al. 2001a) and CX3 has the lowest affinity for dsDNA (Kurumizaka et al. 2001; Masson et al. 2001a). Interestingly, CX3 complex promotes DNA aggregation suggestive of a role in annealing complementary DNA during the homology search of RAD51 filaments (Kurumizaka et al. 2001; Masson et al. 2001a). Together, this data suggests that CX3 may have an early function in RAD51 filament assembly. Similarly suggesting a role of the BCDX2 complex in RAD51 filament assembly, the BCDX2 complex exhibits a modest ATPase activity in the presence of ssDNA but not in the presence of 5' or 3' tailed DNA or dsDNA (Masson et al. 2001b). Electron microscopy analysis also indicates a role for the BCDX2 complex in RAD51 filament assembly where recombinant BCDX2 complex bound to both ssDNA as well as gaps and nicks in duplexed DNA (Masson et al. 2001b). Walker A and Walker B motifs have been shown to bind and hydrolyze ATP such as for RAD51 (Sung and Stratton 1996). Given that the RAD51 paralogs contain Walker A and B motifs, their role in RAD51 filament mediation may utilize ATP hydrolysis. For example, the BC heterodimer or the DX2 heterodimer alone also binds ssDNA,

and this binding stimulates ATPase activity (Braybrooke et al. 2000; Sigurdsson et al. 2001). Furthermore, the DX2 heterodimer ssDNA binding is enhanced upon ATP addition (Braybrooke et al. 2000; Kurumizaka et al. 2001). The roles of BCDX2 and CX3 in filament formation are most strongly supported by cellular studies discussed below (Takata et al. 2001; Chun et al. 2013). Furthermore, work with the yeast RAD51 paralogs support this presynaptic role. *In vitro* analysis has revealed that both the yeast RAD51 paralog containing complexes, RAD55-RAD57 and Shu complex, promote RAD51 presynaptic filament assembly (Sung 1997b; Gaines et al. 2015). How the RAD51 paralogs mechanistically aid in RAD51 filament assembly is still unknown (Figure 3). It has been hypothesized that perhaps they can either intercalate into the filament (Figure 3A; left side) or even form a co-filament that enables RAD51 elongation after BRCA2-mediated nucleation (Figure 3A; right side). For example, DX2 and CX3 were observed to form filament structures on ssDNA, although these structures significantly differed from RAD51 nucleoprotein filaments (Kurumizaka et al. 2001; Kurumizaka et al. 2002). Alternatively, the RAD51 paralogs could potentially cap the DNA ends to prevent RAD51 filament disassembly similar to what has been observed in yeast for Rad55-Rad57 (Figure 3B) (Liu et al. 2011). Lastly, it has been hypothesized that different RAD51 paralog-containing complexes may promote HR depending upon the nature of the DNA lesion, particularly for the Shu complex (Godin et al. 2016b; Martino and Bernstein 2016; McClendon et al. 2016; Abreu et al. 2018). For example, the Shu complex shows specificity for promoting tolerance of DNA damage, such as an abasic site, in a replication-specific context (Godin et al. 2016b).

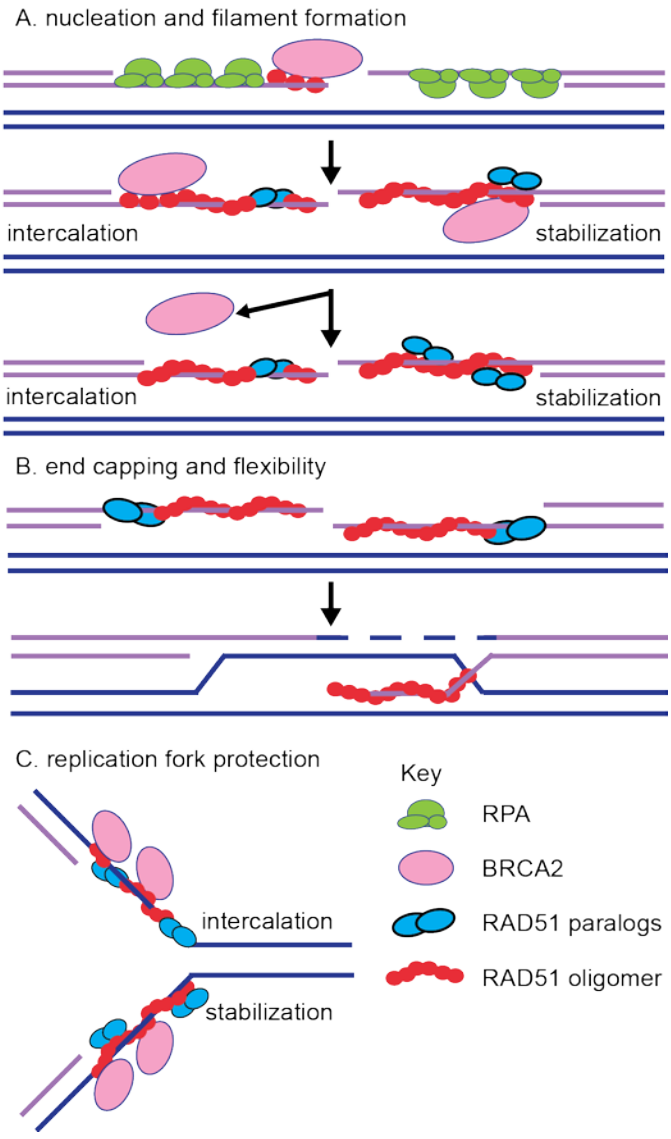

Figure 3. Proposed functions for the RAD51 paralogs.

A. Nucleation and filament formation. Traditionally, the RAD51 paralogs (blue circles) are thought to aid RAD51 (red circle) in filament formation with BRCA2 (pink circle), which nucleates RAD51 monomers onto ssDNA (purple lines). The RAD51 paralogs may act by intercalating into the RAD51 filament directly (shown on left) or by binding to the RAD51 filament to stabilize RAD51 (shown on right). Subsequently, BRCA2 is removed as the filament is stabilized and elongated. B. RAD51 paralog function in RAD51 filament end capping and flexibility were recently proposed (Taylor et al. 2015; Taylor et al. 2016). These functions would aid in RAD51 downstream activity to promote strand invasion. C. Replication fork protection function has also been proposed for the RAD51 paralogs (Somyajit et al. 2015b). During fork protection, the RAD51 paralogs could

potentially intercalate into (top strand) or stabilize (bottom strand) the RAD51 filament at a stalled replication fork.

Conflicting biochemical evidence has also described post-synaptic roles for the RAD51 paralogs as well. For example, contradictory evidence suggests that CX3 either does or does not aid RAD51-mediated D-loop formation (Kurumizaka et al. 2001; Masson et al. 2001a). Suggesting a role for DX2 and BC in strand exchange, the DX2 heterodimer also catalyzes homologous pairing enabling D-loop formation (Kurumizaka et al. 2002) while the BC heterodimer enhances RAD51-mediated strand exchange in the presence of RPA (Sigurdsson et al. 2001). It is possible that incorporation of the RAD51 paralogs into the RAD51 filament could change the conformation of the RAD51 filament to enable increased flexibility for strand exchange as well as promoting filament disassembly to allow the subsequent steps of HR to proceed (Figure 3B). Work on the *C. elegans* RAD51 paralogs, RFS-1 and RIP-1, have provided the most convincing biochemical evidence for a role for the RAD51 paralogs increasing filament remodeling to facilitate a confirmation that enables base pairing and strand exchange using stop flow experiments and cryo-EM (Taylor et al. 2015; Taylor et al. 2016). Simon Boulton's group propose a model in which BRCA2 nucleates RAD51 displacing RPA, and the RAD51 paralogs act downstream to stabilizing the filament. The RAD51 paralogs change RAD51 pre-synaptic filament conformation by capping the 5' end and remodeling up to 40 nucleotides of the 5'-3' filament (Taylor et al. 2015; Taylor et al. 2016). These RAD51 paralog activities are dependent on nucleotide binding but not ATP hydrolysis (Taylor et al. 2015; Taylor et al. 2016). Beyond these initial characterizations, more detailed *in vitro* studies with the human RAD51 paralogs are lacking. For example, the human RAD51 paralogs have not yet been purified individually nor have crystal structures been determined. Therefore, most of our current understanding of RAD51 paralogs function comes from

molecular studies in numerous vertebrate cell lines that have addressed at what steps of repair the RAD51 paralogs act.

1.2.3 *In vivo* characterization of RAD51 paralog function in vertebrates

1.2.3.1 RAD51 paralog knockout mice and MEFs

Since their initial discovery, technical challenges have limited the study of the RAD51 paralogs *in vivo* (Thacker 1999; Godin et al. 2016a). For example, mouse knockout models for the five canonical RAD51 paralogs result in embryonic lethality (Summarized in Table 1). Supporting unique functions for each RAD51 paralog, the knockout models arrest at different developmental stages *RAD51B* (E7.5-E8.5), *RAD51C* (E8.5), *RAD51D* (E9.0-E10.0), *XRCC2* (E10.5-died at birth), and *XRCC3* (unpublished data, personal communication with Maria Jasin) (Shu et al. 1999; Deans et al. 2000; Pittman and Schimenti 2000; Kuznetsov et al. 2009)]. This embryonic lethality mirrors that of *BRCA2* knockout mice (~E8-E9) and provided early evidence that the RAD51 paralogs, like BRCA2, have important HR and developmental functions (Hakem et al. 1998). Recently, the highly divergent RAD51 paralog SWSAP1 and its binding partner SWS1 were shown to produce viable, but sterile, knockout mice (Abreu et al. 2018). The sterility observed in these mice is due to defects in RAD51- and DMC1-mediated meiotic recombination. These mouse models provide new opportunities to examine RAD51 paralog function that has not been possible with the canonical RAD51 paralogs.

RAD51 Paralog	Complex Member	Mouse Knockout	$p53^{-/-}$ Rescue	MEF MMC Sensitivity	MEF MMS Sensitivity	Other Phenotypes
RAD51B	BCDX2	E7.5-8.5	partial	NA	NA	NA
RAD51C	BCDX2, CX3, PALB2-RAD51-RAD51C-BRCA2	E8.5	partial	2-3 fold ($p53^{-/-}$)	2-3 fold ($p53^{-/-}$)	↓ SCEs ↓ IR-RAD51 foci ($p53^{-/-}$)
RAD51D	BCDX2	E9-E10	partial	17.6 fold ($p53^{-/-}$)	6.3 fold ($p53^{-/-}$)	↓ SCEs ($p53^{-/-}$) ↓ IR-RAD51 foci ($p53^{-/-}$)
XRCC2	BCDX2	E10.5- died at birth	yes died 6d P/N	4.5 fold (p53+)	NA	↓ SCEs ↓ IR-RAD51 foci
XRCC3	CX3	NA (EL)	NA	NA	NA	NA
SWSAP1	Shu Complex (SWS1)	Viable/ Infertile	NA	NA	NA	NA

Table 1. RAD51 paralog knockout mice and derived MEF phenotypes.

The phenotypes of RAD51 paralogs (RAD51B, RAD51C, RAD51D, XRCC2, XRCC3, and SWSAP1) are described. The complex where each RAD51 paralog is associated is indicated, the viability and lethality of the mouse knockout model indicated, the degree of rescue by p53 deletion is shown, and mitomycin C (MMC) or methyl methanesulphonate (MMS) sensitivity from derived MEFs indicated. Not applicable is indicated by NA. Other phenotypes noted include sister chromatid exchanges (SCE), ionizing radiation-induced RAD51 foci (IR-RAD51), and a downward arrow indicates a reduction. EL indicates embryonic lethality and P/N is post-natal.

In addition to lack of animal models for the canonical RAD51 paralogs, creating mouse embryonic fibroblasts (MEFs) from these knockout embryos has been challenging., MEFs could not be derived from *RAD51C* $^{ko/ko}$ or *RAD51D*$^{ko/ko}$ mice and conditional *RAD51C* knockout MEFs could not be propagated suggesting *RAD51C* and *RAD51D* are essential (Pittman and Schimenti 2000; Kuznetsov et al. 2009). In contrast to *RAD51C* $^{ko/ko}$ and *RAD51D* $^{ko/ko}$, *XRCC2*$^{ko/ko}$ MEFs were created and found to exhibit fewer RAD51 foci following ionizing radiation-induced DNA damage, and increased mitomycin C sensitivity with fewer sister-chromatid exchanges (Deans et al. 2003). Most intriguingly, even a *XRCC2*$^{ko/+}$ heterozygote knockout displayed genetic instability

(Deans et al. 2003). This result has important clinical implications for *XRCC2* mutation carriers as increased genomic instability may underlie the cancer predisposition seen in RAD51 paralog mutation carriers.

Interestingly, p53 knockout slightly extended the embryonic development of *RAD51B*, *RAD51C*, and *XRCC2* knockout mice (Table 1) (Shu et al. 1999; Adam et al. 2007; Kuznetsov et al. 2009). The greatest rescue is observed with *XRCC2* knockout mice where *Trp53* disruption extended development 6 days (Adam et al 2007). These results are particularly interesting in the context of ovarian cancer where RAD51 paralog germline and somatic mutations are found in p53 deficient tumors (Meindl et al. 2010; Kondrashova et al. 2017). In this context, p53 disruption could enable growth with RAD51 paralog deficiency. Although mouse models result in embryonic lethality, mouse embryonic fibroblasts (MEFs) have been derived from three of the RAD51 paralog knockout mice in a p53-deficient background (*RAD51C*$^{ko/ko}$;*Trp53*$^{ko/ko}$; *RAD51D*$^{ko/ko}$;*Trp53*$^{ko/ko}$; XRCC2$^{ko/ko}$;*Trp53*$^{ko/ko}$) (Smiraldo et al. 2005; Adam et al. 2007; Kuznetsov et al. 2007; Kuznetsov et al. 2009). These MEFs exhibit defects consistent with decreased RAD51 loading or activity (Summarized in Table 1). For example, *RAD51D*$^{ko/ko}$;*Trp53*$^{ko/ko}$ MEFs treated with the DNA crosslinking agent mitomycin C (MMC) have decreased sister chromatid exchanges (SCEs), which result from RAD51-mediated crossover events (Smiraldo et al. 2005). This is further supported by a decrease in RAD51 foci formation after irradiation (IR) in both *RAD51C*$^{ko/ko}$;*Trp53*$^{ko/ko}$ and *RAD51D*$^{ko/ko}$;*Trp53*$^{ko/ko}$ MEFs (Smiraldo et al. 2005; Kuznetsov et al. 2009). These RAD51 paralog deficient MEFs are chromosomally instable with increased chromatid breaks, gaps, and exchanges (Smiraldo et al. 2005; Kuznetsov et al. 2009). In addition, RAD51 paralog disruption in combination with p53 results in extreme sensitivity to MMC (Smiraldo et al. 2005; Adam et al. 2007; Kuznetsov et al. 2007; Kuznetsov et

al. 2009). Severe sensitivity to crosslinking agents like MMC is a defining feature of cells derived from Fanconi anemia (FA) patients as the FA repair pathway (also called the inter-strand crosslink repair pathway) is responsible for repairing inter-strand crosslinks (ICLs), discussed further in Section 1.3.1 (Nalepa and Clapp 2018). Homologous recombination processes are required during ICL repair, and unsurprisingly, RAD51C (FANCO) and XRCC2 (FANCU) mutations have been uncovered in FA or FA-like patients (Vaz et al. 2010; Shamseldin et al. 2012; Jacquinet et al. 2018; Nalepa and Clapp 2018).

1.2.3.2 RAD51 paralog knockout hamster, chicken, and tumor cell lines

The most progress in understanding the role of mammalian/vertebrate RAD51 paralogs has come from studies in Chinese hamster ovary (CHO) and chicken (DT40) cell lines where the RAD51 paralogs are not essential for survival (Jones et al. 1987; Fuller and Painter 1988; Johnson et al. 1999; Pierce et al. 1999; Takata et al. 2000; Takata et al. 2001). Both CHO and DT40 cells have mutant p53 likely enabling the deletion of RAD51 paralogs to be tolerated in culture (Hu et al. 1999; Takata et al. 2000). CHO cells lacking XRCC2 (*XRCC2*$^{-/-}$, irs1-ionizing radiation sensitive 1) have the greatest sensitivity to MMC but are also sensitive to IR, ultraviolet light, and ethyl methanesulphonate (Jones et al. 1987, Thacker 1999). CHO cells lacking XRCC3 (*XRCC3*$^{-/-}$, irs1SF) also exhibits increased sensitivity to IR and fails to form RAD51 foci after damage (Fuller and Painter 1988; Bishop et al. 1998; Thacker 1999). Like CHO cells, DT40 (derived from B-lymphocytes) cells are p53 deficient and tolerate loss of any of the five canonical RAD51 paralogs unlike MEFs (Takata et al. 2000; Takata et al. 2001). DT40 RAD51 paralog knockouts exhibit genomic instability as revealed by spontaneous chromosomal breaks, a reduction in MMC-induced SCEs, and decreased IR-induced RAD51 foci (Takata et al. 2000; Takata et al. 2001). Furthermore, each RAD51 paralog DT40 knockout cell line shows increased sensitivity to DNA damaging

agents such as IR, MMC, and cisplatin (Takata et al. 2000; Takata et al. 2001). These DT40 cell lines have been complemented with human or mouse cDNA which rescued genome instability phenotypes in *RAD51B*$^{-/-}$, *RAD51D*$^{-/-}$, *XRCC2*$^{-/-}$, and *XRCC3*$^{-/-}$ (Takata et al. 2000; Takata et al. 2001). Interestingly, *RAD51C*$^{-/-}$ DT40 could not be complemented with human RAD51C and this has limited RAD51C functional analysis (Takata et al. 2001). Since their initial characterization, these cell lines have complemented and confirmed the results obtained from the mouse models.

Knockdown of RAD51 paralogs in human cancer cell lines (HeLa, HT1080, MCF7 and U2OS) has also proved challenging in studying RAD51 paralog function. For example, siRNA depletion of an individual RAD51 paralog de-stabilizes binding partners within its subcomplex (i.e. siXRCC2 decreases expression of endogenous RAD51D), and siRNAs have variable levels of knockdown efficiency (Lio et al. 2004; Chun et al. 2013). RAD51C is particularly problematic as it is a member of both the BCDX2 and CX3 complexes and its depletion destabilizes members of both subcomplexes (Lio et al. 2004). The dependence of the RAD51 paralogs on one another for expression makes understanding their unique contributions particularly difficult. Furthermore, knockdown of RAD51C is highly toxic to HeLa cells as measured by plating efficiency and delays cell cycle progression from G_1 phase into S and G_2 phases (Lio et al. 2004).

The importance of each human RAD51 paralog in HR has been demonstrated in MCF7 breast cancer and U2OS osteosarcoma cell lines by measuring HR following an endonuclease-induced DSB and by monitoring cells for DNA damage sensitivity (Lio et al. 2004; Chun et al. 2013). Consistent with an HR function, the elevated IR-sensitivity of RAD51C-depleted HeLa cells was specific to S/G_2 cell cycle phase when HR is most active while G_1 phase cells were equally sensitive as controls when other repair pathways predominate (Lio et al. 2004). Furthermore, increasing evidence suggests that the RAD51 paralog subcomplexes likely have non-

overlapping roles. For example, knockdown of siRAD51D, which disrupts the BCDX2 complex specifically, results in decreased RAD51 foci formation following IR exposure whereas knockdown of siXRCC3, which disrupts the CX3 complex specifically, does not (Chun et al. 2013). Concurrent siRNA knockdown of both RAD51B and RAD51D does not further impair RAD51 foci formation upon IR treatment (Chun et al. 2013). These results suggest that the CX3 and BCDX2 complexes function independently. Furthermore. BCDX2 likely acts upstream of RAD51, whereas the CX3 complex may function after RAD51 filament formation (Chun et al. 2013). Depletion of either BCDX2 or CX3 does not impair BRCA2 foci formation after IR suggesting BRCA2 recruitment is independent of the RAD51 paralogs (Chun et al. 2013). These cell-based studies support the notion that the RAD51 paralogs might function during both pre- and post-synaptic filament assembly (Figure 3).

1.2.4 The RAD51 paralogs function at replication forks

The RAD51 paralogs also play critical roles at damaged replication forks (Somyajit et al. 2015b). RAD51 paralog disruption leads to sensitivity to genotoxic agents that could cause replication-associated damage such as the alkylating agent methylmethane sulfonate (MMS) (Kuznetsov et al. 2009; Deans and West 2011). Alkylation damage is primarily repaired through the base excision repair pathway (BER); however, if the replication fork encounters a BER DNA processing intermediate, these DNA adducts can slow or even collapse replication forks (Tercero and Diffley 2001). Similar to agents that directly induce DSBs, both RAD51C$^{ko/ko}$;Trp53$^{ko/ko}$ and RAD51D$^{ko/ko}$;Trp53$^{ko/ko}$ MEFs are sensitive to MMS (Table 1) (Kuznetsov et al. 2009; Deans and West 2011). Similarly, knockdown of the human Shu complex members, SWS1 or SWSAP1 also exhibited MMS sensitivity and reduced RAD51 foci formation (Martin et al. 2006; Liu et al. 2011).

Interestingly, the Shu complex function is specific to these types of lesions as SWS1 or SWSAP1 knockdown cells do not exhibit sensitivity to IR (Liu et al. 2011). This is consistent with the role for the yeast Shu complex in tolerance of MMS-induced DNA damage during S phase (Godin et al. 2016b).

In mammalian cells, emerging new roles in replication fork protection and restart have been identified for BRCA2 (Schlacher et al. 2011; Schlacher et al. 2012). Fiber spreading methods have revealed that BRCA2 protects replication forks from MRE11-mediated degradation (Schlacher et al. 2011). RAD51 has also been implicated to have a role in fork protection (Hashimoto et al. 2010). Direct evidence for a role of the human RAD51 paralogs at replicative damage has only recently been investigated (Somyajit et al. 2015b). A study by Somyajit et al examined the consequences of loss of three RAD51 paralogs, RAD51C, XRCC2, and XRCC3, using RAD51 paralog hamster mutant cell lines and HeLa cell knockdowns (Somyajit et al. 2015b). In DNA fiber spreading experiments, loss of RAD51C, XRCC2, and XRCC3 increased MRE11-mediated degradation of nascently replicated DNA (Figure 3C). This implicates both the BCDX2 and CX3 complexes as being involved in replication fork protection (Somyajit et al. 2015b). However, XRCC2 was dispensable for replication fork restart, and only RAD51C and XRCC3 were important for restart in fiber spreading experiments. Somyajit et al propose that the CX3 complex, but not the BCDX2 complex, plays a role in fork restart and that this activity depends on their Walker A motifs (Somyajit et al. 2015b). This result suggests that the RAD51 paralog subcomplexes may play unique functions during repair of replication damage (Somyajit et al. 2015b).

1.3 RAD51 MEDIATORS AND DISEASE

Since HR is a high-fidelity DSB repair mechanism, mutations in HR genes are particularly deleterious to the cell. The importance of maintaining this repair pathway is highlighted by the link between mutations in HR genes and several cancer-associated diseases. Defects in HR genes are associated with many genetic syndromes, such as ataxia-telangiectasia, Nijmegen break syndrome, FA, and Bloom's syndrome (Thompson and Schild 2002). Specifically, the RAD51 mediators and their interaction partners are correlated to diseases defined by genomic instability that predispose individuals to cancer.

1.3.1 Genetic syndromes linked to RAD51 mediators

While defects in HR genes are linked to several genetic syndromes, the RAD51 mediators are most closely associated with FA (Moldovan and D'Andrea 2009). FA affects many systems of the body causing bone marrow failure, anemia, congenital abnormalities, and cancers amongst other clinical conditions (Moldovan and D'Andrea 2009). Most notably these patients have an early predisposition to several cancers of the blood, bone marrow, and solid tumors, which vary by complementation group (Moldovan and D'Andrea 2009; Nepal et al. 2017). FA is diagnosed by sensitivity to the crosslinking agents MMC or diepoxybutane resulting in chromosomal breaks and radials (Moldovan and D'Andrea 2009; Nalepa and Clapp 2018). This MMC sensitivity is due to defects in ICL repair either in removal of the crosslink itself or in downstream HR steps (Moldovan and D'Andrea 2009). FA is caused by single gene defects in any one of these factors and are named for their complementation groups (A-W to date) (Nalepa and Clapp 2018; Knies et al 2017). Importantly RAD51 and its mediators make up a significant portion of these complementation

groups including BRCA2 (FANCD1), PALB2 (FANCN), RAD51C (FANCO), RAD51 (FANCR), and XRCC2 (FANCU) (Nalepa and Clapp 2018). The addition of RAD51, RAD51C, and XRCC2 to the FA family has been quite recent likely due to the availability and decreased cost of DNA sequencing. While RAD51C is classified as a FANC complementation group, it does not share all of the phenotypes that present in other FA subtypes. It is therefore considered a Fanconi-like syndrome (Vaz et al. 2010; Jacquinet et al. 2018). The emerging role of RAD51C and potentially other RAD51 paralogs in ICL repair is still an emerging field of study, and we have yet to determine if these proteins are playing roles upstream of canonical HR during ICL repair.

1.3.2 Cancers associated with defects in homologous recombination

While patients with biallelic mutations in RAD51 and its mediators have been identified in FA patients, monoallelic germline mutations in RAD51 mediators are correlated to predisposition to cancer (Meindl et al. 2010; Pennington et al. 2014). This is thought to be frequently caused by a somatic loss-of-heterozygosity (LOH) event where the second functional copy of the gene is deleted, resulting in genomic instability and cancer development (Ollier et al. 2015; Maxwell et al. 2017). The most common cancer associated mutations are found in BRCA1 and BRCA2 and can be both germline and somatic. *BRCA1* and *BRCA2*, initially named as breast cancer susceptibility genes 1 and 2, are most associated with breast and ovarian cancers (Pennington et al. 2014; Ollier et al. 2015; Tung et al. 2016). Mutations in *BRCA1* and *BRCA2* genes are routinely screened for in women and men with a family history of breast or ovarian cancer (Tung et al. 2016). BRCA1 mutations account for about 16.3% of ovarian cancers and BRCA2 mutations account for 6% of ovarian cancers (Pennington et al. 2014). *BRCA1/2* mutations are somewhat less frequent in breast cancers accounting for 5.5-6.1% of patients (Tung et al. 2016). Interestingly,

overall mutation frequency of *BRCA1/2* decreases with age in breast cancer patients, suggesting deleterious mutations in *BRCA1/2* are found in earlier-onset cancers (Tung et al. 2016). Mutations in these genes are diverse and range from single amino acid changes to methylation silencing of promoters (Pennington et al. 2014; Tung et al. 2016; Bernards et al. 2018). More recently, mutations in additional RAD51 mediators are increasingly being identified and screened for in the clinic (BARD1, BRIP1, PALB2, RAD51C, RAD51D) (Pennington et al. 2014; Tung et al. 2016; Couch et al. 2017). HR gene mutations are particularly abundant in breast, ovarian, and endometrioid cancers but have also been found in other cancers such as pancreatic and colon (Pelttari et al. 2012; Pennington et al. 2014; Witkiewicz et al. 2015; Forbes et al. 2017). A number of the RAD51 mediators have now been added to the more comprehensive breast and ovarian cancer screening panels (i.e. PALB2, RAD51C, RAD51D, XRCC2). Due to the technical challenges in studying these proteins described above, the vast majority of the mutations identified are variants of unknown significance. However, hundreds of epidemiology studies have tried to correlate specific RAD51 paralog mutations with cancer predisposition using population studies. HR-deficiency is most prevalent in ovarian carcinomas and an HR-deficient mutational signature is found in approximately 20% of breast cancers (Nik-Zainal and Morganella 2017). In the most lethal type of ovarian cancer, high-grade serous carcinomas, up to 51% of tumors are HR-deficient from either inherited or somatic mutations or promoter methylation (Pennington et al. 2014; Stover et al. 2016; Bernards et al. 2018)(TCGA, 2011). It has been estimated that 3% of hereditary ovarian cancer patients have a mutation in RAD51C whereas 5% have a mutation in RAD51D (Pennington et al. 2014). Standard of care for HR-deficient ovarian cancer patients includes aggressive surgery and a combination of platinum and taxane chemotherapy (TCGA, 2011) (Vencken et al. 2011; Pennington et al. 2014; Matondo et al. 2017). However, the five-year survival rate is only 30%

and within 12 months, 30-40% of patients relapse (Matondo et al. 2017). To remedy these startling statistics, it is essential to target these patients with targeted chemotherapy. There remains a critical need to identify all HR-deficient tumors to determine who will most benefit from therapies used to currently treat BRCA1/2 patients.

1.3.3 Therapeutic strategies for HR-deficient breast and ovarian cancers

New treatment strategies targeting DDR factors have shown promising success in clinical trials (O'Connor 2015; Stover et al. 2016). These therapies can effectively kill cancer cells with defects in DNA repair through synthetic lethality (Stover et al. 2016). However, understanding which tumors will be vulnerable to a specific therapy is central to determining efficacy of a drug for an individual tumor. This precision medicine approach requires detailed molecular analysis of variants of unknown significance (VUS) to determine if the target gene is truly deleterious and a good candidate for targeted therapy. Synthetic lethality with the HR pathway has proved especially effective for *BRCA*-deficient cancers (Fong et al 2009; Bryant et al 2005). Similarly, emerging evidence suggests these therapies will also be efficacious in targeting other HR gene defects. In addition to traditional chemotherapeutic drugs that induced DNA damage, HR-deficient tumors are currently being targeted with small molecule inhibitors of Poly (ADP-ribose) polymerase (PARP), DDR signaling molecules, and NHEJ factors (Maxwell et al. 2017). These inhibitors have had varying levels of success, and some have already been introduced to the clinic while others remain in various stages of clinical testing as described below.

1.3.3.1 Synthetic lethality in BRCA and BRCA-like cancers

Synthetic lethality induces cell death by the loss of two somewhat redundant functions that alone would have been viable, such as the impairment of two DNA repair pathways that respond to the same DNA lesions (Stover et al. 2016). Synthetic lethality can be achieved through numerous targeting strategies in cancer cells with a genetic loss-of-function mutation. Cancer cells typically lose some component of the DDR pathway that has enabled genomic instability and has therefore been selected for as it allows the tumor to grow (Bryant et al. 2005; Jackson and Bartek 2009; O'Connor 2015). This loss-of-function is specific to the tumor and causes the tumor cells to have greater dependence on remaining pathway(s) for survival relative to normal cells. An effective strategy in specifically targeting cancer cells for cell death takes advantage of DDR impairment in the tumor by pharmacologically impairing a complementary pathway that becomes essential for cell survival (Bryant et al. 2005; O'Connor 2015). The protection of normal cells from this same lethality is an advantage to traditional chemotherapies that induce DNA damage in all cells (Bryant et al. 2005; O'Connor 2015).

As discussed above, *BRCA*-deficient cancer cells typically arise through a LOH event that enables tumor growth through an increased tolerance for genomic instability (O'Connor 2015; Maxwell et al. 2017). However, the surrounding cells still maintain one normal copy of the *BRCA* gene and are therefore considered *BRCA*-proficient (Maxwell et al. 2017). The tumor then relies on alternative repair pathways while the surrounding tissue can still use HR. Therefore, a drug impairing only the HR alternative pathways will have little effect on normal cells limiting its toxicity (O'Connor 2015). This difference between the two tissue types provides an opportunity for targeted therapy. By increasing the damage burden of the cell through classical chemotherapy and/or inhibiting back-up repair pathways (SSA or alt-NHEJ) through small molecules, the tumor

cells can be specifically targeted (Jasin and Rothstein 2013). This minimizes the impact on normal cells while effectively killing cancer cells (Fong et al. 2009). This concept has produced a variety of therapies to treat *BRCA* and *BRCA-like* cancers (Stover et al. 2016). It is interesting that HR-defective tumors are sensitive to PARP inhibitors which was designed to target PARP1 and increase ssDNA breaks that can become DSBs in a replicative context (O'Connor 2015). New findings suggest that PARP1 might also play a critical role during Okazaki fragment ligation during replication to facilitate repair (Hanzlikova et al 2018). Currently, HR-deficient cancers are primarily clinically specific to *BRCA*-deficient cancers as other HR factors are less well characterized in a clinical setting but could benefit from the same strategies.

1.3.3.2 Chemotherapeutics currently in the clinic

Classically, ovarian cancers have been treated with platinum-based chemotherapeutics and more recently triple-negative breast cancer patients have increased progression free survival using platinum therapy (Deans and West 2009). BRCA1/2-deficient tumors show increased sensitivity to platinum based therapy resulting in an improved overall survival (Matondo et al. 2017; Maxwell et al. 2017). Platinum-based drugs including cisplatin and carboplatin are effective inducers of inter- and intra-strand cross links that require ICL and subsequently HR repair to resolve (Deans and West 2009; Moldovan and D'Andrea 2009). In BRCA1/2-deficient tumors, HR is incapable of resolving ICLs and DSBs will be repaired by error-prone alternative pathways leading to cell death in the tumor cells. The increased DNA damage is much more toxic to the HR-deficient tumor cells than to the surrounding HR-proficient cells. While few large-scale studies have shown the same trends for *BRCA1/2*-independent HR gene mutations, emerging studies show similar platinum sensitivities for mutations in HR genes including *RAD51C* and *RAD51D* (Norquist et al, 2017). While initially effective, subsequent platinum-resistance often leads to recurrence of the

tumor (Pennington et al. 2014). In this scenario, ovarian cancer patients have now been approved for use of PARP inhibitors (Kristeleit et al. 2016).

PARP inhibitors (PARPi) are small molecule inhibitors that have recently been approved for platinum-sensitive relapsed and platinum-resistant ovarian cancers harboring *BRCA1* or *BRCA2* mutations (Bryant et al 2005; Fong et al. 2009; O'Connor 2015; Kristeleit et al. 2016). PARPi in HR-deficient tumor cells are much more toxic than in surrounding HR-proficient tissue. The relationship between PARP and HR is complex as PARP is a single-strand break repair factor. PARP acts as a signaling molecule by binding DNA at ssDNA breaks to recruit repair factors but must be removed for repair to proceed (Murai et al. 2014). Without this signaling, the ssDNA break collapses replication forks requiring HR to repair the resultant dsDNA break (Bryant et al 2005). PARPi range in their ability to trap PARP on DNA through the competitive binding of the inhibitor where NAD+ activates PARP releasing it from the DNA (O'Connor 2015)(Murai et al. 2014). However, when PARP dissociation from DNA is inhibited, it becomes trapped on DNA and will block DNA replication (O'Connor 2015). This replication block generates stalled or collapsed replication forks that require HR for repair. If HR is impaired, as occurs in *BRCA*-deficient tumor cells, more deleterious HR alternative pathways repair the damage and lead to rampant genome instability and eventually cell death (O'Connor 2015). Currently, Olaparib and Rucaparib are two PARPi approved for use in the United States (Brown et al, 2016). These drugs show different levels of PARP trapping on the DNA where niraparib, olaparib, and rucaparib are medium trappers relative to other PARPi such as talazoparib and veliparib which are stronger or weaker trappers (Murai et al. 2014). Success of these drugs in platinum-resistant ovarian cancers holds promise for expanded approval for a larger set of ovarian cancers as well as breast cancers (O'Connor 2015). Currently, clinical trials are testing non-*BRCA* HR deficient tumors that have

other HR gene mutations including *RAD51C* and *RAD51D* show PARPi response (Swisher et al. 2017).

One of the major problems in treating ovarian cancers with PARPi is acquired resistance to the PARPi therapy due to a strong drive for reversion mutations and therefore restoration of HR. The first-line treatment of combined platinum and PARPi may be able to more effectively eliminate the tumor before resistance can arise. Recently, the acquisition of PARPi-resistance has been investigated in *BRCA1*-deficient cancer cells and has also been observed in RAD51C and RAD51D patients (Kondrashova et al. 2017). In addition to reversion mutations restoring BRCA1 function directly, mutations in other genes that restore HR through alternative mechanisms has also been uncovered. For example, in BRCA deficient tumors, additional loss of 53BP1 or the shieldin genes rescues HR-deficiency by allowing the HR pathway to be engaged (Ghezraoui et al. 2018; Gupta et al. 2018; Mirman et al. 2018; Noordermeer et al. 2018). The numerous resistance mechanisms to overcome loss of HR decreases the efficiency of monotherapies and allows the tumor to evade the therapeutic strategy. New strategies need to more efficiently kill tumor cells to prevent the opportunity for evasion mechanisms. PARPi may therefore be most effective when used in combination with classical DNA damage-inducing agents rather than as a monotherapy. In this scenario, a weaker PARP trapper may be necessary to minimize cytotoxicity.

As RAD51 regulation is essential to maintaining HR and thus preserving genome stability, we aimed to understand the functions of factors that regulate RAD51. RAD51 paralogs assemble into multiple complexes each of which regulates aspects of RAD51 activity. We first investigated the highly conserved Shu complex, a RAD51 paralog-containing complex, in a multicellular organism. We sought to characterize the composition of the *C. elegans* Shu complex and determine how its functions promote genome stability. We then investigated RAD51C, a RAD51 paralog

contained in two RAD51 paralog complexes in humans. Mutations in *RAD51C* are associated with familial breast and ovarian cancers, but the impact of these mutations on RAD51C function has remained unknown. We aimed to identify mutations in *RAD51C* that would disrupt RAD51 paralog complexes and impair the function of RAD51C in HR. By clarifying the basic functions of RAD51 paralog complexes in HR, we can understand their role in cancer predisposition.

2.0 SWS-1 FUNCTIONS WITH THE RAD-51 PARALOGS TO PROMOTE HOMOLOGOUS RECOMBINATION IN *CAENORHABDITIS ELEGANS*

Homologous recombination (HR) repairs cytotoxic DNA double-strand breaks (DSBs) with high fidelity. Deficiencies in HR result in genome instability. A key early step in HR is the search for and invasion of a homologous DNA template by a single-stranded RAD-51 nucleoprotein filament. The Shu complex, comprised of a SWIM domain-containing protein and its interacting RAD51 paralogs, promotes HR by regulating RAD51 filament dynamics. Despite Shu complex orthologs throughout eukaryotes, our understanding of its function has been most extensively characterized in budding yeast. Evolutionary analysis of the SWIM domain identified *Caenorhabditis elegans sws-1* as a putative homolog of yeast Shu complex member, Shu2. Using a CRISPR-induced nonsense allele of *sws-1*, we show that *sws-1* promotes HR in mitotic and meiotic nuclei. *sws-1* mutants exhibit sensitivity to DSB-inducing agents and fail to form mitotic RAD-51 foci following treatment with camptothecin. Phenotypic similarities between *sws-1* and the two RAD-51 paralogs, *rfs-1* and *rip-1*, suggest they function together. Indeed, we detect direct interaction between SWS-1 and RIP-1 by yeast-two-hybrid that is mediated by the SWIM domain in SWS-1 and the Walker B motif in RIP-1. Furthermore, RIP-1 bridges an interaction between SWS-1 and RFS-1, suggesting RIP-1 facilitates complex formation with SWS-1 and RFS-1. We propose that SWS-1, RIP-1, and RFS-1 comprise a *C. elegans* Shu complex. Our work provides a new model for studying Shu complex disruption in the context of a multicellular organism that has important

implications as to why mutations in the human RAD51 paralogs are associated with genome instability.

2.1 INTRODUCTION

DNA double-strand breaks (DSBs) are extremely cytotoxic lesions that threaten genome integrity. DSBs arise from both endogenous sources such as replicative damage, or exogenous sources such as ionizing radiation (IR) and chemotherapeutic agents. To ensure the maintenance of the genome, DSBs need to be repaired by high-fidelity repair pathways, the most robust of which is homologous recombination (HR), in which DNA from a sister chromatid or homologous chromosome provides a repair template. Initial processing of DSB ends by resection forms 3' single-stranded DNA (ssDNA) overhangs that are coated with the ssDNA-binding protein RPA. Several RAD51 mediators then facilitate the exchange of RPA for the recombinase enzyme RAD51 to form a RAD51 filament. This presynaptic filament then performs the homology search and strand invasion of homologous DNA templates to form displacement loop structures. Subsequent stabilization of HR intermediates then requires removal of RAD51 from the double-stranded DNA to allow access to the DNA polymerization machinery. Given the central role of the RAD51 filament in HR, its assembly and disassembly are tightly regulated to ensure the fidelity of repair (Krejci et al. 2012; Jasin and Rothstein 2013; Heyer 2015).

Key mediators of RAD51 filament assembly are the RAD51 paralogs. In humans, there are six RAD51 paralogs: RAD51B, RAD51C, RAD51D, XRCC2, XRCC3, and the newly identified SWSAP1 (Liu et al. 2011; Karpenshif and Bernstein 2012; Prakash et al. 2015). The RAD51 paralogs form multiple sub-complexes including a novel complex containing SWSAP1 and its

binding partner SWS1 (Miller et al. 2002; Liu et al. 2011). Mutations in the RAD51 paralogs are associated with cancer predisposition and, in some cases, Fanconi anemia-like syndromes (Vaz et al. 2010; Wang et al. 2015), underscoring the importance of these proteins in maintaining genome stability. Nevertheless, progress in understanding the roles of these complexes in metazoans has been hampered by the embryonic lethality observed in mouse knockouts and the difficulty in attaining purified proteins for biochemical studies (Deans et al. 2000; Thacker 2005; Kuznetsov et al. 2009; Suwaki et al. 2011).

Much of our understanding of the RAD51 paralogs comes from studies in budding yeast in which the Rad51 paralogs form two sub-complexes, the Shu complex (also called the PCSS complex) and the Rad55-Rad57 complex. The Shu complex is an obligate hetero-tetramer comprised of Psy3, Csm2, Shu1, and Shu2 which facilitates HR-mediated DSB repair by stimulating Rad51 filament formation (Shor et al. 2005; Mankouri et al. 2007; Ball et al. 2009; Godin et al. 2013; Hong and Kim 2013; Sasanuma et al. 2013; Gaines et al. 2015; Godin et al. 2015). Csm2 and Psy3 are Rad51 paralogs whereas Shu2 is a member of the SWS1 protein family, defined by a highly conserved SWIM domain (Makarova et al. 2002; Martin et al. 2006; Godin et al. 2015). Yeast with Shu complex disruptions exhibit sensitivity to the alkylating agent methyl methanesulfonate (MMS), increased mutations, decreased meiotic crossover (CO) formation, and reduced spore viability (Shor et al. 2005; Hong and Kim 2013; Sasanuma et al. 2013; Godin et al. 2015). Unlike yeast and humans, only two RAD-51 paralogs, RFS-1 and RIP-1, are known in *C. elegans*. Both paralogs function in HR, mediating repair of DNA lesions in the mitotic and meiotic regions of the worm germ line (Ward et al. 2007; Yanowitz 2008; Ward et al. 2010; Taylor et al. 2015). Nevertheless, the relationship of the RAD-51 paralogs to a worm Shu complex remains largely unknown.

Although Shu complex function was thought to be conserved throughout eukaryotes, the poor amino acid conservation across species precluded identification of functional paralogs in other systems until recently. Evolutionary analyses of the SWIM domain led to the identification of *C. elegans sws-1* as the homolog of *S. cerevisiae* Shu2 (Godin et al. 2015). *C. elegans* provides several advantages for probing the function of *sws-1*. The germ line is spatially and temporally organized such that the stages of meiotic prophase I – and integrity thereof – can be readily distinguished by DNA morphology (visualized by DAPI). The germ line is a reliable source of programmed DSBs induced by the topoisomerase-like SPO-11 (Keeney et al. 1997), and HR is the favored repair mechanism due to the need to form crossovers between homologous chromosomes (Cole et al. 2010). Populations of *C. elegans* exist primarily as self-fertilizing hermaphrodites with two X chromosomes; rare nondisjunction of the X chromosome (<0.2% in wild type) results in viable males with a single X chromosome (XO). Nondisjunction of autosomes, by contrast, is lethal in most cases and can be ascertained by the presence of unhatched eggs (Hodgkin et al. 1979). Thus, progeny viability and male frequency (*h*igh *i*ncidence of *m*ales phenotype) can intimate meiotic HR repair defects, although those phenotypes are not sufficient indicators on their own.

Using CRISPR/Cas9, we created a nonsense allele of *sws-1* in *C. elegans*, generating an mRNA product that underwent nonsense mediated decay, and probed the role of this conserved DNA repair factor in both mitotic and meiotic cells of the germ line. We find that *sws-1* is the functional homolog of *S. cerevisiae* Shu2, showing that: 1. *sws-1* mutants exhibit DNA damage sensitivity; 2. disruption of *sws-1* results in reduced RAD-51 foci formation following camptothecin (CPT) treatment; and 3. SWS-1 interacts with the known *C. elegans* RAD-51 paralogs RFS-1 and RIP-1 (Ward et al. 2007; Taylor et al. 2015). Our findings show for the first

time the mitotic and meiotic role of *sws-1* in the context of a metazoan and expand upon the known RAD-51 paralog-interacting proteins in worms.

2.2 MATERIALS AND METHODS

2.2.1 Culture and strains

For all experiments, worms were cultured on NGM plates seeded with OP50 and grown at 20°C unless otherwise noted (Brenner 1974). Mutant strains used in this study were: LG I, *syp-3(ok758)*, *dog-1(gk10)*; LG III, *rip-1(tm2948)*, *rfs-1(ok1372)*, *helq-1(tm2134)*; LG V, *sws-1(ea12)* (generation of strain described below); LG X, *unc-58(e665)*. *rip-1*, *rfs-1 rip-1*, and *helq-1* were kindly provided by Simon Boulton; *syp-3* by Sarit Smolikove; and *dog-1* by Ann Rose. Other strains were provided by the Caenorhabditis Genetics Center. Double and triple mutants generated for this work were done so using standard genetic techniques and are listed in Supplemental Table 1. *helq-1;sws-1* double mutants were maintained as heterozygotes due to lack of suitable genetic balancers and were genotyped in all experiments to confirm homozygosity of markers. Control animals used in this study are the homozygous wild-type self-progeny of an *sws-1* heterozygote and did not differ phenotypically from our N2 stock (Table 2, rows A and B).

2.2.2 Generation of *sws-1(ea12)*

Unique CRISPR guides near the start and stop codons of *sws-1* were selected using the CRISPR design tool at crispr.mit.edu (see Supplemental Table 2 for sequences of the primers used in

sgRNA design). Primers were inserted into pDD162 (P*eft-3::Cas9::tbb-2* 3' UTR) using the Q5 Site-Directed Mutagenesis Kit (NEB) as described (Dickinson et al. 2013). DNA from positive clones was isolated using the PureLink®HQ Mini Plasmid DNA Purification kit (Invitrogen) and sequenced to verify the insertion. An injection mix consisting of 30 ng/µl *dpy-10(cn64)* repair oligo (Arribere et al. 2014) and 50 ng/µl each gRNA in pDD162 (one for *dpy-10*, two for *sws-1*) diluted in PureLink EB buffer (Invitrogen) was prepared and injected into N2 day 1 adult hermaphrodites. Roller progeny (*dpy-10(cn64)/+*) of injected hermaphrodites were isolated and allowed to lay eggs before being lysed in buffer for DNA isolation (0.1 M Tris pH 8.5, 0.1 M NaCl, 0.05 M EDTA, 1% SDS, 0.1 µg/mL proteinase K). A region ~300 bp around each Cas9 target site was amplified by PCR and resolved on a 2-3% agarose gel to identify products differing in size from an uninjected control (Supplemental Table 2, Figure 4A-B). This approach yielded one candidate founder strain with an insertion near the start codon; we did not detect any mutations near the stop codon (data not shown). PCR product from the founder strain was purified (NucleoSpin Gel and PCR Clean-up kit, Macherey-Nagel), sequenced, and aligned with wild-type sequence to identify mutations. The candidate allele was outcrossed to N2 multiple times to lose the *dpy-10(cn64)* allele and any potential (though unanticipated) off-target mutations (Paix et al. 2014).

2.2.3 Gene expression

A population of approximately 1000 day 1 adult hermaphrodites were washed thrice in 1x M9 buffer (3 g/L KH_2PO_4, 6 g/L Na_2HPO_4, 5 g/L NaCl, 1 mM $MgSO_4$), resuspended in Trizol (Invitrogen) and vortexed for ~60 seconds before being flash frozen and stored at -80°C. Worms were further disrupted by 3 freeze-thaw cycles in which samples were thawed in cold water,

vortexed 30 seconds, and frozen at -80°C. RNA was isolated by chloroform extraction and isopropanol precipitation, and resuspended in nuclease-free water. Genomic DNA was removed using the DNaseI kit (Sigma-Aldrich, AMPD1-1KT) according to manufacturer's instructions. RNA quality was measured by a spectrophotometer.

Reverse transcription was performed using the TaqMan High Capacity RNA-to-cDNA kit (Applied Biosystems) according to manufacturer's instructions. Comparative C_T experiments were performed according to the manufacturer's instructions using TaqMan Fast Universal No AmpErase UNG PCR Master Mix and TaqMan gene expression assays for CELE_Y39B6A.40 (*sws-1*) and reference gene *rpl-32* (Hoogewijs et al. 2008) (Thermo Fisher Scientific). Reactions were run in triplicate and analyzed with Applied Biosystems Fast PCR System and StepOne Software using the comparative C_T method (Schmittgen and Livak 2008).

2.2.4 Brood size/lethality/Him frequency

L4 hermaphrodites of a given genotype were individually plated and transferred to a clean plate every 12 hours until egg-laying ceased. After transfer, the number of eggs and L1s on the plate was counted and recorded. Three to four days later, each plate was scored for the number of adult hermaphrodites and males. Timepoint data from each individual parent was combined to give total eggs, total adult brood, and total males. Percent hatching was calculated by dividing total adults by total eggs and multiplying by 100, then subtracting from 100 to give percent lethality. Percent lethality is normalized to N2 to account for 3% error in egg counts. To calculate male frequency, the total number of males was divided by the total number of adults. The data are presented as the mean ± SEM from isogenic parents.

2.2.5 Developmental arrest assay

Developmental arrest in unstressed larvae was assayed as previously described (Craig et al. 2012). Briefly, 100 L1 larvae of a given genotype were plated onto center-seeded 3-cm dishes in triplicate. After 48-60 hours, the number of adult, L3-L4, and L1-L2 worms on each plate was counted. To calculate larval arrest, the number of worms in each developmental stage was divided by the total number of worms counted.

2.2.6 Mutation frequency

Mutation frequency of *sws-1(ea12)* was assessed as described previously (Harris et al. 2006). Briefly, *sws-1(ea12);unc-58(e665)* and *unc-58(e665)* homozygotes were grown on 40 6-cm plates until starvation, then transferred by chunking to approximately 100 10-cm plates containing a streak of OP50 opposite the agar chunk. Plates were scored by eye for the presence of Unc revertants that could reach the OP50. Mutation frequency was calculated as described (Harris et al. 2006). Mutation frequency of *sws-1(ea12)* in the *dog-1* background was assessed as described previously (Youds et al. 2006). Briefly, generation-matched (F3) *dog-1(gk10)* and *dog-1(gk10);sws-1(ea12)* day 1 adults were individually lysed in buffer for DNA isolation. The poly G/C tract of *vab-1* was amplified by PCR (primers and conditions described in (Youds et al. 2006)) and resolved on a 1.5% agarose gel. The presence of one or more bands below the expected product size signified a deletion event.

2.2.7 Genotoxin Sensitivity Assays

Details for each genotoxin exposure are described below. For each genotoxin, drug doses and exposure times were optimized using wild type worms. In all assays, the number of eggs and L1s were counted at the end of the collection window. Three to four days later, each plate was scored for the number of adult progeny. Survival was calculated as the number of adult progeny divided by the number of eggs/L1s relative to untreated worms ± SEM from 22-50 adults over two trials.

2.2.7.1 Ionizing Radiation (IR)

L4 hermaphrodites were plated on each of 4 6-cm plates with 30-100 worms/plate depending on genotype and IR dose. The following day, worms were exposed to 0, 10, 50, or 100 Gy of IR from a ^{137}Cs source (Gammacell®1000 Elite, Nordion International Inc.). Twelve hours post-irradiation, worms were plated (2 worms per 3-cm dish) and allowed to lay for 12 hours before removal and egg counts.

2.2.7.2 Methyl Methanesulfonate (MMS)

L4 hermaphrodites were incubated in 0%, 0.0025%, 0.005%, and 0.01% MMS (50-9480886, Fisher Healthcare) dissolved in 1x M9 buffer for 12 hours at room temperature with mild agitation. Following exposure, worms were washed, transferred to plates, and allowed to recover for 12 hours. Post recovery, worms were plated (2 worms per 3-cm dish) and allowed to lay for 12 hours before removal and egg counts.

2.2.7.3 Camptothecin (CPT)

CPT exposure was performed as described with minor alterations (Kessler and Yanowitz 2014). Briefly, young adult hermaphrodites were incubated in 0 nM, 250 nM, 500 nM, and 1000 nM CPT (ICN15973250, Fisher Healthcare) dissolved in 1x M9 pH 6.0 buffer and 0.2% DMSO for 18 hours at room temperature with mild agitation. Following exposure, worms were washed, transferred to plates, and allowed to recover for three hours. Post recovery, worms were plated (5 worms per 3-cm dish) and allowed to lay for 4 hours before removal and egg counts.

To assess DNA damage-induced apoptosis in response to CPT, young adult hermaphrodites were treated, washed, and allowed to recover as described above. Post recovery, worms were exposed to acridine orange (AO, Invitrogen A3568) as previously described (Lant and Derry 2014). Worms that were verified to have taken up the stain were mounted in levamisole and observed on a compound microscope with fluorescence. Cells in the pachytene-diplotene region of the germ line that retained AO were scored as apoptotic. The data are presented as mean AO-positive nuclei ± SEM from 25 germ lines.

2.2.7.4 Hydroxyurea (HU)

Hydroxyurea (H8627, Sigma-Aldrich) was dissolved in approximately 60°C NGM to final concentrations of 0 mM, 8 mM, 12 mM, and 25 mM, poured into 3-cm dishes to solidify, and used within 24 hours. Plates were seeded with heat-killed OP50 (Kessler and Yanowitz 2014) and dried for 45-60 minutes under a fume hood. L4 hermaphrodites were incubated on HU plates for 20 hours at 20°C. Following exposure, worms were moved to plates with drug-free NGM and live OP50 (2-4 worms per 3-cm dish) and allowed to lay for 12 hours before removal and egg counts.

2.2.8 Immunofluorescence

Day 1 adult hermaphrodites were dissected in PBS/levamisole and fixed in 0.5% triton/1% PFA for 5 minutes in a humid chamber. Slides were freeze-cracked and briefly immersed in methanol. Following fixation, slides were washed in PBST and incubated in primary antibody (α-RAD-51, kindly provided by Verena Jantsch, 1:5000; α-XND-1 (Wagner et al. 2010), 1:2000) overnight at 4°C. Next day, slides were washed and incubated in secondary antibody (α-rabbit 568, 1:2000; α-guinea pig 633, 1:2000) for 2 hours at room temperature in the dark. Slides were mounted in Prolong Gold with DAPI (Life Technologies) and imaged on a Nikon A1r confocal microscope using a 63x Plan Fluor objective with 0.2 µm step sizes. Images were quantified using Volocity 3D software (PerkinElmer). RAD-51 foci were quantified by dividing the region from leptotene (transition zone) through the pachytene/diplotene border into 6 even zones (based on physical distance in µm), and individually scoring RAD-51 foci in each nucleus by scrolling through the images in the Z-dimension. RAD-51 counts were confirmed by examining 3D renderings of nuclei. Graphs represent the averages of three germ lines for each genotype.

2.2.9 Yeast-two- and three-hybrid plasmid construction

A population of predominately adult N2 hermaphrodites were washed thrice in 1x M9 buffer, flash frozen in RNAzol (Invitrogen), and stored at -80°C. RNA was isolated by chloroform extraction and isopropanol precipitation, and resuspended in DEPC water. Purity was verified by spectrophotometry. cDNA synthesis was performed as described previously (Fukushige and Krause 2012). cDNA was diluted 1:15 in deionized water prior to further use.

Yeast-two-hybrid (Y2H) plasmids were created from pGAD-C1 and pGBD-C1. The additional plasmid used in yeast-three-hybrid (Y3H) analysis was created from pRS-ADH-416. pGAD-SWS-1 was synthesized by Genewiz (Genewiz Inc., Gene Synthesis Services, South Plainfield, NJ) using a codon-optimized sequences for expression in *S. cerevisiae*. pGBD-SWS-1 was created by subcloning SWS-1 into pGBD using 5'SmaI and 3'BglII restriction sites. SWIM domain mutants were made by site-directed mutagenesis of the pGAD-SWS-1 plasmid for SWS-1-C133S (SWS-1.C133S.F and SWS-1.C133S.R) and SWS-1-A156T (SWS-1.A156T.F and SWS-1.A156T.R) (Supplemental Table 2). pGAD-RIP-1 and pGAD-RFS-1 were constructed using standard restriction digestion and ligation techniques. First, PCR amplification was used for the coding regions of both *rip-1* and *rfs-1* genes from N2 cDNA using oligonucleotide pairs RIP-1.F/RIP-1.R and RFS-1.F/RFS-1.R, respectively (Supplemental Table 2). *rip-1* was subcloned into pGBD and pRS-ADH-416 using 5'BamHI and 3'SalI restriction sites. Walker B motif mutant was made by site-directed mutagenesis (RIP-1.D131A.F and RIP-1.D131A.R; Supplemental Table 2) of pGBD-RIP-1. *rfs-1* was subcloned into pGBD using 5'EcoRI and 3'BglII restriction sites. All other plasmids were constructed as previously described (Godin et al. 2015).

2.2.10 Yeast-two- and three-hybrid assays

Yeast strains, media, and yeast-two-hybrid assays were performed as previously described (Godin et al. 2015) with the following modifications. For Y2H analysis, pGAD and pGBD plasmids were co-transformed into the PJ69-4A Y2H strain (James et al. 1996) and 1mM histidine competitive inhibitor, 3-Amino-1,2,4-triazole (3AT) was used to detect more stringent Y2H interactions (SC-LEU-TRP-URA+3AT; Sigma Aldrich). For Y3H analysis, pGAD, pGBD, and pRS-ADH-416 (with URA selection marker) plasmids were co-transformed into the PJ69-4A Y2H strain. Yeast

were selected for expression by growth on SC-LEU-TRP (Y2H) or SC-LEU-TRP-URA (Y3H) solid medium. Plates were grown for 2-4 days at 30°C and photographed.

2.3 RESULTS

2.3.1 *sws-1* contributes to germline HR repair

We generated an *sws-1* allele using CRISPR/Cas9 mediated genome engineering (Figure 4A-B, Materials and Methods) (Dickinson et al. 2013; Arribere et al. 2014). Using this approach, we identified a founder strain with a 3 bp deletion/83 bp insertion in exon 2 just downstream of the predicted Cas9 cleavage site, designated as *ea12* (Figure 4A-B and Supplemental Figure 1). Interestingly, the *dpy-10(cn64)* repair oligo donated most of the sequence for the insertion. *sws-1(ea12)* (hereafter referred to as *sws-1*) is predicted to produce the first 19 amino acids of the wild-type SWS-1 protein followed by 32 frameshifted amino acids prior to truncation (Figure 4C). Given the substantial truncation of the protein including the conserved SWIM domain encoded in exon 4 (Figure 4A), and that disruption of the SWIM domain in *S. cerevisiae* Shu2 results in a non-functional protein (Godin et al. 2015), we expect *ea12* to be a null allele. Consistent with the presence of a premature stop codon, which triggers nonsense mediated mRNA decay, we detect approximately 5-fold less *sws-1* mRNA in *sws-1(ea12)* hermaphrodites compared to wild type (Figure 4D).

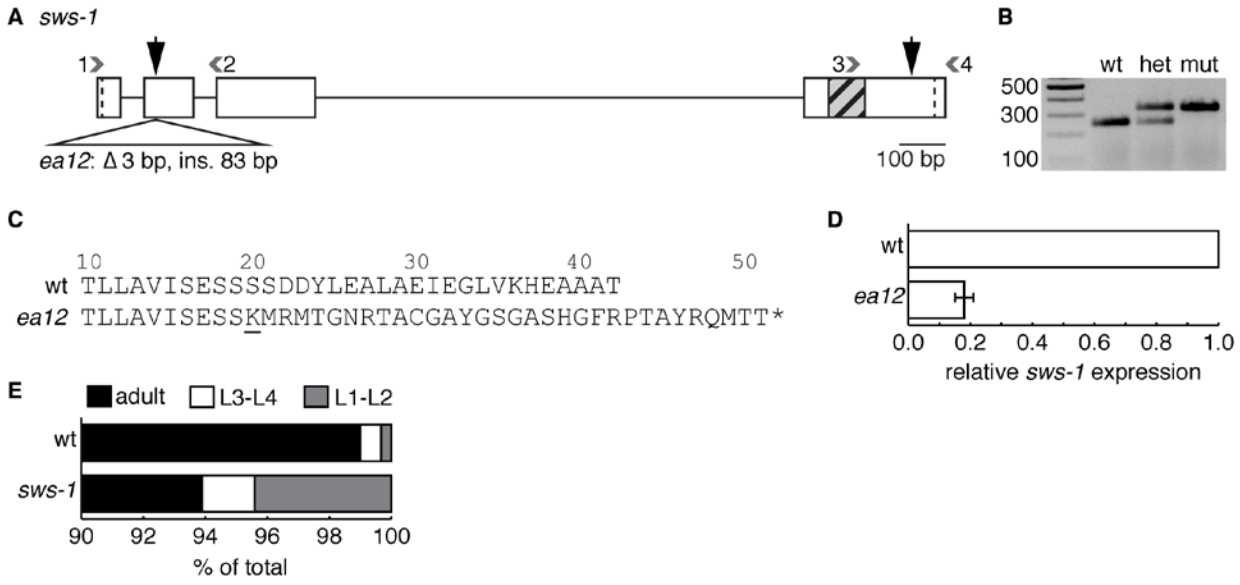

Figure 4. sws-1(ea12) is an insertion/deletion that results in an early stop codon.

Diagram of *sws-1* coding region. Boxes and straight lines represent exons and introns, respectively. Start and stop codons demarcated by dotted lines. Gray hatched box shows DNA encoding the SWIM domain. Large black vertical arrows mark predicted Cas9 cleavage sites for each injected gRNA; small gray numbered arrowheads represent primers used for screening (primer sequences listed in Table 2). *ea12* is a 3 bp deletion/83 bp insertion in exon 2. B. Representative image of *ea12* genotyping using primer combination 1 and 2 as shown in (A). The mutant allele is readily detected as the slower migrating band on a 2% agarose gel indicated in base pairs (bp). C. Predicted protein sequence of exon 2 of wt (top) and *ea12* (bottom) SWS-1. *sws-1(ea12)* is predicted to produce the first 19 amino acids of the wild-type SWS-1 protein followed by 32 frameshifted amino acids prior to truncation (underlined text marks beginning of frameshift). D. Expression of *sws-1* mRNA in wt and *sws-1(ea12)* hermaphrodites. The data are presented as the mean expression of *sws-1* relative to reference gene *rpl-32* ± SEM for 2 biological replicates. E. Developmental progression of wt and *sws-1*. For each genotype, 100 L1s were plated in triplicate and scored 50 hours later as L1-L2, L3-L4, or adult. The results shown are the percent of total worms in each developmental stage. A subset of *sws-1* mutants arrested as L1-L2 larvae ($p<0.001$ vs. wt, Fisher's exact test).

sws-1 homozygotes are viable, although they exhibit decreased survival compared to their wild-type counterparts (p=0.0399, Mann-Whitney) (Table 2, rows B-C). This decrease in survival

is not solely attributable to embryonic lethality, as we found a small but significant percentage of *sws-1* homozygotes fail to develop past the L2 stage ($p<0.001$ vs. wt, Fisher's exact test) (Figure 4E). We also observed a four-fold increase in male frequency compared to their wild-type counterparts ($p=0.0114$, Mann-Whitney) (Table 2, rows B-C). These results suggest that *sws-1* is required for both normal development and X chromosome disjunction.

	Genotype	n	Avg. Brood ± SEM	% lethal ± SEM	% male ± SEM
A	N2	12	232.42 ± 5.97	0.00 ± 0.67	0.07 ± 0.05
B	wild type	6	227.17 ± 9.28	0.56 ± 1.49	0.16 ± 0.16
C	*sws-1*	25	203.84 ± 10.35	8.45 ± 2.05*	0.63 ± 0.08*
D	*rip-1*	6	265.33 ± 8.02	6.33 ± 1.11	1.78 ± 0.72
E	*rip-1;sws-1*	16	268.00 ± 9.72	2.59 ± 0.49	0.87 ± 0.10
F	*rfs-1*	10	212.90 ± 7.59	9.36 ± 1.48	2.22 ± 0.31
G	*rfs-1;sws-1*	13	206.77 ± 9.59	7.84 ± 2.00	1.78 ± 0.26
H	*rfs-1,rip-1*	11	177.00 ± 9.00	8.47± 1.29	2.20 ± 0.31
I	*rfs-1,rip-1;sws-1*	22	164.23 ± 9.97	12.33 ± 1.94	2.43 ± 0.29

Table 2. General characteristics of strains used in this study.

Brood size, lethality, and male frequency were collected as described in Section 2.2.4 (n=number of worms). % lethal ± SEM is normalized to N2 (row A) to account for counting error. Differences between wild type and *sws-1* were assessed by Mann-Whitney (* $p<0.05$); differences in lethality and male frequency among genetic combinations of *sws-1*, *rip-1*, and *rfs-1* were assessed using one-way ANOVA with multiple comparisons (Supplemental Tables 3 and 4).

In other eukaryotes, such as *S. cerevisiae,* the Rad51 paralogs and a SWIM domain-containing protein form the Shu complex and share HR phenotypes (Shor et al. 2005; Mankouri et

al. 2007). Therefore, we asked whether *sws-1* mutants would exhibit similar phenotypes to RAD-51 paralog mutants in worms. In *C. elegans*, loss of the two known RAD-51 paralogs, RFS-1 and RIP-1, confer reduced survival and *him* phenotypes (Ward et al. 2007; Yanowitz 2008; Taylor et al. 2015). Importantly, the reduced survival and *him* phenotypes of *sws-1* resembled those of *rfs-1* and *rip-1* (Table 2, rows D and F), suggesting *sws-1* may have an analogous role in HR repair. To test this, we analyzed the viability and cytology of *helq-1;sws-1* double mutants. *helq-1* encodes a conserved DNA helicase (human HELQ) that functions in HR-mediated repair during replication stress and meiosis (Muzzini et al. 2008; Ward et al. 2010). In meiosis, *helq-1* exhibits synthetic lethality with both *rfs-1* and *rip-1* due to persistent HR intermediates, suggesting *helq-1* and *rfs-1/rip-1* perform overlapping roles in DSB repair (Ward et al. 2010; Taylor et al. 2015). Whereas *helq-1* single mutants exhibited low levels of lethality (~3.6%), *helq-1;sws-1* double mutants displayed ~63% lethality in the F2 generation (Figure 5A). Analysis of diakinesis-stage nuclei in *helq-1;sws-1* hermaphrodites revealed chromatin abnormalities associated with impaired DSB repair – including decondensed chromatin, DNA fragments, and chromosome aggregates – in nearly all nuclei scored (Figure 5B-C). The redundancy with *helq-1* indicates that *sws-1* functions in HR repair and the raises the possibility that *sws-1* functions with the RAD-51 paralogs in this role.

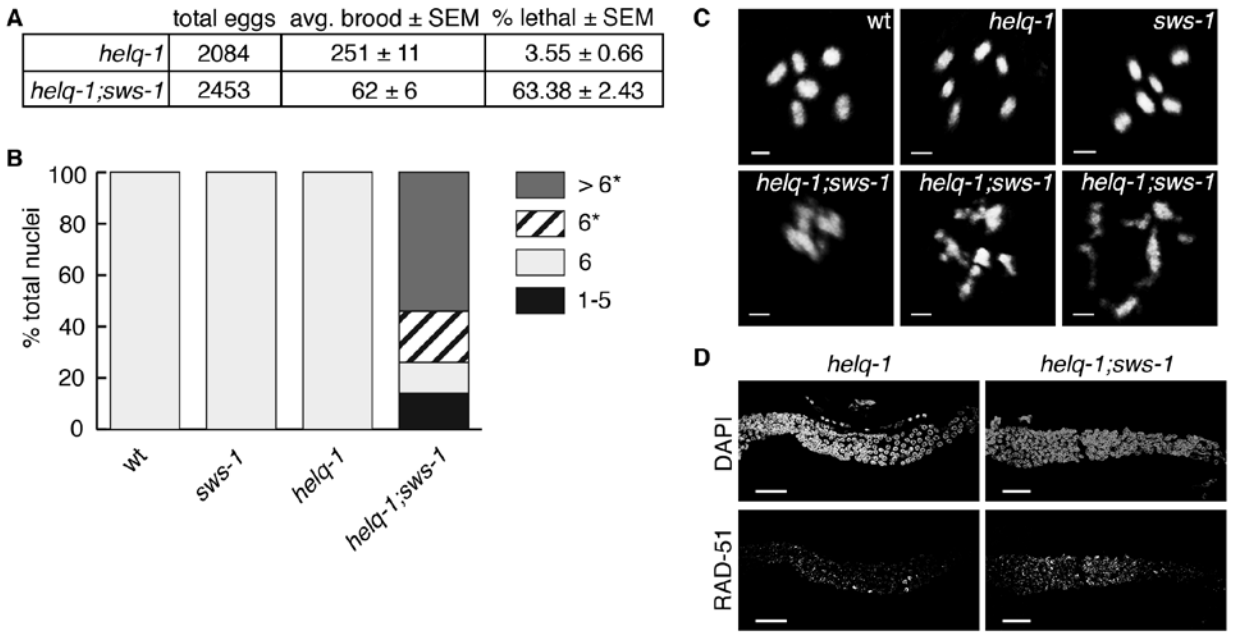

Figure 5. *sws-1* is synthetic lethal with *helq-1*.

A. Brood size and viability of *helq-1* and *helq-1;sws-1* mutants. B. Quantification of the number of DAPI-staining bodies at diakinesis in wt, *sws-1*, *helq-1*, and *helq-1;sws-1* germ lines. Only the -1 oocyte was used for analysis (n=20 for wt and *helq-1*; n=50 for *sws-1* and *helq-1;sws-1*). Asterisk indicates chromosomal abnormalities. C. Representative images of -1 oocytes analyzed as described in (B). Scale bar is 2 µm. D. Representative images of RAD-51 foci from the transition zone (left) to late pachytene (right) in *helq-1* and *helq-1;sws-1* germ lines. Scale bar is 20 µm.

We reasoned that, if *sws-1* is required for HR repair during meiosis, we might observe a change in RAD-51 dynamics compared to wild type. We quantified RAD-51 foci in wild-type and *sws-1* germ lines from the onset of leptotene (transition zone, TZ) through pachytene, the time at which SPO-11-induced DSBs breaks are made and repaired (Figure 6). In wild-type germ lines, RAD-51 foci first appear in the TZ, peak during early-pachytene, then disappear by late-pachytene as HR progresses ((Alpi et al. 2003) and Figure 6 (wt)). Similar to wild type, most *sws-1* nuclei had no RAD-51 foci upon entry to meiosis (Figure 6, zone 1), and RAD-51 foci slowly

accumulated as nuclei progressed into pachytene. However, in later stages of pachytene, a greater proportion of *sws-1* nuclei had 7 or more RAD-51 foci than their wild-type counterparts (Figure 6A, $p<0.05$ for 7-8 foci in zone 3, $p<0.0001$ for 9+ foci in zone 3, $p<0.05$ for 9+ foci in zone 4, Student's t-test). Although this may be explained by increased formation of DSBs, the exclusively late pachytene persistence of RAD-51 foci suggests that *sws-1* nuclei were delayed in removing RAD-51 foci. At the late-pachytene/diplotene border, the proportion of nuclei containing RAD-51 foci was again similar to wild type (Figure 6, zone 6), indicating that all DSBs are eventually repaired.

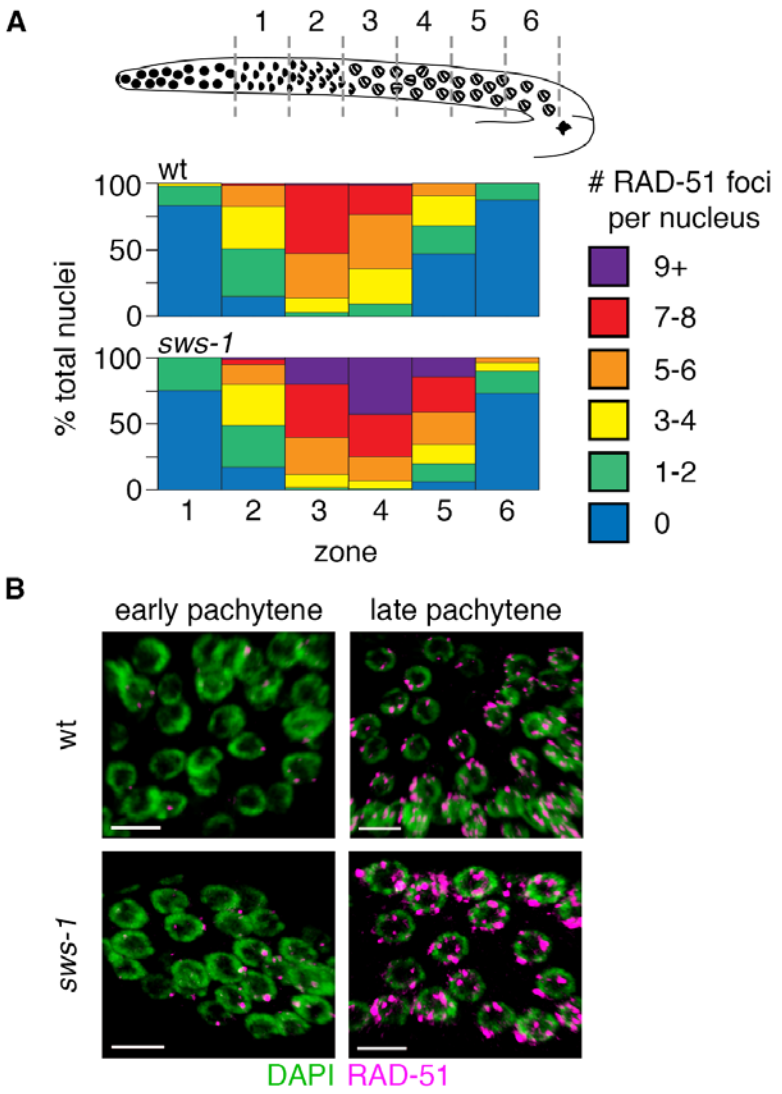

Figure 6. sws-1 alters meiotic RAD-51 dynamics

A. Quantitative analysis of RAD-51 foci during meiotic prophase. Diagram depicts organization of the hermaphrodite germ line with meiotic prophase prior to diplotene divided into six equal-sized zones (gray dashed lines) based on physical distance. The heat map shows percent of total nuclei per zone with the indicated number of RAD-51 foci from wt (top) and *sws-1* (bottom) germ lines (color code, legend). B. Representative images of early and late pachytene nuclei in wt (top) and *sws-1* (bottom) showing higher levels of RAD-51 foci (magenta) on DNA (green). Scale bar is 5 µm.

The observation that RAD-51 foci eventually resolve in *sws-1* germ lines (Figure 5B and 6A) left us curious about the cause of lethality in *sws-1* mutants. *C. elegans* exhibits strong CO control such that only one DSB per chromosome pair becomes an interhomolog CO (Barnes et al. 1995; Meneely et al. 2002; Hillers and Villeneuve 2003). One possible explanation for the lethality, then, is that *sws-1* mutants are deficient in HR repair of DSBs not designated to be repaired as interhomolog COs. To test this hypothesis, we analyzed the competency of *sws-1* mutants for inter-sister HR by examining the cytology of diakinesis-stage oocytes in *syp-3;sws-1* double mutants (Supplemental Figure 2). *syp-3* is a component of the synaptonemal complex (SC) that holds homologs together during meiosis. In the absence of the SC, HR repair between homologous chromosomes cannot occur, and DSBs are repaired from the sister chromatids. Consequently, *syp-3* mutants exhibit an average of 11.6 condensed DAPI-staining bodies at diakinesis (Supplemental Figure 2 and (Smolikov et al. 2007a; Smolikov et al. 2007b)). We did not observe a significant change in either number or morphology of DAPI-staining bodies at diakinesis between *syp-3* and *syp-3;sws-1* mutants (Supplemental Figure 2), suggesting that *sws-1* mutants are competent for intersister HR.

unc-58(e665) BACKGROUND	TRIAL	PLATES WITH REVERTANTS/TOTAL PLATES	MUTATION FREQUENCY ± SEM
wild type	1	0/40	$7.06 \times 10^{-7} \pm 7.06 \times 10^{-7}$
	2	1/38	
	3	0/39	
	4	0/36	
sws-1	1	2/41	$2.00 \times 10^{-6} \pm 1.26 \times 10^{-6}$
	2	0/40	
	3	0/37	
	4	1/39	

Table 3. Spontaneous revertant frequencies of unc-58(e665).

***Unc-58* reversion assay carried out as described in Section 2.2.6. Mutation frequency was calculated by dividing the proportion of plates with reversion events by the number of haploid genomes per plate. The data are presented as the mean mutation frequency ± SEM for four trials.**

A second possibility is that *sws-1* mutants have an increased reliance on error-prone DSB repair pathways. If this is the case, *sws-1* might be expected to show an increase in spontaneous mutation rate, which can be assessed by the reversion to wild-type movement of *unc-58(e665)*, a missense gain-of-function mutation that confers paralysis (Harris et al. 2006). Although not significantly different from controls, *sws-1;unc-58* mutants exhibited a trend toward increased mutation rate with an approximately 3-fold increase in reversion to non-Unc offspring compared to *unc-58* alone (Table 3, p=0.4058, Student's t-test). These observations are consistent with what has been reported for *rfs-1* mutants (Yanowitz 2008), and may suggest that HR factors are not critical for correction of mismatches during DNA replication. However, HR factors – including

rfs-1 – have been shown to be important for maintaining the integrity of poly G/C tracts in the absence of the helicase *dog-1*, which prevents the formation of deletions in G/C-rich DNA by unwinding secondary DNA structures that hinder replication fork progression (Cheung et al. 2002; Youds et al. 2006; Ward et al. 2007). We observed increased deletion frequency in *dog-1;sws-1* mutants compared to *dog-1* alone (Figure 7, p=0.0386, Fisher's exact test), suggesting increased reliance on mutagenic repair pathways in the absence of *sws-1*. Collectively, these results suggest that *sws-1* functions in HR, and is important for maintaining genome integrity during DNA replication.

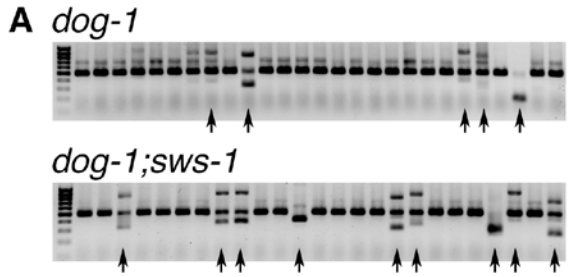

B

	n	# animals with deletions
wt	95	0
sws-1	96	1
dog-1	191	35
dog-1;sws-1	192	53*

Figure 7. sws-1 maintains G/C tract stability in the absence of dog-1.

A. Amplification of the *vab-1* G/C tract in *dog-1* (top) and *dog-1;sws-1* (bottom) mutants. Deletions in the amplified region are observed as faster-migrating bands on a 1.5% agarose gel (black arrows). B. Quantification of deletion frequency in wt, *sws-1*, *dog-1*, and *dog-1;sws-1* mutants. Number of individual animals with one or more deletions in the *vab-1* G/C tract as described in (A) are indicated. * p<0.05, Fisher's exact test.

2.3.2 *sws-1* mutants are sensitive to genotoxins that induce HR substrates

In *C. elegans*, both *rfs-1* and *rip-1* mutants display sensitivity to DSB-inducing agents, especially those that obstruct replication fork progression (Ward et al. 2007; Taylor et al. 2015). To further investigate the role of *sws-1* in HR repair, we exposed hermaphrodites to a subset of genotoxins that create HR repair substrates: IR, MMS, hydroxyurea (HU), or camptothecin (CPT). The survival of the offspring laid post-exposure reflects the repair capacity in the hermaphrodite germ line. As shown in Figure 8, we observed a modest, but statistically significant, increased sensitivity of *sws-1* mutants to IR, MMS, and HU compared to their wild-type counterparts (Figure 8A-C). By contrast, *sws-1* mutants were dramatically more sensitive than wild type to CPT (Figure 8D). The reduced progeny survival following CPT treatment was accompanied by a 2-fold increase in apoptotic germline nuclei (Supplemental Figure 3), indicating that *sws-1* meiotic nuclei were unable to repair CPT-induced DSBs. This increased sensitivity to CPT may suggest that *sws-1* plays a more prominent role in the repair of a specific subset of DSB-inducing lesions.

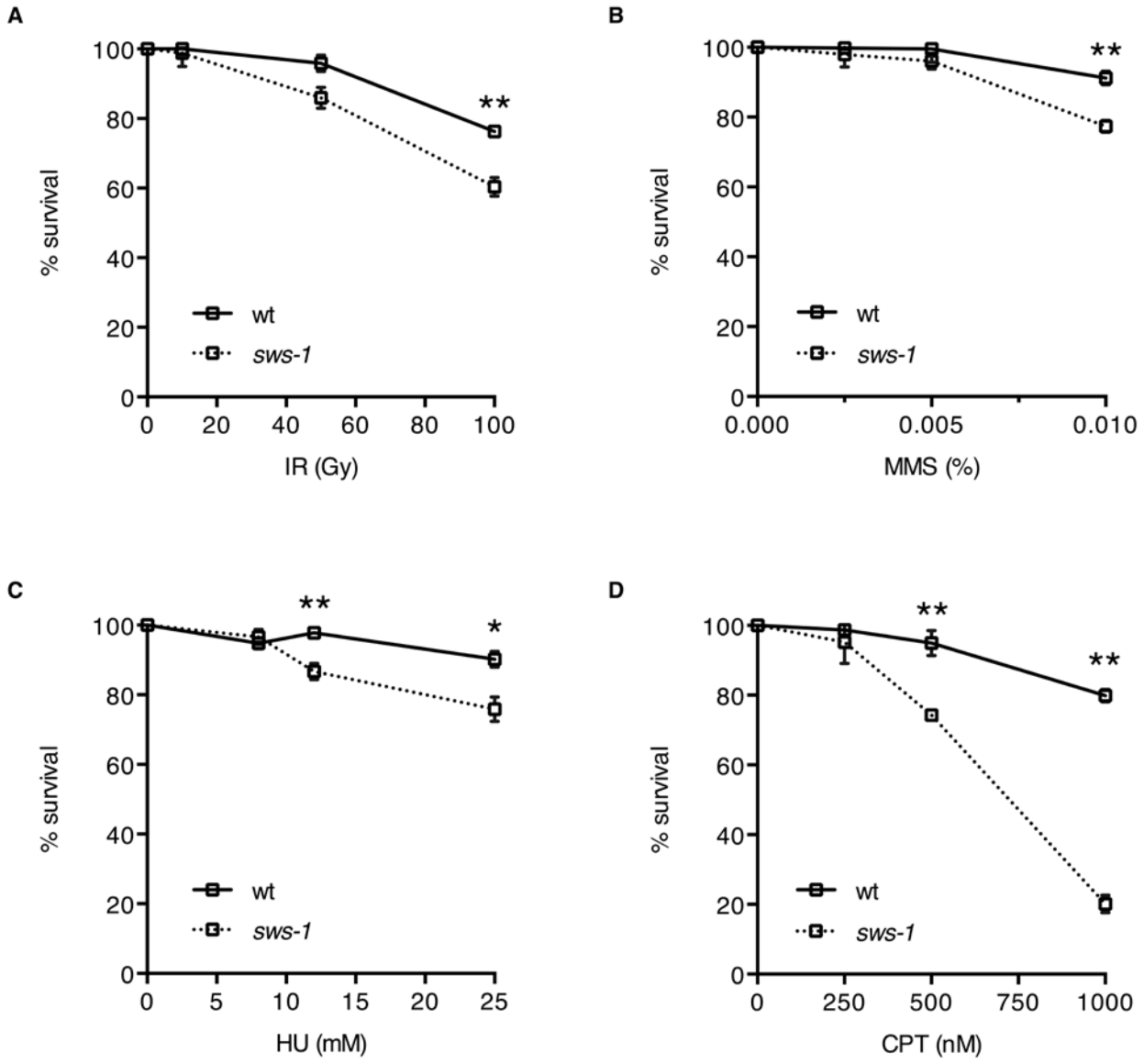

Figure 8. sws-1 mutants are sensitive to genotoxins that induce HR repair

Progeny survival of hermaphrodites treated with IR (A), MMS (B), HU (C), or CPT (D) as described in Materials and Methods. Survival was calculated as the number of adult progeny divided by the number of eggs and L1s relative to untreated worms ± SEM from at least 22 adults over two trials. Statistical analysis was performed using Student's t-test (* $p<0.01$, ** $p<0.0001$).

The *S. cerevisiae* Shu complex has been shown *in vitro* to promote Rad51-mediated repair in concert with Rad52 and the Rad55-Rad57 heterodimer by stimulating Rad51 loading onto

ssDNA and stabilizing it thereafter (Gaines et al. 2015). Further studies in *S. cerevisiae* suggest that the Shu complex promotes Rad51 assembly on meiotic chromosomes *in vivo* based on a reduced number of Rad51 foci in Shu complex mutants (Sasanuma et al. 2013). In *C. elegans*, the RAD-51 paralogs, *rfs-1* and *rip-1*, stabilize RAD-51 foci in response to cisplatin, nitrogen mustard, and UV (Ward et al. 2007; Taylor et al. 2015). We reasoned that the increased sensitivity of *sws-1* mutants to CPT may stem from a failure to stabilize RAD-51 presynaptic filaments at damage sites. To test this hypothesis, we visualized RAD-51 foci by immunofluorescence (Figure 9). In wild-type and *sws-1* germline nuclei under normal conditions, RAD-51 foci were rarely – if at all – seen in the mitotic zone (Figure 9A). In response to CPT treatment, RAD-51 foci were readily visible throughout the mitotic zone nuclei in wild-type germ lines, indicative of ongoing HR repair (compare Figure 9A and 9C). In contrast, we observed a striking absence of RAD-51 foci in the mitotic zone of *sws-1* germ lines following CPT exposure (compare Figure 9B and 9D). These results suggest that the sensitivity of *sws-1* mutants to CPT may be due to a failure to undergo HR repair.

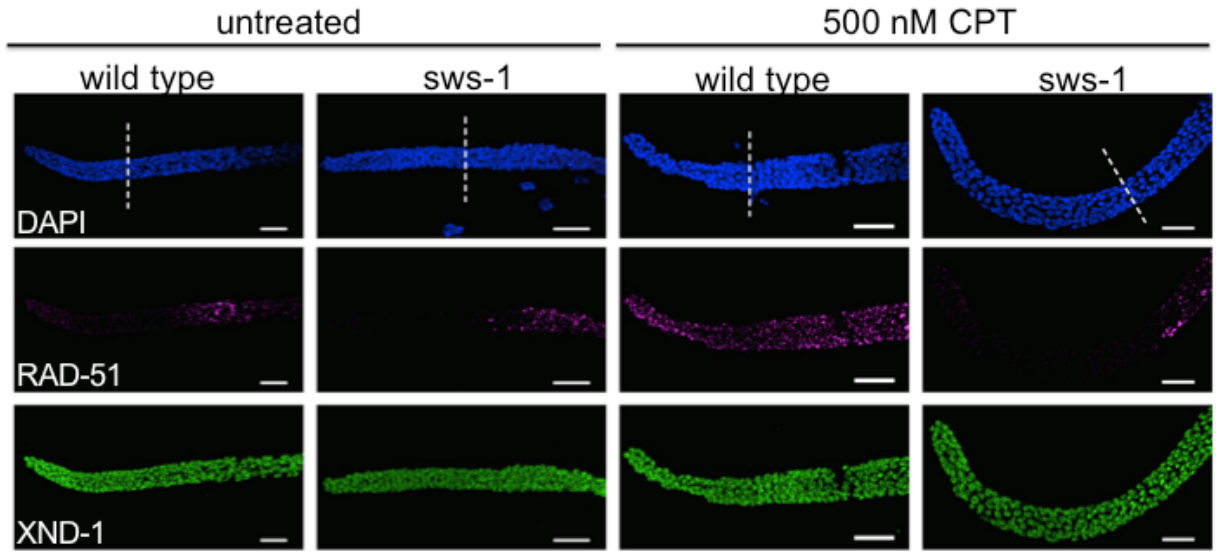

Figure 9. sws-1 fails to form mitotic RAD-51 foci following CPT treatment.

Immunofluorescence of RAD-51 with or without CPT exposure in germ lines of wt (A, C) and *sws-1* (B, D) hermaphrodites. Treated worms were exposed to 500 nM CPT as described in Materials and Methods and dissected at the end of the recovery period. Immunostaining conditions described in Materials and Methods. White dashed line marks beginning of transition zone. XND-1 immunofluorescence serves as a staining control. Scale bar is 20 µm.

2.3.3 RIP-1 interacts with SWS-1 by yeast-two-hybrid and bridges an interaction between SWS-1 and RFS-1 by yeast-three-hybrid

The HR repair defects of *sws-1* mutants, including synthetic lethality with *helq-1*, resemble those of RAD-51 paralogs *rfs-1* and *rip-1* (Ward et al. 2007; Ward et al. 2010; Taylor et al. 2015). To further explore if these factors act in the same pathway, we compared the lethality and male frequency of double and triple mutant combinations of *sws-1*, *rfs-1*, and *rip-1* (Table 2, rows C-I). We observed that the incidence of lethality was statistically unchanged between the *rfs-1,rip-1;sws-1* triple mutant and any of the single mutants (ANOVA, $p>0.05$). Curiously, the lethality of *rip-1;sws-1* double mutants exhibited reduced lethality compared to the *rfs-1,rip-1;sws-1* triple

mutant ($p<0.05$, Tukey's test, Supplemental Table 3), although there was no statistical difference in lethality between *rip-1;sws-1* and either *rfs-1;sws-1* or *rfs-1,rip-1* double mutants. Furthermore, the lethality of the *rfs-1,rip-1;sws-1* triple mutant is well below the additive value predicted from each single mutant, suggesting the cause of lethality is shared. The male frequency of *rfs-1,rip-1;sws-1* triple mutants was unchanged from either *rfs-1* or *rip-1* single mutants, but significantly increased compared to *sws-1* single mutants ($p<0.05$, Tukey's test, Supplemental Table 4). This result is consistent with the observation in yeast that *psy3* or *csm2* mutants exhibit more severe phenotypes compared to *shu1* or *shu2* mutants (Sasanuma et al. 2013; Godin et al. 2015) and highlights the importance of the RAD-51 paralogs in Shu complex function.

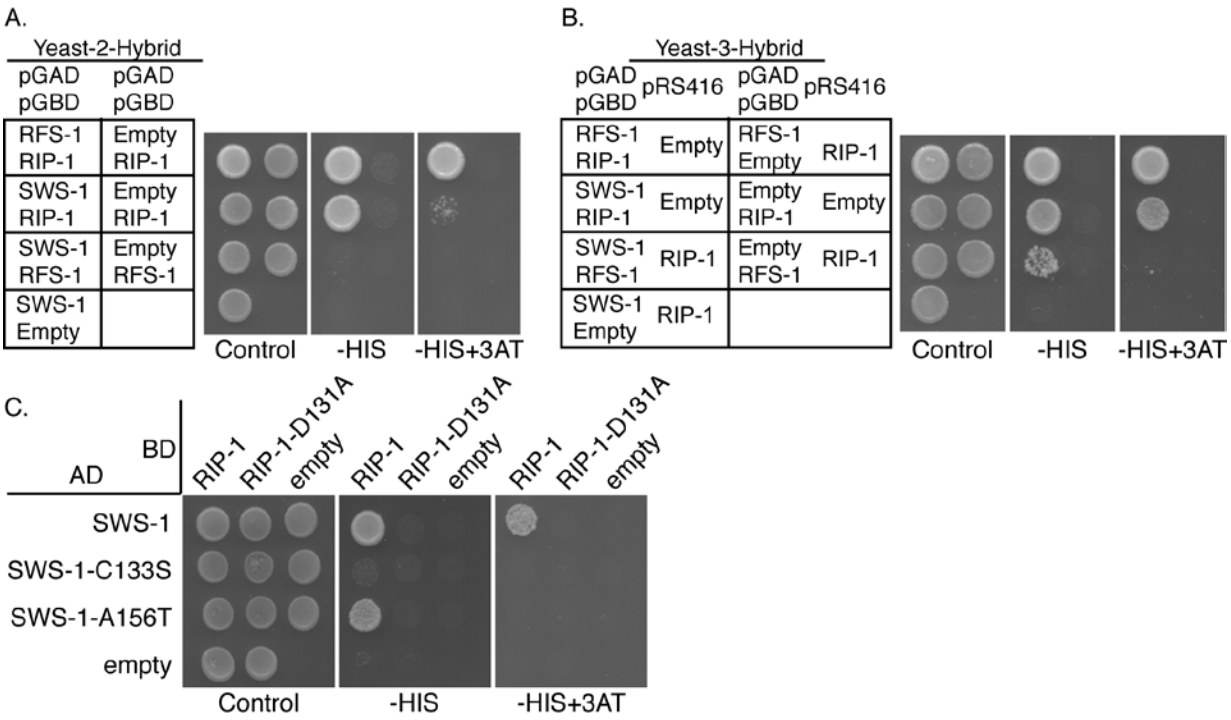

Figure 10. RIP-1 interacts with SWS-1 and bridges an interaction between SWS-1 and RFS-1.

Y2H (A, C) and Y3H (B) panels from left to right show plating controls on SC-LEU-TRP or SC-LEU-TRP-URA respectively with the additional dropout of histidine (-HIS) and histidine with 3-amino-1,2,4-triazole (-HIS+3AT) indicating interaction a Y2H or Y3H interaction. Within each panel, the left column shows potential interactions between two proteins and the right column shows an empty vector control. RIP-1 interacts with both SWS-1 and RFS-1. SWS-1 and RFS-1 do not interact (A). With constitutive expression of RIP-1, SWS-1 and RFS-1 promote growth on SC-LEU-TRP-URA-HIS indicating a Y3H interaction (row 3, B). Two SWIM domain mutations were created in SWS-1, C133S and A156T. SWS-1-C133S disrupts interaction with RIP-1 (row 2, C). SWS-1-A156T decreases interaction with RIP-1 on –HIS+3AT (row 3, C). A Walker B motif mutation was introduced into RIP-1 that disrupts interaction with SWS-1, SWS-1-C133S, and SWS-1-A146T (column 2, C).

In yeast and human cells, Shu2/SWS1 is found in complexes with the Rad51 paralogs Csm2-Psy3 and SWSAP1, respectively (Martin et al. 2006; Liu et al. 2011; Godin et al. 2013; Godin et al. 2015). To determine if SWS-1 similarly interacts with the known RAD-51 paralogs

in *C. elegans*, we performed yeast-two-hybrid (Y2H) analysis, fusing SWS-1, RFS-1, or RIP-1 to the GAL4 activation domain (pGAD) and the GAL4 DNA-binding domain (pGBD). By Y2H, SWS-1 interacted directly with RIP-1 but not RFS-1 in both configurations (Figure 10A, Supplemental Figure 4). Since yeast Shu2 interacts with the other Shu complex members Shu1 and Psy3, and human SWS1 directly interacts with SWSAP1, we next examined if worm SWS-1 could interact with the any other member of the yeast Shu complex or with human SWSAP1 by Y2H. We were unable to detect a cross-species Y2H interaction between worm SWS-1 and the other yeast or human Shu complex members (Supplemental Figure 5 and data not shown). These data make it unlikely that the yeast Shu complex members are bridging an interaction between SWS-1 and RIP-1. Rather, these data support the conclusion that SWS-1 and RIP-1 directly interact and comprise core components of the worm Shu complex.

Based on the known Y2H interaction between RIP-1 and RFS-1 ((Taylor et al. 2015) and Figure 10A), we hypothesized that RIP-1 may bridge an interaction between SWS-1 and RFS-1. To test this possibility, we performed a yeast-three-hybrid (Y3H) assay in which SWS-1 was again expressed as a fusion with the GAL4 activation domain and RFS-1 as a fusion with the GAL4 DNA-binding domain, but in this case a third, untagged vector expressing RIP-1 or an empty vector was co-expressed (pRS416-RIP-1 or pRS416, respectively) (Figure 10B). By Y3H, we find that in the presence of RIP-1, but not the empty vector control, SWS-1 and RFS-1 confers growth on the Y3H medium suggesting that these proteins are now able to interact (Figure 10B). Together, these studies suggest that RIP-1 facilitates ternary complex formation with SWS-1 and RFS-1.

2.3.4 The SWIM domain in SWS-1 and the Walker B motif in RIP-1 are important for their yeast-two-hybrid interaction

We originally identified SWS-1 because of its invariant SWIM domain, a zinc-finger binding-like motif ($CxCx_nCxHxxA$, n being 6-25 residues), which we found to be important for Sws1 protein family Y2H interactions with the Rad51 paralogs in yeast and humans (Godin et al. 2015). Therefore, we wondered whether the SWIM domain of SWS-1 would be important for its interaction with RIP-1. We mutated the second cysteine of the SWIM domain to serine (*sws-1-C133S*) in the Y2H expression vector and retested the functionality of this protein to support growth on SC-HIS medium or the more stringent SC-HIS+3AT medium, where 3AT is a competitive inhibitor of histidine. As shown in Figure 10, *sws-1-C133S* abrogated the Y2H interaction between SWS-1 and RIP-1 (Figure 10C). Previously we identified a cancer-associated mutation in human SWS1 on the COSMIC database where the invariant alanine was mutated to a threonine (Godin et al. 2015). Therefore, we made the analogous mutation in SWS-1 and found that *sws-1-A156T* maintains its interaction with RIP-1 at lower stringencies but exhibited reduced Y2H interaction upon more stringent conditions (Figure 10C; plating on SC–HIS medium vs. SC–HIS+3AT). Together these results suggest that the SWIM domain in SWS-1 is important for its interaction with RIP-1.

RIP-1 is defined as a RAD51 paralog by the presence of a conserved Walker B-like motif. Therefore, we next asked whether the Walker B motif is important for its interaction with SWS-1. By Y2H, expression of a RIP-1 Walker B mutant, *rip-1-D131A*, disrupts interaction with both wild-type SWS-1 and the SWS-1 SWIM domain mutants (C133S and A156T) (Figure 10C). Interestingly, *rip-1-D131A* was found to maintain its Y2H interaction with RFS-1 under the same

conditions (Taylor et al. 2015). Therefore, RIP-1 interacts with SWS-1 through its Walker-B-like motif.

2.4 DISCUSSION

2.4.1 SWS-1 functions in HR with RFS-1 and RIP-1

C. elegans sws-1 was identified as a putative Shu2 homolog based on the presence of a conserved SWIM domain, although no functional analysis was performed (Godin et al. 2015). Using a nonsense allele of *sws-1* (Figure 4), we show that *sws-1* is involved in HR in the germ line. *sws-1* mutants exhibit mild reduction in viability and increased male frequency compared to wild type (Table 2). The mildness of these *sws-1* phenotypes belies its importance when worms are further compromised by loss of *helq-1*. *helq-1; sws-1* double mutants exhibit synthetic lethality and diakinesis oocytes with severe chromosomal abnormalities (Figure 5). These results indicate functional redundancy of *sws-1* and *helq-1* for meiotic HR repair. Impaired meiotic HR functions become obvious in *sws-1* single mutants based on the sensitivity to DSB-inducing agents, and perhaps most significantly, increased accumulation of RAD-51 in mid-late pachytene nuclei.

The clear substrate preference for SWS-1 at replication forks implicates a mitotic role: first, *sws-1* is needed to maintain poly G/C tract stability in the absence of *dog-1* (Figure 7), which is predicted to function during DNA replication (Youds et al. 2006); second, *sws-1* mutants are most sensitive to CPT, which induces DSBs by blocking replication forks (Figure 8); third, RAD-51 foci were notably absent in *sws-1* mitotic nuclei following CPT treatment (Figure 9). However, the timing of our genotoxin exposure assays is consistent with assessing repair capacity of meiotic

nuclei (Jaramillo-Lambert et al. 2007; Kessler and Yanowitz 2014). Consistent with this, we observed a 2- and 4-fold increase in germline apoptosis following treatment with CPT in *sws-1* and *rfs-1* hermaphrodites, respectively (Supplemental Figure 3). Collectively, these results suggest that *sws-1* promotes HR by stabilizing RAD-51 at specific HR substrates in both mitosis and meiosis, as has been shown for *rfs-1* and *rip-1* (Ward et al. 2007; Taylor et al. 2015). Using this cell biological approach, we cannot distinguish if SWS-1 promotes RAD-51 loading or stabilizes RAD-51 after it has loaded onto ssDNA, as previous work with RFS-1 and RIP-1 has suggested (Taylor et al. 2015). *In vitro* analysis could similarly measure if the Shu complex promotes RAD-51 loading by co-incubating the Shu complex and RAD-51 with RPA-coated ssDNA and measuring filament formation as has been observed for the yeast Shu complex (Gaines et al. 2015). To determine if the Shu complex protects RAD-51 filaments from antirecombinases, *in vitro* studies could challenge RAD-51 coated ssDNA with DNaseI with or without the Shu complex to compare stability of the RAD-51 filament (Taylor et al. 2015).

The similar phenotypes of *sws-1* and the RAD-51 paralogs, *rfs-1* and *rip-1*, (Ward et al. 2007; Ward et al. 2010; Taylor et al. 2015) prompted us to examine whether these genes function together in HR repair. The lack of additive lethality among double and triple mutant combinations strongly suggests that they function together (Table 2 and Supplemental Table 3). In support of this notion, we observe a direct interaction between SWS-1 with RIP-1 and RFS-1 by Y2H (Figure 10). Taken together, our results suggest that SWS-1, RIP-1, and RFS-1 form a conserved complex to promote RAD-51-dependent HR (Figure 11). We note that *rfs-1* mutants have a higher male frequency than *sws-1*, which likely contributes to the increased male frequency in the triple mutants (Table 2 and Supplemental Table 4). While we cannot rule out that *rfs-1* may have additional roles outside of the Shu complex, it may be that mutation of *rfs-1* may have more severe

consequences than other members of the complex because it directly mediates an interaction with RAD-51 (Ward et al. 2010; Taylor et al. 2015).

2.4.2 The *C. elegans* Shu complex is composed of SWS-1, RIP-1, and RFS-1

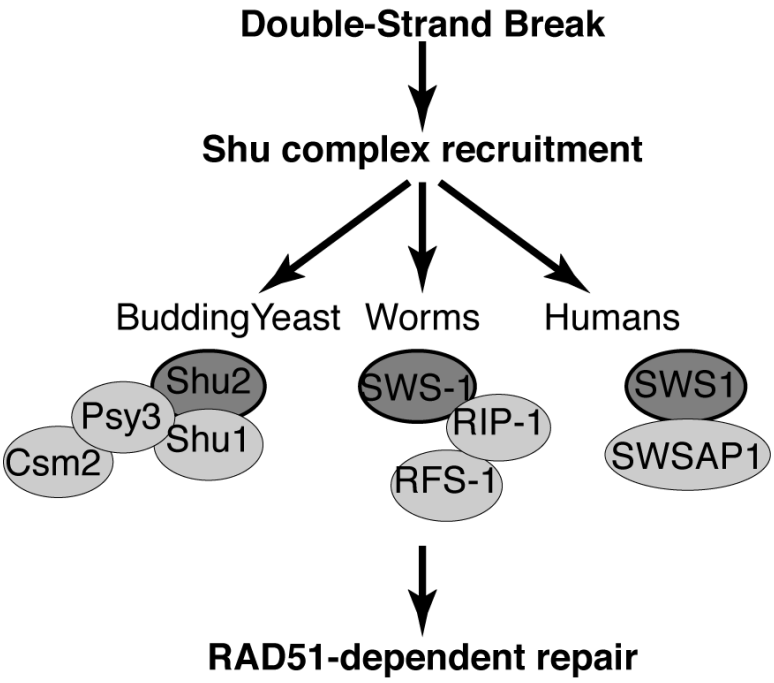

Figure 11. Model of Shu complex function in promoting Rad51-mediated repair.

After a double-strand break occurs, the Shu complex in budding yeast, worms, or humans, is recruited to sites of DNA damage where it subsequently promotes RAD51-dependent repair. In budding yeast, the Shu complex is composed of a SWIM domain containing protein, Shu2, the Rad51 paralogs Csm2-Psy3, and Shu1. In humans the exact components of the Shu complex are not completely known but consist of the SWIM domain containing protein, SWS1, and its associated RAD51 paralog, SWSAP1. Here we define the worm Shu complex to consist of SWS-1 and the RAD-51 paralogs, RFS-1 and RIP-1, where SWS-1 directly interacts with RIP-1 through the SWIM domain of SWS-1 and the Walker-B motif of RIP-1. RIP-1 bridges an interaction between SWS-1 and RFS-1 suggesting that it can interact with both proteins simultaneously. SWS1 family members are depicted by dark gray circles with a black outline and the other Shu complex components by light gray circles.

Budding and fission yeast as well as the human Shu complexes have been defined as consisting of an SWS1 protein family member and its associated RAD51 paralog interacting partners (Shor et al. 2005; Martin et al. 2006; Liu et al. 2011). Using this definition, we propose that *C. elegans* contains a Shu complex comprised of SWS-1, RIP-1, and RFS-1 (Figure 11). Previously, we have shown that yeast Shu2 is most closely related to SWS-1 in *C. elegans* using sequence homology to the conserved SWIM domain*;* however, it remained unknown whether this conservation was limited to its sequence or if it extended to SWS-1 protein function (Godin et al. 2015). Given the embryonic lethality observed in the knockout models of the mouse RAD51 paralogs (Deans et al. 2000; Thacker 2005; Kuznetsov et al. 2009; Suwaki et al. 2011), our work in *C. elegans* provides a unique opportunity to study Shu complex disruption in a multicellular organism. Here we demonstrate the first evidence for a functional worm Shu complex consisting of SWS-1 and RIP-1, which likely directly interact through the SWIM domain of SWS-1 and the Walker B motif of RIP-1. Note that it is possible that the *sws-1* SWIM domain mutants may not be properly folded or expressed. Additionally, RIP-1 bridges an interaction between SWS-1 and RFS-1 (Figures 10 and 11). Unlike yeast and humans, only two RAD-51 paralogs have been identified in worms (Ward et al. 2007; Taylor et al. 2015). One possibility is that the worm RAD-51 paralogs, RFS-1 and RIP-1, are sufficient to perform all the various functions of the RAD-51 paralogs described in other eukaryotes. Alternatively, additional RAD-51 paralogs have yet to be identified in *C. elegans*. Importantly, the budding yeast Csm2 and Psy3 proteins were only shown to be Rad51 paralogs upon crystallization as their sequence conservation to Rad51 is extremely poor (She et al. 2012; Tao et al. 2012; Sasanuma et al. 2013). Further, the poor sequence conservation of Rad51 paralogs between species and our inability to complement yeast harboring disruptions of the Shu complex genes with worm proteins also makes direct comparisons between the individual Rad51

paralogs challenging (data not shown). Therefore, further studies will be important for determining whether additional RAD-51 paralogs exist in worms and which RAD-51 paralogs correlate with the functions attributed to the equivalent human and yeast proteins.

2.4.3 Substrate specificity of the worm Shu complex

We find that *sws-1* mutants are most sensitive to the DNA damaging agent camptothecin (Figure 8). In contrast, budding yeast containing a deletion of the *sws-1* ortholog, *shu2*Δ, exhibits a more pronounced sensitivity to MMS (Shor et al. 2005; Mankouri et al. 2007; Ball et al. 2009). Therefore, it is possible that the different DNA damage sensitivities observed for the Shu complex members relative to other more general HR factors may indicate a specialized role of SWS-1 in repair of specific types of DNA lesions. Camptothecin is a topoisomerase I inhibitor which would specifically become covalently modified on the ssDNA end and would therefore be converted into a DSB upon replication fork progression. It is intriguing to speculate that perhaps the specific sensitivity of *sws-1* worms to camptothecin provides a framework for determining the types of DNA structures created during meiosis. It is possible that SWS-1 performs different functions at different HR substrates as SWS-1 was needed for resolution of RAD-51 foci during meiotic HR and needed to stabilize RAD-51 in CPT-treated mitotic cells. Using mutants of antirecombinase, *rtel-1*, *sws-1* mutants may suppress hyper-recombination of *rtel-1* mutants if SWS-1 activity is upstream of RAD-51 filament activity. Studies in yeast have shown that the Shu complex is important for driving homolog bias during meiosis, where the homologous chromosome is made the preferred partner for repair over the sister chromatid (Hong and Kim 2013; Hong et al. 2013; Sasanuma et al. 2013). Therefore, further studies to delineate the specific lesions that the worm Shu complex are needed to resolve will shed light on their function during both mitotic and meiotic

repair. The *C. elegans* Shu complex may have a specialized role for responding to ICLs. As replication forks encountering ICLs would be blocked causing replication-associated damage, these substrates share similarities to MMS-induced lesions at replication forks for which the budding yeast Shu complex shows specificity. Importantly, our work on the worm Shu complex provides a new way in which to study disruption in the Shu complex in the context of a multicellular organism that will help us to determine why mutations in the human RAD51 paralogs are associated with cancer predisposition and in some cases Fanconi anemia.

2.5 ACKNOWLEDGEMENTS

A modified version of this paper has been accepted at *Genetics*:

*McClendon TB, *** Sullivan MR**, Bernstein KA, and Yanowitz JL (2016) Promotion of Homologous Recombination by SWS-1 in Complex with RAD-51 *Caenorhabditis elegans*. *Genetics*, 203(1):133-145.

*Denotes equally contributing authors

Fig 4A,B,C,E (TBM, JLY); Fig 4D (MRS); Supp Fig 1 (TBM, JLY); Supp Fig 2 (TBM); Table 2 (TBM); Fig 5 (TBM, JLY); Fig 6 (TBM, JLY); Table 3 (TBM, MRS); Fig 7 (TBM); Fig 8 (TBM, MRS); Fig 9 (TBM, MRS, JLY); Supp Fig 3 (TBM, MRS, JLY); Fig 10A,B,C (MRS); Supp Fig 4 (MRS); Supp Fig 5 (MRS)

We are grateful to Tyler Machovina for performing injections and initial screening. We thank Simon Boulton, Ann Rose, and Sarit Smolikov for strains, Verena Jantsch for the anti-RAD-51 antibody, and Francis Gandhi for guidance with qPCR. Some strains were provided by the

Caenorhabditis Genetics Center, which is funded by NIH Office of Research Infrastructure Programs (P40 OD010440). Sequencing of CRISPR constructs and of *sws-1* was performed in the Genomics Research Core at the University of Pittsburgh. This work was supported by the National Institutes of Health grants to K.A.B. (ES024872) and J.L.Y. (GM1040070).

3.0 UNCOVERING HOW *RAD51C* MUTATIONS CONTRIBUTE TO CANCER PREDISPOSITION

Homologous recombination (HR) is a major double strand break (DSB) repair pathway critical for maintaining genome stability. Defects in HR proteins are frequently associated with diseases characterized by genomic instability including cancers and Fanconi anemia. RAD51 regulatory proteins are particularly critical during HR repair and include the RAD51 paralogs. This family of RAD51 regulators includes RAD51B, RAD51C, RAD51D, XRRC2, XRCC3, and SWSAP1 that assemble into subcomplexes *in vivo*. RAD51C has particular clinical relevance as mutations in RAD51C have been found in familial breast and ovarian cancers. However, the specific role of RAD51C has remained elusive as mouse models and non-tumorigenic knockout cell lines are inviable. Therefore, we have identified RAD51C point mutations from breast and ovarian cancer patients to understand how these mutations impair HR and contribute to genomic instability phenotypes. We have found that mutations in RAD51C can impair interactions with binding partners, RAD51B, RAD51D, and XRCC3. Using yeast-two/three-hybrid and co-immunoprecipitation strategies, we identified RAD51C mutations that disrupt RAD51 paralog subcomplexes, which are critical for RAD51C protein stability and for efficient repair. We found that mutations around the Walker A motif were particularly critical for maintaining protein-protein interactions. To investigate these RAD51C mutants in a relevant cell model, we utilized a RAD51C conditional knockout breast epithelial cell line. We complemented these cells with

RAD51C mutants to understand how disruption of RAD51 paralog subcomplexes impacts repair of DSBs. We measured complementation of viability and repair proficiency at I-SceI-induced DSBs through the DR-GFP reporter construct. We found that mutations in RAD51C variably impact repair, and that mutations around the Walker A motif that were important for maintain protein-protein interactions were also important for maintaining HR proficiency. Ultimately, identifying specific RAD51C mutations that disrupt efficient repair informs us clinically of which tumors could respond best to chemotherapeutic therapies that rely on HR-deficiency.

3.1 INTRODUCTION

Faithful repair of DNA double-strand breaks (DSBs) is essential to preserving genome stability. Homologous recombination (HR) is a high fidelity DSB repair pathway used to repair both endogenous and exogenous sources of DNA damage. Unlike error-prone alternatives, HR utilizes a homologous template, such as the sister chromatid or homologous chromosome to restore the information around the DSB site (Jasin and Rothstein 2013). A central HR step is RAD51 filament formation as RAD51 filaments perform the homology search and strand invasion steps that define this repair process (Godin et al. 2016a). Mutations in HR genes are associated with many cancers but are especially prevalent in breast and ovarian cancers (Pennington et al. 2014; Tung et al. 2016). In fact, HR gene mutations occur in 31% of ovarian tumors including both germline and somatic mutations (Pennington et al. 2014). Many of these HR gene mutations occur in RAD51 regulators including *BRCA2*, *PALB2*, *RAD51C*, and *RAD51D* (Pennington et al. 2014; Tung et al. 2016).

HR genes, *BRCA1* and *BRCA2*, are commonly screened for in breast and ovarian tumors and targeted for precision therapy as they are the two most frequently mutated HR genes found in these patients (Pennington et al. 2014; Maxwell et al. 2017). Emerging studies show that mutations in many of the other HR genes (such was *RAD51C*, *RAD51D*, *PALB2*, *BARD1*, *BRIP1*) could also be targeted by similar therapies as *BRCA1* and *BRCA2* deficient tumors (Ollier et al. 2015; Kondrashova et al. 2017). However, many of these genes such as *RAD51C* and *RAD51D* are much less well characterized and thus mutations in these genes are typically classified as variants of unknown significance (Pennington et al, 2014; Kondrashova et al, 2017; Baldock et al. in revision). To determine if specific mutations in these HR genes will be good candidates for HR-deficient targeted therapies, we aimed to understand the consequences of individual mutations. In this study, we focused on cancer-associated mutations and single nucleotide polymorphisms (SNPs) found in the RAD51C gene.

Six RAD51 paralogs have been identified in humans, RAD51B, RAD51C, RAD51D, XRCC2, XRCC3, and SWSAP1. RAD51C and RAD51D are two RAD51 paralogs that have been specifically linked to breast and ovarian cancer predisposition. These proteins share sequence similarity to RAD51 itself and are thought to regulate its activity during HR (reviewed in Sullivan and Bernstein 2018). Walker A and B motifs are common to the RAD51 paralogs and these regions have the most sequence similarity to RAD51 (Thacker J, 1999; Cartwright et al, 1998; Thompson and Schild, 1999; Lin et al, 2006). Walker A and B motifs are used for ATP binding and could be used for ATP hydrolysis in mediating RAD51 filament activity (Sigurdsson et al, 2001; Braybrooke et al, 2000). While precise functions of the RAD51 paralogs remain unknown, their activity is critical for HR proficiency (Chun et al, 2013). Their importance is underscored further as the loss of the RAD51 paralogs are embryonic lethal in mouse models and are variably tolerated

in cell lines (Garcin et al, submitted). In non-tumorigenic cell lines such as MCF10-A cells, RAD51C, RAD51D, XRCC2, and XRCC3 were inviable (Garcin et al, submitted). The RAD51 paralogs interact with one another to form complexes which is required for their stability and function. The RAD51 paralogs assemble into the BCDX2 complex (RAD51B, RAD51C, RAD51D, XRCC2), the CX3 complex (RAD51C, XRCC3) and the Shu complex (SWSAP1, SWS1) (Schild et al., 2000; Miller et al., 2001; Martin et al 2006). RAD51C is unique among the RAD51 paralogs as it is a member of both the BCDX2 and CX3 complexes. RAD51C plays a critical role in canonical HR as well as in replication fork protection and restart (Somyajit et al, 2015b). Due to the incorporation of RAD51C into multiple complexes, RAD51C is thought to play a critical function during several steps of DSB repair and replication-associated repair.

RAD51C heterozygous mutations are associated with cancer predisposition, and biallelic mutations in *RAD51C* have been found in Fanconi anemia-like syndromes (Vaz et al, 2010; Jacquinet et al, 2018). *RAD51C* mutations have been identified in 3% of familial ovarian cancers including frame-shifts and point mutations, as well as promoter methylation (Pennington et al, 2014). Epidemiology work has identified *RAD51C* mutations in families with high incidences of breast and ovarian cancers that are wild-type for *BRCA1* and *BRCA2* mutations (Meindl et al, 2010). Patient samples revealed that *RAD51C* mutations are heterozygous within the patient, and only the tumors had two mutated *RAD51C* alleles suggesting a loss-of-heterozygosity (LOH) event in the tumor (Meindl et al, 2010). These tumors are also p53 deficient which is thought to allow the tumor to tolerate the loss of *RAD51C* (Meindl et al, 2010; Kondrashova et al, 2017). Preliminary studies have suggested that a subset of *RAD51C* mutations are deleterious to RAD51C function during HR as reduced RAD51 foci were observed (Meindl et al. 2010; Clague et al. 2011; Osorio et al. 2012; Thompson et al. 2012; Blanco et al. 2014).

Here we report a comprehensive analysis of *RAD51C* cancer-associated point mutations and SNPs that are observed in highly conserved residues of RAD51C. By using a yeast-two-hybrid and yeast-three-hybrid approach, we screened 32 RAD51C point mutations for altered protein-protein interactions between RAD51C and its binding partners, RAD51B, RAD51D, and XRCC3. RAD51C interactions with RAD51B and XRCC3 were validated by co-immunoprecipitation experiments in human cells, and a subset of these mutants were further analyzed for HR defects using a direct repeat GFP (DR-GFP) recombination assay. Using this approach, we identified that mutations in and surrounding the Walker A motif of *RAD51C* are critical for disrupting RAD51C protein-protein interactions, and this largely correlated with a deficiency in HR function. We then correlated these phenotypes with sensitivities to therapeutic strategies currently used to treat *BRCA1/2*-deficient ovarian cancers. In conclusion, our results suggest that the Walker A motif of RAD51C is critical for RAD51C function during HR and prevention of breast and ovarian cancers.

3.2 MATERIALS AND METHODS

3.2.1 Yeast-two- and three-hybrids and plasmid construction

Yeast-two-hybrid (Y2H) plasmids were created in pGAD-C1 and pGBD-C1 for RAD51B (EcoRI/BglII), RAD51D (EcoRI/SalI), and XRCC3 (EcoI/SalI. The constitutively expressed yeast-three-hybrid (Y3H) plasmid was created in pRS-ADH-416 for RAD51B (EcoRI/SalI). RAD51C mutant vectors were made by sub-cloning RAD51C into the pGAD-C1 or pGBD-C1 vectors using 5'EcoRI and 3'SalI restriction sites. Specific point mutations were introduced by site-directed mutagenesis of the pGAD-RAD51C or pGBD-RAD51C vectors. *RAD51C* cDNA and

RAD51B cDNA were a gift from Jun Huang, *RAD51D* cDNA was a gift from Paul Russell, and pGAD-XRCC3 and pGBT-XRCC3 plasmids were a gift from David Schild.

Y2Hs and Y3Hs were performed as described in McClendon and Sullivan et al, 2016 (Chapter 2) except that the pGAD, pGBD, and pRS-ADH-416 plasmids were co-transformed into the YPJ694a yeast strain. RAD51C mutants were queried in both the pGAD and pGBD vectors for interaction with each binding partner by plating on SC- LEU-TRP -HIS (Y2H interaction), SC -LEU-TRP -URA-HIS (Y3H interaction) and loading controls SC -LEU-TRP (Y2H) or SC -LEU-TRP -URA (Y3H). Images were adjusted for brightness and contrast identically in Adobe Photoshop software. RAD51C mutant interactions were then categorized as complete interaction, partial loss of interaction, or complete loss of interaction compared to wild-type RAD51C for each respective binding partner. Analysis was performed in duplicate with fresh transformations for each biological replicate.

3.2.2 U2OS culture, cell lines, and reagents

Human U2OS cells were cultured at 5%CO_2 in DMEM supplemented with 10% fetal bovine serum (FBS), penicillin and streptomycin. All cells were transfected with the indicated cDNA and *Trans*IT-LT1 transfection reagent (Mirus Bio) diluted in OptiMEM serum free media according to manufacturer's instructions. *RAD51C* cDNAs were expressed in pCMV2B FLAG tagged plasmids and *RAD51B* and *XRCC3* cDNAs were expressed in pCMV3B MYC tagged plasmids. Mutations were generated in *RAD51C* through site-directed mutagenesis as for Y2H plasmids.

U2OS-Myc-RAD51B cells were generated by transfecting pCMV3B-Myc-RAD51B and selecting with G418 for 5 days and plated at colony forming density to select individual clones and generate a stable cell line over-expressing Myc-RAD51B. Expression was verified by Western

blot for the Myc tag (c-Myc (A-14) (sc-789, Santa Cruz; 1:500)). These cells were then used for co-immunoprecipiation and cycloheximide chase experiments.

3.2.3 Co-immunoprecipitation and Western blot experiments

2.0 X 10^6 U2OS-Myc-RAD51B cells were seeded on 15cm plates (~40% confluence) and transfected 24 hours later with each pCMV2B-RAD51C mutant or pCMV2B empty vector. Cells were harvested 24 hours later (~70% confluence) and lysed in NP-40 lysis buffer (50mM Tris base, 100mM NaCl, 2mM $MgCl_2$, 10% glycerol, 0.1% NP-40) supplemented with protease inhibitor cocktail (A32965, Pierce) and phosphatase inhibitor cocktail (A32957, Pierce). Cells were lysed on ice for 20 minutes with benzonase (70746, Millipore Sigma) to eliminate protein-protein interactions mediated by DNA. Lysates were cleared by centrifugation and 10% volume was then removed as the input. Samples were incubated with 40 µl Anti-c-Myc Magnetic beads (Thermo Scientific Pierce, 88842) overnight, rotating at 4°C. The following morning, cells were washed four times in the same lysis buffer and the remaining 90% was loaded in the gel as the IP fraction. SDS-sample buffer was added to input and IP samples, and were boiled 5 minutes at 99°C.

The same method was used for XRCC3 interaction with the following changes. pCMV3B-XRCC3 was co-transfected with pCMV2B-RAD51C. 20 µl XRCC3 antibody (Novus Biologicals, NB100-180) was incubated with the lysate overnight and the following morning 40 µl G protein beads (Thermo Scientific Pierce, 88847) were added for 2 hours rotating at 4°C.

The entire volume of each sample was loaded in 10% SDS-PAGE gels and run at 80V. Protein was then transferred onto PVDF membrane (Immobilon-FL, Millipore) at 100V for 2 hours and blocked for 1 hour with Odyssey blocking buffer (927-50000, Licor). Antibodies were diluted

into Odyssey blocking buffer and Tris phosphate buffer (TBS) at a 1:1 ratio supplemented with 0.2% Tween-20. Antibodies included FLAG-M2 (F3165, Sigma; 1:2000), c-Myc (A-14) (sc-789, Santa Cruz; 1:500), XRCC3 (Novus Biologicals, NB100-180; 1:500), and GAPDH (Santa Cruz sc-25778; 1:500). Secondary antibodies were all used at 1:20,000 and included Goat anti-Mouse IgG Light-Chain Specific (AlexaFluor 790-conjugated; Jackson ImmunoResearch 115-655-174), IRDye680RD Goat anti-rabbit (Licor 926-6807). Membranes were then imaged using the Licor Odyssey CLx imaging system. This imaging software was used to quantify intensities of all blots and each immunoprecipitation was normalized to the respective input to control for transfection differences. Inputs were additionally normalized to GAPDH in the input to account for loading differences. Co-immunoprecipitations were then divided by immunoprecipitations to find a ratio of interaction. All images were adjusted for brightness and contrast identically in Adobe Photoshop software.

3.2.4 Cycloheximide chase experiments

2.5 X 10^6 U2OS-Myc-RAD51B cells were seeded and transfected 24 hours later with the indicated Flag-RAD51C mutant construct. The next day, 0.5 million cells were seeded for each time point of the experiment. The following day, 50µg/ml cycloheximide (Sigma C4859) was added for the indicated amount of time (0, 0.5, 1, 2, 4, or 6 hours). Cells were harvested and lysed on ice for 20 minutes in RIPA buffer (150 mM NaCl, 50 mM Tris-HCl pH 7.2, 1% Triton X-100, 0.5 Na-deoxycholate, 0.1% SDS, 1mM EDTA) supplemented with 2 mM PMSF, protease inhibitor cocktail (A32965, Pierce), phosphatase inhibitor cocktail (A32957, Pierce), and Benzonase (70746, Millipore Sigma). Lysates were cleared by centrifugation and diluted in 2X SDS-sample buffer and boiled 5 minutes, 99°C. Western blots were run as in co-immunoprecipitation

experiments. Blots were quantified using the Licor Odyssey CLx imaging system software and each lane was normalized to GAPDH loading control. Data was graphed as bar graphs in Excel as averages with standard error of the mean. In addition to graphing the averaged data as a bar graph, an exponential model was used to fit to the data. A one phase decay model was fit to the data using Prism software. [(Y=(Y0 - Plateau)*exp(-K*X) + Plateau) in which X is time, Y0 is Y at time 0, plateau is the Y value at infinite time, K is the rate constant].

3.2.5 ConSurf alignments and sequence Logo generator for Walker A region of RAD51C

WebLogo was used to compare ConSurf alignments of 9 species, *Homo sapiens*, *Danio rerio*, *Gallus gallus*, *Macaca mulatta*, *Pan troglodytes*, *Bos Taurus*, *Canis lupu familiaris*, *Mus musculus*, and *Rattus norvegicus*. Amino acids 117-142 are represented as stacked symbols indicating the overall conservation of the residue and frequency of the amino acid (Crooks et al, 2004; Schneider et al, 1990). Amino acids were color coded as polar in green (GSTYC), neutral in purple (QN), basic in blue (KRH), acidic in red (DE), and hydrophobic in black (AVLIPWFM).

3.2.6 MCF10A culture and Cre treatment

MCF10A cells containing an integrated DR-GFP reporter (Feng and Jasin 2017) were grown in DMEM HG/F-12 supplemented with 5% horse serum, 1% penicillin and streptomycin, 100 ng/mL cholera toxin, 20 ng/mL epidermal growth factor, 0.01 mg/mL insulin, and 500 ng/mL hydrocortisone at 37°C with 5% CO_2 atmosphere.

Cells were seeded at 500,000 cells/60mm dish 24 hours before infection. The next day, one dish was counted to determine MOI (density X 375 for the volume of diluted AdCre). Cells were treated

with AdenoCre (Baylor College of Medicine, Ad5-CMV-Cre) diluted 1:100 in MCF10A media and Genejammer (Aligent 204132). Cells were incubated with virus for 4 hours at which point infection media was diluted 1:3 overnight. The following morning virus was removed, and cells were washed with PBS and incubated another 48 hours in MCF10A media before use.

3.2.7 MCF10A genotyping post Cre treatment

After Cre treatment, cells were grown for 48 hours and harvested for genotyping. Genomic DNA was extracted, and PCR was performed for the LoxP flanked RAD51C at the *AAVS1* locus with the following primers: ATTGTGCTGTCTCATCATTTTGGC (forward) and CTGGGATACCCCGAAGAGTG (reverse). Expected PCR product sizes are ~2.5 kb (before Cre) and ~1.3 kb (after Cre).

3.2.8 MCF10A Western blot, complementation and HR reporter assay

Nuclear extracts were collected from MCF10A cells using the cytoplasmic lysis buffer (10 mmol/L Tris-HCl, 0.34 mol/L sucrose, 3 mmol/L $CaCl_2$, 2 mmol/L magnesium acetate, 0.1 mmol/L EDTA, 0.5% NP-40, protease inhibitor) and nuclear lysis buffer (20 mmol/L HEPES, 3 mmol/L EDTA, 10% glycerol, 150 mmol/L potassium acetate, 1.5 mmol/L $MgCl_2$, 0.1% NP-40, protease inhibitor). Nuclear protein (30 μg) was used for detection. Protein was separated on 10% acrylamide gels and transferred to PVDF membranes, and protein was detected on a LiCor CLX scanner. RAD51C expression was detected with RAD51C antibody (ab55728 1:500; Abcam), and equal nuclear loading was detected using PCNA antibody (sc-56 1:250; Santa Cruz

Biotechnology), and IR dye secondary antibodies from LiCor Biosciences. The image was adjusted for brightness and contrast using Photoshop (Adobe Systems Inc.).

The DR-GFP reporter was introduced into MCF10A cells as previously described in Kondrashova et al 2017. Cre recombinase was expressed in conditional *RAD51C*$^{-/-}$ MCF10A cells to remove an ectopic floxed *RAD51C* gene and in isogenic wild-type cells as a control. After Cre expression, cells were infected with an I-SceI– expressing lentivirus. GFP^{+} cells were measured by flow cytometry (BD FACScan) 48 hours after infection, and data were analyzed using FlowJo software. Without I-SceI expression, the number of GFP^{+} cells was ≤0.01.

3.2.9 MCF10A clonogenic survival and genotoxin sensitivity

48 hours after Cre treatment, MCF10A cells were seeded at colony forming density on 60mm dishes for clonogenic survival. For genotoxin sensitivity studies, cells were seeded in triplicate and treated 24 hours after plating with the following drugs. Cells were exposed to cisplatin for 24 hours for both cisplatin exposure alone and in combination with Olaparib. Cells were exposed to Olaparib (Selleck Chem, AZD2281) continuously, replacing the media with fresh Olaparib every 3 days. Cells were grown for 10 days (beginning with treatment Day 1), and fixed in 100% methanol. Plates were stained with crystal violet, scanned on a FluorChem M (proteinsimple), and quantified for area density using the Colony Count Analysis Tool (AlphaView SA software). Area was graphed relative to untreated plates.

3.2.10 RAD51C modeling using I-TASSER server

The I-TASSER (iterative threading assembly refinement) server is a structure prediction server from the Yang Zhang lab at the University of Michigan (Yang and Zhang 2015). Several RAD51C PBD structural analogs were identified, and the closest structure was *M. voltae* Rad51 homolog (PDB: 1XU4). This structure was used for mapping the Walker A and B motifs and RAD51C mutants in purple.

3.3 RESULTS

3.3.1 *RAD51C* cancer-associated point mutations and single nucleotide polymorphisms are found at highly conserved residues

To investigate the consequences of *RAD51C* cancer-associated mutations and SNPs on RAD51C function, we used the COSMIC database, epidemiology literature, and exome sequencing from the Broad Institute to identify point mutations in the *RAD51C* gene. We limited our analysis of both cancer-associated mutations and SNPs to highly conserved residues, which we determined using the ConSurf alignment of several vertebrate RAD51C sequences (Supplemental Figure 6) (Glaser et al. 2003; Landau et al. 2005). Mutations and SNPs were identified throughout the RAD51C protein (Figure 12A). Cancer-associated RAD51C mutations are shown in red text on the top of the RAD51C schematic whereas SNPs are shown in blue text below the schematic (Figure 12A). Germline mutations were derived primarily from epidemiology studies identifying familial incidences of cancer in families that had wild-type *BRCA1*/2 genes but contained *RAD51C*

mutations (Table 4) (Blanco et al., 2014; Clague et al., 2011; Meindl et al., 2010; Osorio et al., 2012; Thompson et al., 2012). Additionally, RAD51C mutations from spontaneous tumors were identified through several databases as indicated (Table 4) (COSMIC (Tate et al. 2018), Memorial Sloan Kettering Cancer Center, SU2C ovarian cancer dream team). Interestingly, some SNPs were also found to be cancer-associated (indicated by a # in Tables 4 and 5). For each SNP analyzed, we indicated the population in which this SNP was observed and the frequency of occurrence (Table 5). We also determined whether the mutation or SNP analyzed would be predicted to be functionally important by using the PolyPhen2 analysis software (Adzhubei et al. 2010). PolyPhen2 analysis software predicts whether a given amino acid substitution may be damaging to protein function using phylogenetic and structural information to produce a score between 0 and 1 from benign to probably damaging. In total, 23 cancer-associated mutations and 10 SNPs were chosen for analysis (Table 6, left column; Figure 12A). We additionally included the Fanconi anemia-like (FA-like) RAD51C point mutation, R258H (Vaz et al, 2010).

Mutation	Tissue Origin	Somatic vs. Germline	Reference
P21S	Breast Invasive Carcinoma	somatic	(1)
D108Y	Colorectal adenocarcinoma	not determined	MSK
T121R	Not available	somatic	SU2C
G125V	Breast Cancer	germline	(4)
A126T#	Breast and Ovarian Cancer	germline	(4) (5) (6) (7)
T132P	Not available	germline	SU2C
C135Y	Breast and Ovarian Cancer	germline	(6)
M136L	Lung Adenocarcinoma	somatic	(19)
L138F	Breast and Ovarian Cancer	germline	(4) (6)
G153D	Breast Cancer	germline	(5)
D159N	Breast Cancer	germline	(4)
G162E	Breast and Ovarian Cancer	germline	(9)
L219S#	Breast and Ovarian Cancer	germline	(6) (7)
Y224H	BladderUrothelialCarcinoma	somatic	(20)
P247L	Malignant Melanoma	somatic	(10)
R249C#	Breast Cancer	not determined	(9) MSK
L257V	Liver Cancer	somatic	(21)
R258H	Fanconi anemia-like syndrome	germline	(12)
A279V	EndometrioidCarcinoma	not determined	(13)
T287A#	Breast and Ovarian Cancer	germline	(4) (5) (7) (9)
A308T	Not available	somatic	SU2C
R312W#	Large intestine Carcinoma	somatic	(15) (16)
A324T	Colorectal Adenocarcinoma	somatic	(17)
P330H	Urinary Tract Carcinoma	somatic	(18)
# Mutation also found in SNPs from the population			

Table 4. RAD51C cancer-associated mutation origins.

RAD51C cancer-associated mutations were selected using the COSMIC database and primary literature from the following references: (1) COSMIC. Breast Invasive Carcinoma (TCGA, US) Curated Study (2) MSKCC-D108Y (3) SU2C-T121R (4) Meindl A., et al, 2010 Nature Genetics (G125V, A126T, L138F, T287A) (5) Clague, J., et al, 2011 PlosOne (A126T,G153D, T287A) (6) Osorio A., et al, 2012 Human Molecular Genetics (A126T,C135Y,L138F,L219S) (7) Blanco A., et al 2014 Breast Cancer Research and Treatment (A126T,L219S,T287A) (8) SU2C-T132P (9) Thompson, E., et al, 2012 Human Mutation (G162E,R249C,T287A)

(10) COSMIC. Krauthammer M et al. (2012) Exome sequencing identifies recurrent somatic RAD51C mutations in melanoma. Nature genetics 44(9):1006-14. (11) MSKCC-R249C (12) Vaz et al, 2010, Nature Genetics (R258H, shown in green) (13) COSMIC. Uterine Corpus Endometrioid Carcinoma (TCGA, US) import from ICGC Curated Study (14) SU2C-A308T (15) COSMIC. Colon Adenocarcinoma (TCGA, US) Curated study (16) COSMIC. Cancer Genome Atlas Network (2012) Comprehensive molecular characterization of human colon and rectal cancer. Nature 487(7407):330-7 (17) TCGA (2012) Colorectal Adenocarcinoma. Nature 487(7407):330-7; TCGA patient: TCGA-AA-A00J (18) COSMIC. Bladder Urothelial Carcinoma (TCGA, US) import from ICGC Curated Study.

Mutation	Population	Allele Count	Total Frequency
R12W	European*	1/121184	8.252×10^{-6}
G125S	NA	NA	NA
A126T#	most: European*	422/119592	0.003529
M136L	East Asian	2/121412	1.647×10^{-5}
I144T	European*	4/121412	3.295×10^{-5}
R212C	most: South Asian	5/121122	4.128×10^{-5}
R214C	most: East Asian	6/ 121136	4.953×10^{-5}
L219S#	Latino	1/ 121144	8.255×10^{-6}
R249C#	European*	1/ 121404	8.237×10^{-6}
L257V	most: African	3/121404	2.471×10^{-5}
R260W	most: East Asian	2/121402	1.647×10^{-5}
L262V	most: European*	7/121400	5.766×10^{-5}
T287A#	European*	658/ 120450	0.005463
A308S	African	7/ 120930	5.788×10^{-5}
R312W#	Latino	1/ 120886	8.272×10^{-6}
*Non-Finnish descent			
# Mutation also found in cancer-associated context			

Table 5. RAD51C SNPs sourced from EXOME and NCBI databases.

All SNPs in RAD51C were sourced from EXOME with the exception of G125S which was sourced from dbSNP on NCBI. In the population column, most indicates the most prevalent population in which the mutation was identified for mutations found in multiple populations.

Mutation	PolyPhenscore	Prediction
R12W	1.00	Probably Damaging
P21S	0.054	Benign
D108Y	1.00	Probably Damaging
T121R	1.00	Probably Damaging
G125S	1.00	Probably Damaging
G125V	1.00	Probably Damaging
A126T	0.066	Benign
T132P	1.00	Probably Damaging
C135Y	1.00	Probably Damaging
M136L	0.006	Benign
L138F	0.995	Probably Damaging
I144T	0.885	Probably Damaging
G153D	1.00	Probably Damaging
D159N	1.00	Probably Damaging
G162E	1.00	Probably Damaging
R212C	1.00	Probably Damaging
R214C	0.001	Benign
L219S	1.00	Probably Damaging
Y224H	0.001	Benign
P247L	0.109	Benign
R249C	1.00	Probably Damaging
L257V	0.238	Benign
R258H	1.00	Probably Damaging
R260W	1.00	Probably Damaging
L262V	0.883	Possibly Damaging
A279V	0.883	Possibly Damaging
T287A	0.988	Probably Damaging
A308S	0.771	Possibly Damaging
A308T	0.992	Probably Damaging
R312W	1.00	Probably Damaging
A324T	0.981	Probably Damaging
P330H	0.997	Probably Damaging

Table 6. Damaging RAD51C mutation predictive analysis by PolyPhen2.

RAD51C mutations were scored for predictive functional consequences using the Polymorphism Phenotyping version 2 (PolyPhen-2) software. PolyPhen was used to predict the impact of amino acid substitutions in

RAD51C on both structure and function to categorize mutations as benign, possibly damaging, or probably damaging. Cancer-associated mutations are red, SNPs are blue, and FA-like is green. Mutations identified as both cancer-associated and as SNPs are indicated in blue.

3.3.2 RAD51C mutants disrupt BCDX2 and C3X protein complexes by yeast-two and three-hybrid assays

RAD51C is a member of the BCDX2 and CX3 complexes where it directly interacts with RAD51B and RAD51D in the BCDX2 complex and XRCC3 in the CX3 complex. By analyzing RAD51C protein-protein interactions of our mutants, we aimed to determine if the BCDX2 or CX3 complex remained intact. Therefore, using this pool of 34 mutations (18 cancer-associated, 10 SNPs, 5 mutants found as both SNPs and cancer-associated and 1 FA-like mutant), we conducted a large-scale screen of RAD51C mutants for altered protein-protein interactions (Figure 12). Yeast-two-hybrid (Y2H) analysis was initially used to determine the composition of RAD51 paralog complexes as these protein-protein interactions are readily observed using this high-throughput approach (Schild et al, 2000). We used Y2H analysis to screen for RAD51C interactions with RAD51B or XRCC3 (representative Y2Hs, Figure 12B; Supplemental Figures 7,9). RAD51C interaction with RAD51D is very weak in the Y2H system, so we employed a yeast-three-hybrid (Y3H) approach where constitutive expression of RAD51B functions to stabilize RAD51C and thus enables its interaction with RAD51D to be more readily visualized (Supplemental Figures 8,9). As RAD51B does not interact with RAD51D itself, RAD51B serves to stabilize the RAD51C mutants in these experiments. Y2H and Y3H screening was performed bi-directionally as a confirmation of the Y2H or Y3H results. In some cases, differences were observed depending upon whether RAD51C point mutation was expressed in the pGAD or the pGBD vector. In these

instances, we divided the square into triangles where the pGAD-RAD51C interaction is shown on the bottom and the pGBD-RAD51C Y2H interaction shown in the top triangle (Figure 12E; see Supplemental Figures 7-9). *RAD51C* mutations were classified as fully disrupting individual protein-protein interactions (shown in red), partially disrupting protein-protein interactions (shown in yellow), or proficient for protein-protein interactions (shown in green) (summarized in Figure 12E).

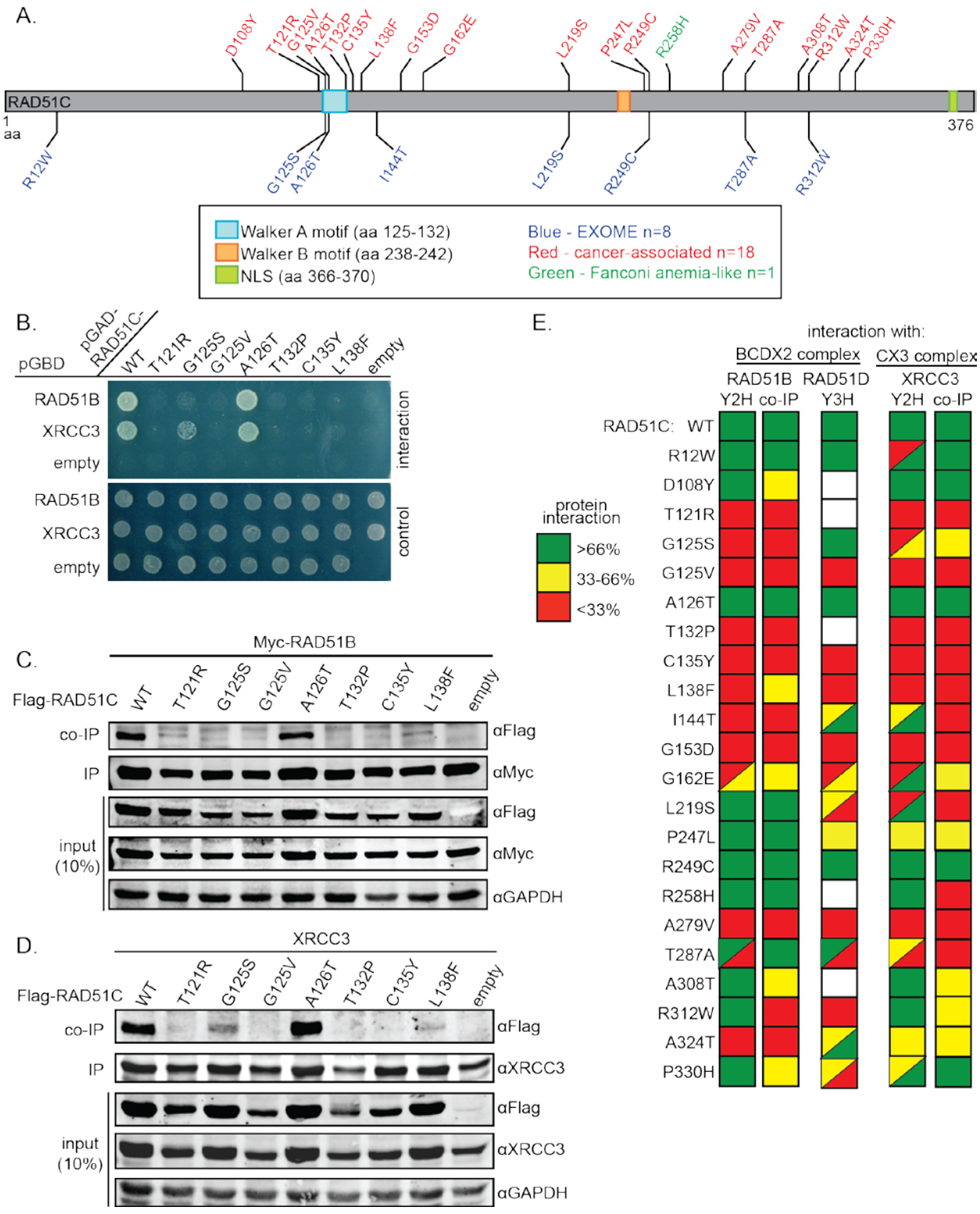

Figure 12. RAD51C mutants disrupt protein-protein interactions.

A. RAD51C schematic (aa1-376) shows cancer-associated point mutations above in red, an FA-like point mutation above in green, and SNPs below in blue. B. Representative Y2H interactions of RAD51C and RAD51C point mutations in the pGAD vector and RAD51B and XRCC3 interaction partners in the pGBD vector. Interaction is indicated by growth. C. and D. Representative co-immunoprecipitations are shown for RAD51C and RAD51C point mutations (as in B) with RAD51B or XRCC3, respectively. IP indicates immunoprecipitations of either Myc-RAD51B or XRCC3. co-IP indicates Flag-RAD51C or Flag-RAD51C point mutations bound to the IP. Inputs are 10% of the total sample. E. Heat map indicates protein-protein interactions for the complete set of RAD51C mutations and corresponds to supplemental data (Supplemental Figures 7-12). Green squares indicate 66%-100% interaction, yellow squares indicate 33%-66% interaction, red squares indicate 0-33% interaction.

3.3.3 Disrupted protein-protein interactions of RAD51C mutants validated in U2OS cells

To validate the Y2H/Y3H results, 22 of the 34 RAD51C mutants were further analyzed by co-immunoprecipitation (co-IP) for interactions with RAD51B and XRCC3 (Figure 12E). To avoid confounding variables in these experiments, IPs were performed on the binding partner (RAD51B or XRCC3) rather than each RAD51C mutant to avoid misinterpretation of an interaction if a particular RAD51C mutant was expressed at a lower level than wild type RAD51C. RAD51C interaction with RAD51B or XRCC3 was interrogated as representative of interactions within the BCDX2 or CX3 complexes, respectively (representative co-IPs, Figure 12C, 12D; Supplemental Figures 10-12). The co-IP results revealed that approximately 95% of RAD51C interactions with RAD51B were either identical or had less than a 30% difference between the Y2H and co-IP experiments (i.e. complete loss of interaction vs. partial loss of interaction). Approximately 64% of RAD51C co-IP interactions with RAD51B were identical to the Y2H results. Similarly, the RAD51C co-IP results with XRCC3 revealed that approximately 91% were identical or had less

than a 30% difference between the Y2H and co-IP experiments. Approximately 68% of RAD51C co-IP interactions with XRCC3 were identical to the Y2H results (Figure 12E). Representative co-IP experiments between RAD51C with RAD51B or XRCC3 are shown (Figure 12C,D). Indicating that point mutations are expressed, we observed protein expression of RAD51C mutants in the input lanes of the IP by western blot. To confirm that a loss of RAD51C protein-protein interactions was not solely due to a loss of RAD51C protein stability, cycloheximide chases were performed on seven RAD51C mutants (six of which had disrupted protein-protein interactions by both Y2H/Y3H and co-IP and one of which maintained its protein interactions) (Figure 13). The cycloheximide chases revealed that each mutant exhibited similar stability to the wild-type RAD51C. While we did not see gross changes in RAD51C protein stability, RAD51C-C135Y exhibited a small but reproducible change in protein stability at the later time points. Therefore, we concluded that protein stability alone does not account for the loss of RAD51C mutant's protein-protein interactions for the mutants tested.

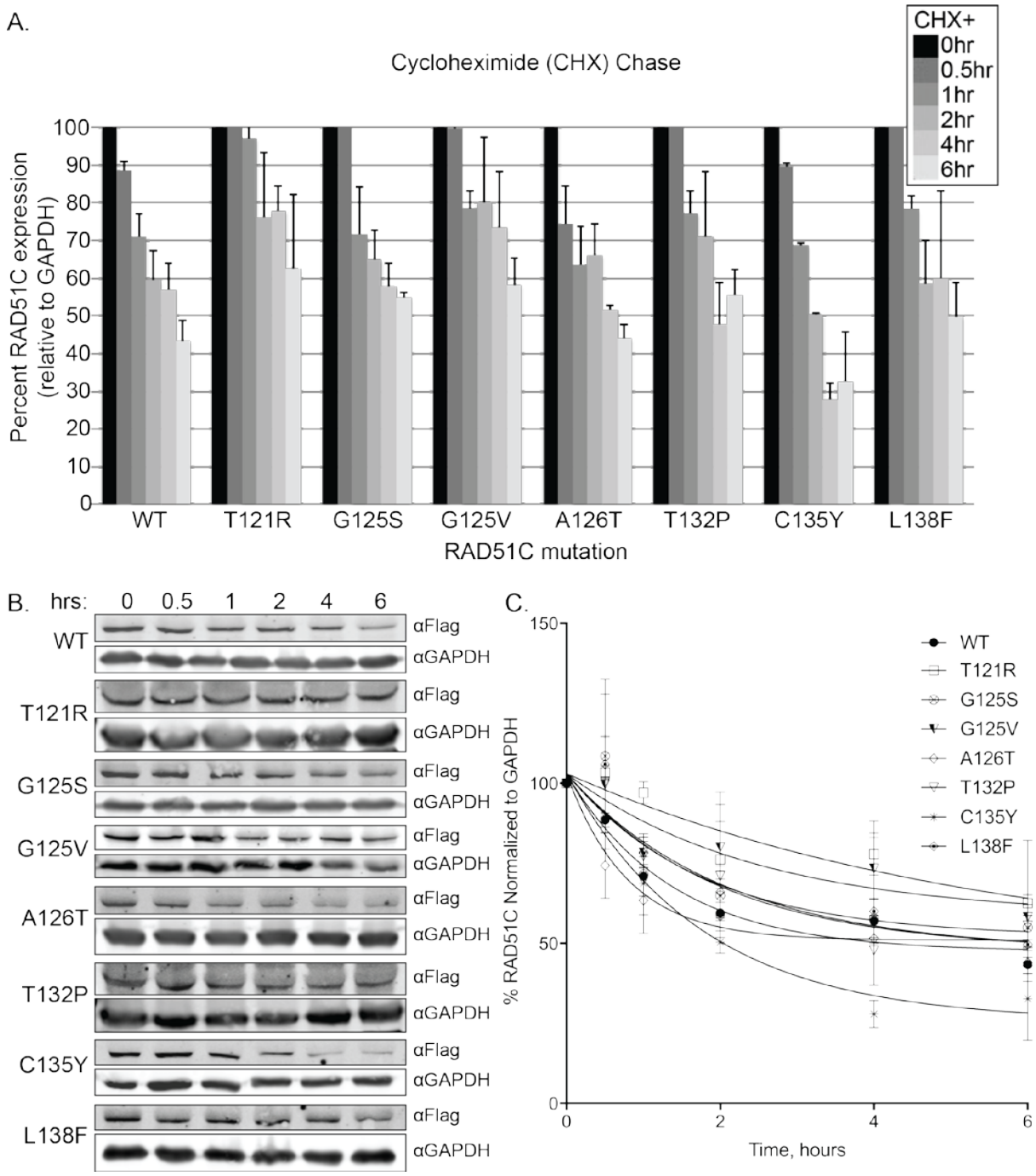

Figure 13. RAD51C mutant stability differences do not account for reduced protein-protein interactions. Cycloheximide chases were performed for RAD51C mutants in the ATPase region of RAD51C. A. Relative RAD51C expression was normalized to time 0, and wild type RAD51C and RAD51C mutants showed similar protein stability over a six hour time course. While not statistically significant, C135Y appears slightly less stable than other mutants analyzed. B. Transiently transfected U2OS cells were subjected to cycloheximide

treatment for 0-6 hours as indicated and lysed to assess protein stability of Flag-RAD51C over time. C. An exponential curve was fit to the cycloheximide data using a one phase decay model [(Y=(Y0 - Plateau)*exp(-K*X) + Plateau) in which X is time, Y0 is Y at time 0, plateau is the Y value at infinite time, K is the rate constant].

Upon further analysis, we found that RAD51C mutations between amino acid 121 and 162 frequently resulted in loss of protein interactions by Y2H/Y3H and co-IP experiments (Figure 12E; red boxes). Within this region is the highly conserved Walker A motif of RAD51C (aa125-132, GXXXXGKT/S; Figure 12A). Since the Walker A motif is an ATPase domain found in many DNA binding proteins, we wanted to further investigate the significance of mutations within and around this motif in RAD51C. We observed six residues in or surrounding the RAD51C Walker A motif that disrupted its protein-protein interactions (T121R, G125S, G125V, T132P, C135Y, and L138F; Figure 12B-E; Supplemental Figure 13). Additionally, we selected RAD51C-A126T as a control as it maintained its protein-protein interactions. Interestingly, these six mutations were all highly conserved throughout vertebrate species and were largely invariant amongst 9 of these species (Supplemental Figure 6; Supplemental Figure 13). RAD51C-A126T is a notable exception of where A126 falls in a non-conserved position of the Walker A motif (Schneider and Stephens 1990; Crooks et al. 2004).

3.3.4 MCF10A cells expressing RAD51C mutants have impaired viability, homologous recombination, and sensitivity to chemotherapeutic agents

To determine if RAD51C mutants that alter its protein-protein interactions lead to a loss of cellular viability or HR defects, we utilized a RAD51C conditional knockout cell line that was created by Dr. Rohit Prakash in Dr. Maria Jasin's laboratory at Memorial Sloan Kettering Cancer Center

(Supplemental Figure 13). The MCF10A cells represent a normal breast epithelial cell line. In this cell line, the two endogenous copies of RAD51C are disrupted by TALENs. To overcome the lethality of RAD51C knockout, a conditional copy of RAD51C integrated into the AAVS1 locus and contains flanking LOXP sites. Following lentiviral CRE-infection, RAD51C is excised resulting in a loss of cell viability without complementation of a wild-type copy of RAD51C (Figure 14A,B). RAD51C conditional MCF-10A cells were previously characterized (Garcin et al, submitted). Mutations within or proximal to the Walker A motif were introduced into this cell line to assess the importance of this region of RAD51C on cellular survival (Supplemental Figure 14). Using this approach, RAD51C-T121R, G125V, and C135Y mutations do not complement cell survival, whereas G125S, A126T, and L138F do complement survival (Figure 14C, T121R not shown). Interestingly, T121R, G125V, and C135Y RAD51C mutants exhibit complete loss of protein-protein interactions, which correlates with a lack of cellular survival (Figure 12 and Figure 14C). Conversely, G125S, A126T, and L138F RAD51C mutants maintained or exhibited partial loss of RAD51C protein-protein interactions and these mutants are viable (Figure 12 and Figure 14C). These results suggest that RAD51C protein-protein interactions are necessary for cellular survival and that partial protein-protein interactions are sufficient for cellular growth.

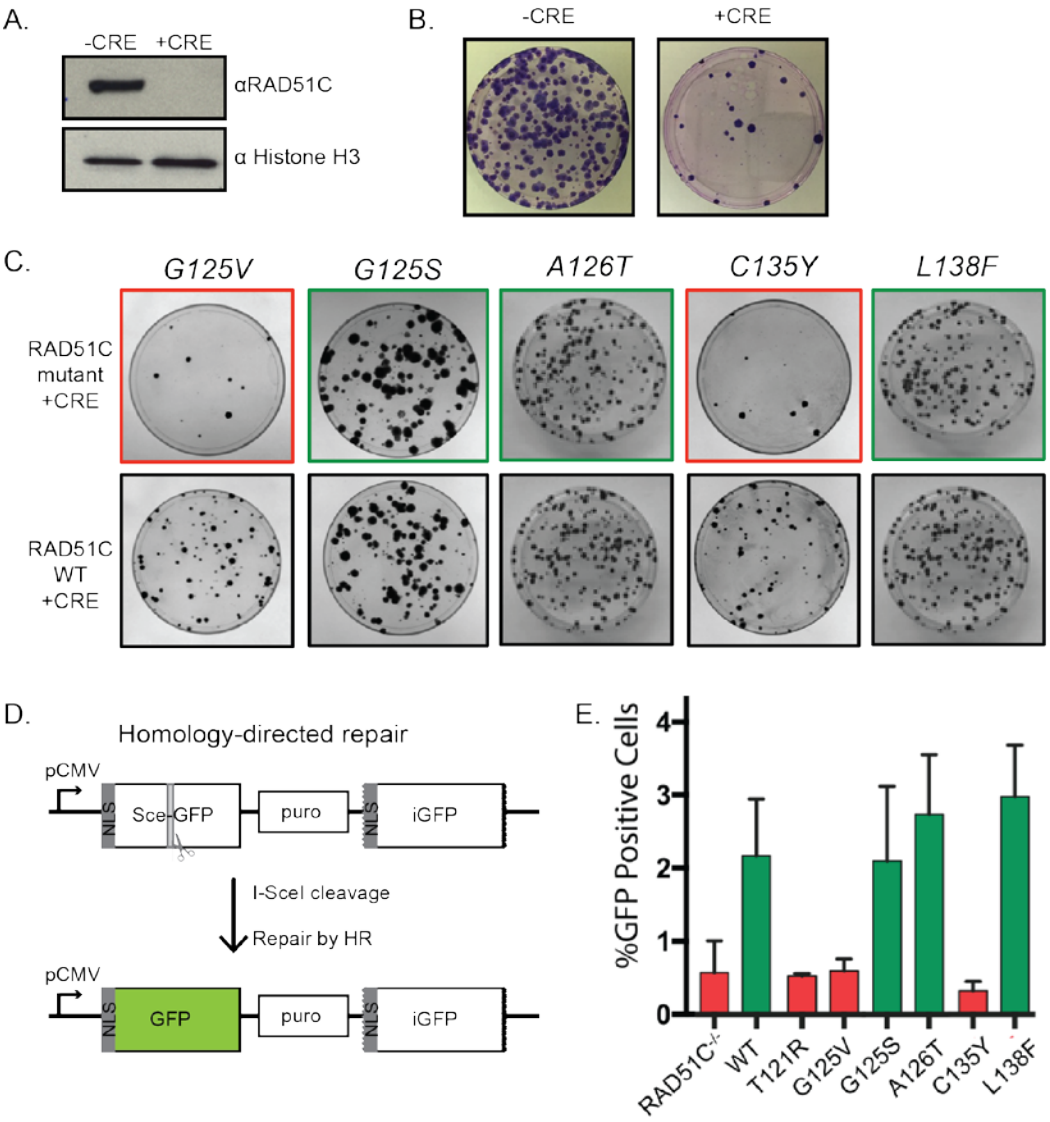

Figure 14. MCF10A cells expressing RAD51C mutants have impaired viability and HR.

A. Nuclear extracts of conditional RAD51C expression in MCF10A cells before and after addition of CRE + 48 hours. Histone H3 serves as a nuclear loading control. B. After 7 days of growth MCF10A cells treated with Cre do not survive. Remaining colonies were sequenced and still expressed RAD51C. C. MCF10A cells were complemented with the indicated RAD51C mutant or wild-type (WT) RAD51C and treated with CRE. Cells were allowed to grow for one week before imaging. RAD51C-G125V and -C135Y (outlined in red) did not complement survival relative to WT RAD51C shown below. RAD51C-G125S, -A126T, and –L138F (outlined in green) complemented survival. D. Direct repeat GFP (DR-GFP) assay depiction. The GFP reporter construct is integrated into the MCF10A conditional cell line. Upon I-SceI cleavage, a DSB is produced which when

repaired by the downstream template provided using HR will produce a full length copy of GFP which can be measure by fluorescence-activated cell sorting (FACS). E. Percent GFP expression for MCF10A cells 72 hours after CRE treatment complemented with the indicated RAD51C mutant.

Next, we analyzed whether mutations in or proximal to RAD51C Walker A motif are HR proficient. To do this, we utilized a DR-GFP reporter construct that is stably integrated into the RAD51C conditional MCF10A cells, and HR can be assayed before cellular death occurs (Figure 14D). In this assay, a DSB can be introduced by expression of the I-*Sce*I endonuclease, which cleaves a non-functional copy of GFP. GFP expression can be restored using HR by utilizing a downstream repair template and can be measured by FACS (Figure 14D). Using this assay, we observe that RAD51C-T121R, G125V, and C135Y exhibit impaired HR (Figure 14E). These results are consistent with a lack of viability and impaired protein-protein interactions observed. In contrast, RAD51C-G125S, A126T, and L138F were HR proficient (Figure 14E). These results are consistent with cellular viability observed and maintained or partial protein-protein interactions. These results suggest that a loss of RAD51C protein-protein interactions results in loss of cellular viability and HR defects.

In addition to *RAD51C* mutations in or surrounding the Walker A motif, we analyzed the cell viability and HR proficiency of 12 additional RAD51C mutants. Of these additional RAD51C point mutations, we find that RAD51C SNPs are largely HR proficient, whereas many of the cancer-associated mutations, including the FA-like mutation R258H, displayed impaired HR proficiency relative to wild-type RAD51C (Supplemental Figure 15). Similarly, RAD51C mutants that did not rescue viability also were deficient for HR. RAD51C mutants that complemented viability were partially proficient or fully proficient for HR. These results suggest that RAD51C-mediated HR is essential for viability.

Next we sought to determine whether cells expressing *RAD51C* mutations in or surrounding the Walker A motif are sensitive to chemotherapy agents currently used to treat BRCA-deficient tumors. BRCA-deficient ovarian cancer patients are currently treated with platinum compounds and have been approved for treatment with the PARP inhibitor, Olaparib. Therefore, we asked whether cells expressing RAD51C mutants exhibit cisplatin and/or PARP inhibitor (PARPi) sensitivity. Unfortunately, we are unable to examine RAD51C- T121R, -G125V, and -C135Y mutants because of their lack of cellular survival. However, in preliminary experiments we found that RAD51C-G125S and RAD51C-L138F expressing MCF10A cells show sensitivity to a combination of Olaparib and cisplatin exposure (Figure 15B) but not to cisplatin alone (Figure 15A). In contrast, RAD51C-A126T exhibited similar sensitivity to the wild-type RAD51C-expressing cells to cisplatin, or the combination therapy. These results suggest that tumors with partial defects in RAD51C protein-protein interactions may still respond to combination therapeutic approaches.

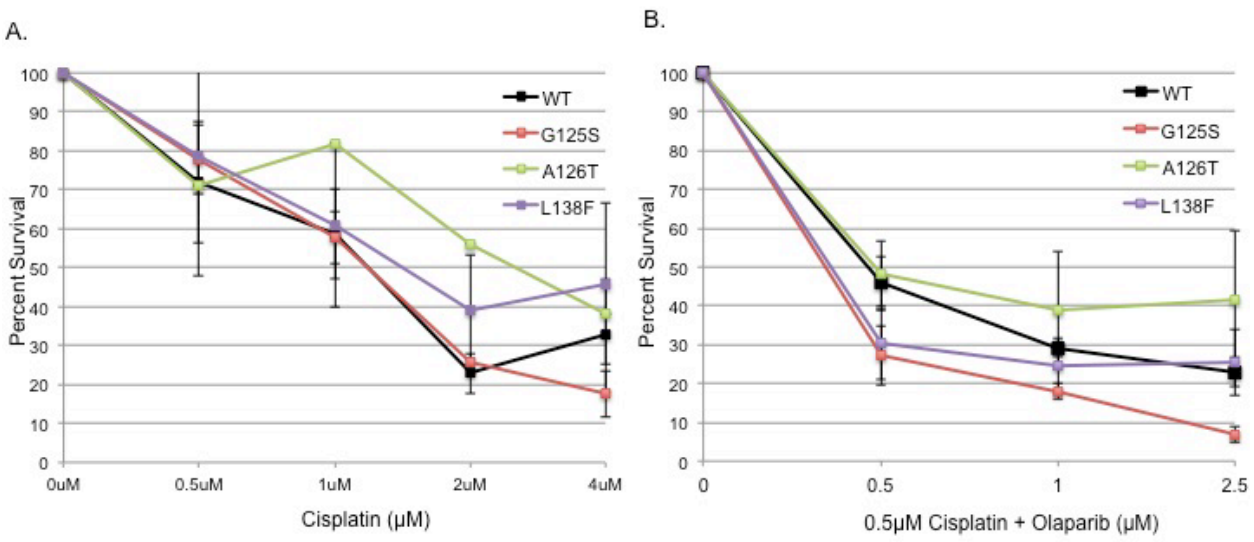

Figure 15. Clonogenic survival of RAD51C Walker A mutants exposed to Cisplatin and Olaparib.

MCF10A cells expressing RAD51C-G125S, -A126T, or –L138F were exposed to cisplatin for 24 hours (A) or cisplatin for 24 hours and olaparib continuously (B) at colony forming density. Cells were allowed to grow for 10 days and then fixed, stained, and quantified for area of growth. A. No RAD51C mutants showed increased sensitivity to cisplatin alone. B. RAD51C-G125S and –L138F showed increased sensitivity to combined cisplatin and olaparib exposure.

3.3.5 *RAD51C* mutations are associated with acquired resistance to PARPi

Unfortunately, tailored treatment strategies for patients who harbor mutations in the RAD51 paralogs are lacking compared to BRCA-deficient tumors. Our findings described here are consistent with other studies analyzing ovarian cancer patients harboring a RAD51C or RAD51D mutation for response to PARP inhibitors (Kondrashova et al, 2017). In the Kondrashova study, which was part of the ARIEL2 phase II clinical trial, we found that a patient with a RAD51C point mutation that truncated the protein at amino acid 193 resulted in impaired protein-protein interactions and HR function. This RAD51C truncation resulted in rucaparib sensitivity. Patient profiling revealed *RAD51C* was the only HR-related gene mutation within the tumor and had bi-

allelic mutations in *RAD51C* causing an early stop codon (R193X) (Figure 16). We showed that the RAD51C-193X truncation protein did not interact with RAD51B or XRCC3 through Y2H (Figure 17A). Western blots analysis revealed that the RAD51C-R193X truncation was also not expressed in yeast suggesting it is unstable (Figure 17B). MCF10A cells complemented with RAD51C- R193X also exhibited HR repair deficiency in the DR-GFP reporter assay and MCF10A nuclear extracts revealed no RAD51C- R193X protein was detected (Figure 17C,D).

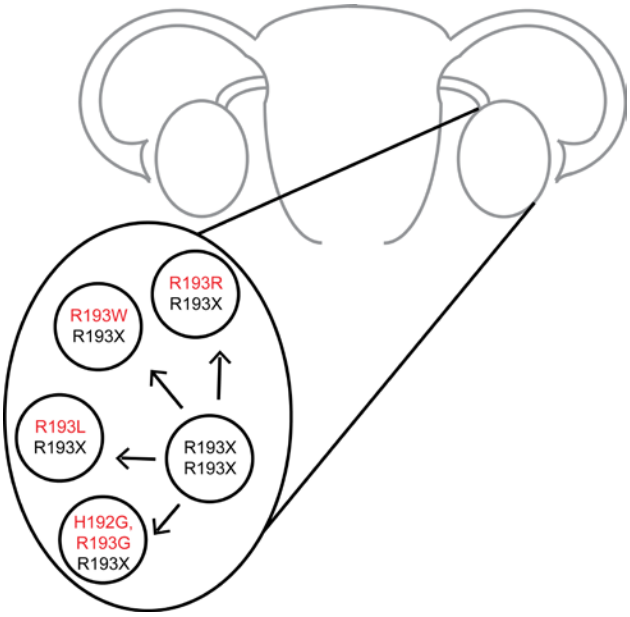

Figure 16. RAD51C reversion mutations summary.

An ovarian tumor, initially treated with platinum therapy, had two mutated RAD51C alleles (R193 early stop codon). During treatment with rucaparib, resistance occurred and tumor sequencing revealed four separate reversion mutations in *RAD51C* had restored the reading frame of one RAD51C allele indicated in red (R193R, R193W, R193L, H192G, R193G).

However, over time this patient stopped responding to PARPi and the tumor was re-sequenced and several RAD51C reversion mutations were detected (Figure 16; Kondrashova et al, 2017)). We demonstrated that these *RAD51C* secondary mutants restore RAD51C R193X Y2H interactions with RAD51B and XRCC3 (Figure 17A) and this correlated with restored HR function

(Figure 17C). Expression of all four *RAD51C* secondary mutants was also now observed by Western blot (Figure 17B,D). Mouse models confirmed that resistance to rucaparib was associated with secondary mutations in *RAD51C*, which restored its HR function (Kondrashova et al, 2017). This study highlights the importance of treating patients with PARPi early and in combination with other chemotherapies to prevent the emergence of secondary mutations that are resistant to therapy.

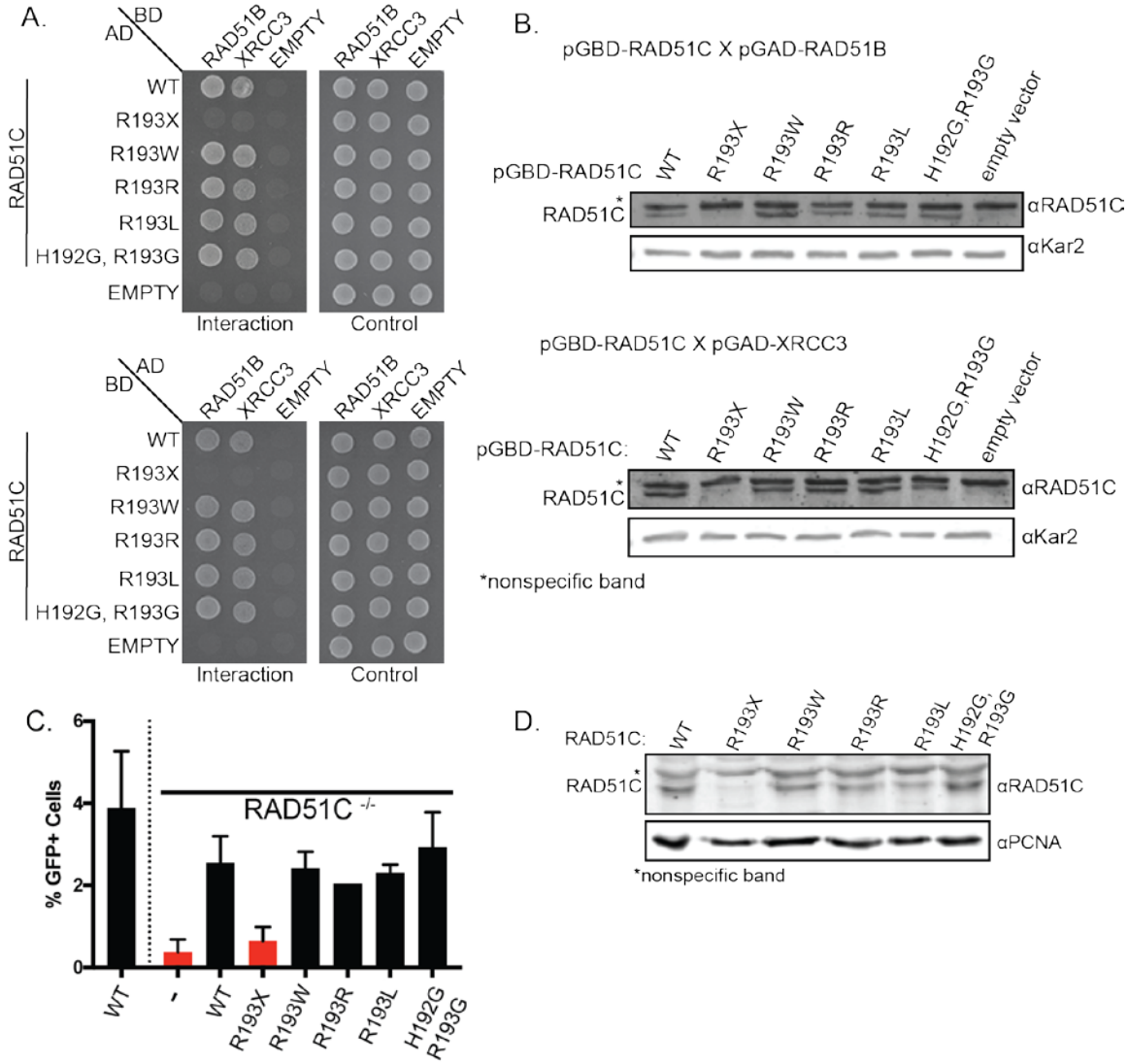

Figure 17. RAD51C reversion mutations restore expression, protein complexes, and HR.

A. RAD51C truncation mutation R193X does not interact with RAD51B or XRCC3 by Y2H. RAD51C reversion mutations restore interactions by Y2H. Y2Hs were performed bi-directionally with each binding partner expressed in either the pGAD (AD) or pGBD (BD) vectors. Growth represents interactions on the plate labeled interaction, and control indicates the presence of each plasmid. B. RAD51C expression of the lower Y2H experiment in which RAD51C mutants are expressed in the BD construct. Yeast expressing pGBD-

RAD51C with either pGAD-RAD51B or pGAD-XRCC3 were lysed and Western blotted for RAD51C expression. RAD51C-R193X truncation mutant does not express. Each RAD51C reversion mutation restores expression. * indicates a non-specific band of the RAD51C antibody. Kar2 serves as a loading control. C. DR-GFP analysis in MCF10A cells measures HR proficiency which is lost for RAD51C-R193X and restored for each reversion mutation. D. MCF10A nuclear extracts show that RAD51C-R193X is not expressed and each RAD51C reversion mutation restores RAD51C expression. PCNA serves as a loading control.

By performing thorough analysis of RAD51C cancer-associated mutations and SNPs, we identified regions of RAD51C critical for its protein-protein interactions and HR function. We aim to use this information to identify patients who will be candidates for current therapies directed toward HR-deficient tumors, such as PARPi. By re-categorizing variants of unknown significance in RAD51C into clinically useful and treatable information, cancer patients can be better and more selectively treated with the most appropriate therapy to increase overall survival.

3.4 DISCUSSION

3.4.1 *RAD51C* point mutations impair genome stability

Here we examined RAD51C cancer-associated mutations and SNPs for altered protein-protein interactions, viability, HR function, and response to chemotherapy. We find that residues in and around the Walker A motif of RAD51C are important for its protein-protein interactions, HR function, viability, and resistance to genotoxic agents. We propose that maintenance of the Walker A motif of RAD51C is a critical region for function of RAD51C and thus for the prevention of breast and ovarian cancer and that mutations in this region that impair RAD51C function may

predispose individuals to cancer. Furthermore our work suggests that these patients may be good candidates for combination therapies that are currently being used to treat BRCA-deficient tumors. By uncovering which RAD51C mutations will be vulnerable to therapies targeting HR-deficiency, clinicians can be better identify patients that will benefit from therapies currently exclusively used for BRCA1/2 patients.

Our results highlight the importance of the Walker A motif of RAD51C, not only for function, but also for maintaining protein-protein interactions. One could have predicted that the Walker A motif would be critical for RAD51C function, but it was surprising that the Walker A motif was also necessary for maintaining protein-protein interactions with the other RAD51 paralogs. While no crystal structures of RAD51C or any of the other human RAD51 paralogs currently exist, we used the I-TASSER server to generate a predictive RAD51C structure (Figure 18). Within this structure, the ATP binding region, highlighted in purple, is in close proximity to the seven residues that are in or proximal to the Walker A motif (Figure 18). RAD51C-T132, C135, L138 are all part of the predicted alpha helix of the ATP binding region, and A126 and T132 are the predicted ATP binding residues of the Walker A motif. If A126 indeed binds ATP, it is interesting that the mutation confers no deleterious phenotypes. It is possible that the alanine to threonine substitution does not impair coordination of the ATP molecule. This residue varies between alanine and valine in vertebrate species (Supplemental Figure 14) and was also a prevalent SNP in the population (Table 5). Because we observed different phenotypes for RAD51C-G125S and RAD51C-G125V in maintaining protein-protein interactions, our data suggests that location of the mutation as well as the amino acid change affects cell survival and HR phenotypes. Similarly, future work will also investigate the importance of the specific amino acid change at the cysteine 135 residue. A recently identified a breast/ovarian cancer mutation C135R will be

compared to the phenotypes observed for C135Y (Ding et al. 2017). As C135Y and G125V did not interact with RAD51 paralogs or complement survival in MCF10A cells, testing survival of C135R will be informative to understand if this cysteine residue is critical for survival or if like glycine 125 these phenotypes are specific to the amino acid change. Preliminary results suggest that C135R similarly loses protein-protein interactions with RAD51 paralogs by Y2H (McKenzie Grundy, unpublished data). While we were able to analyze single point mutations in RAD51C, we did not investigate phenotypes of truncation mutations to identify regions that may be critical for binding or activity. Truncation mutations in RAD51C resulted in a loss of expression of RAD51C (see below, and data not shown). *In vitro* work may help to clarify the importance of these residues and mutations for ATP binding and promotion of RAD51 filament formation. These studies will test complex formation of RAD51C mutants G125V, T132P, and C135Y, within the BCDX2 and CX3 complexes which could help clarify if ATP binding is required for RAD51C interaction with the other RAD51 paralogs or if ATP binding is only required for activity of the complex.

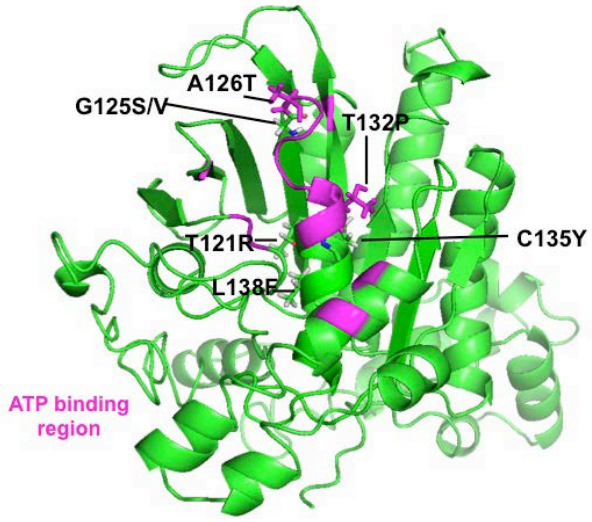

Figure 18. RAD51C Walker A mutant model.

RAD51C mutants around the Walker A motif are predicted to cluster around the ATP binding region indicated in purple. RAD51C Walker A mutants include, T121R, G125S, G125V, A126T, T132P, C135Y, and L138F. I-TASSER server was used to predict a RAD51C structure (Yang et al. 2015).

3.4.2 Walker A and B motifs are critical to RAD51 paralogs

Walker A and B motifs are maintained in all of the human RAD51 paralogs (Miller et al, 2004; Lin et al, 2006). Biochemical evidences suggests the RAD51 paralog Walker A and B motifs are needed for ATP binding and could also hydrolyze ATP to promote RAD51 filament formation *in vitro* (Masson et al, 2001a, Masson et al, 2001b, Sigurdsson et al, 2001; Braybrooke et al, 2000; Kurumizaka et al, 2002). Recently, the two *C. elegans* RAD51 paralogs, RFS-1 and RIP-1, have been purified. These RAD51 paralogs were shown to increase RAD51 filament remodeling to promote strand exchange activity (Taylor et al, 2015; Taylor et al, 2016). Importantly, these studies revealed that RFS-1 and RIP-1 activity required nucleotide binding but not ATP hydrolysis and that mutations in either the Walker A or B motif of RFS-1 disrupted its interaction with RIP-1 and

compromised strand exchange (Taylor et al, 2015; Taylor et al, 2016). The *C. elegans* RAD51 paralogs provide new *in vitro* insights for possible activities of human RAD51 paralogs.

While *in vitro* work on the RAD51 paralogs has been limited, cellular studies have demonstrated the importance of Walker A motif. Two mutations around the Walker A motif in RAD51D have similarly been shown to have disrupted protein-protein interactions and decreased HR proficiency. In fact, RAD51D-G107V is the first glycine residue of the Walker A motif and is the same position and amino acid change as RAD51C-G125V (Baldock et al. in revision). This RAD51D mutation disrupts its interaction with both RAD51C and XRCC2 (the two binding partners of RAD51D) mirroring the RAD51C disrupted interactions with RAD51B, RAD51D, and XRCC3. Also similar to RAD51C-G125V, RAD51D-G107V also showed decreased HR proficiency by the DR-GFP assay in RAD51D knockout U2OS cells (Baldock et al. in revision). These similarities suggest that defects in the Walker A motif of the RAD51 paralogs could be a common mechanism in cancer predisposition. The Walker A motifs of the RAD51 paralogs may not be needed for ATPase activity directly, but they are required for maintaining protein-protein interactions between RAD51 paralogs. These interactions are necessary for maintaining function as the RAD51 paralogs are only stable within complexes. To more precisely define the step of HR leading to decreased HR proficiency by the DR-GFP assay, each HR step could be monitored by immunofluorescence assays. In cells with individual RAD51 paralog mutations, foci formation/persistence of canonical HR proteins (i.e. MRE11, RPA, RAD51, BLM) could identify the step(s) in the HR process impacted by mutation of individual RAD51 paralogs.

3.5 ACKNOWLEDGEMENTS

A modified version of this paper is in preparation for submission:

Uncovering how *RAD51C* mutations contribute to cancer predisposition

*__Sullivan MR__, *Prakash R, Baird J, Mihalevic MJ, Swisher E, Jasin M, Bernstein KA

* Denotes equally contributing authors

Table 4 (MRS); Table 5 (MRS); Supp Fig 6 (MRS); Table 6 (MRS); Fig 12A,B,C,D (MRS), E (MRS, MJM, JB); Supp Fig 7 (MRS, JB, MJM); Supp Fig 8 (MRS, MJM); Supp Fig 9 (MRS); Supp Fig 10 (MRS); Supp Fig 11 (MRS); Supp Fig 12 (MRS); Supp Fig 13 (RP); Fig 13 (MRS); Fig 14A (MRS), B (RP); C (MRS; RP); D,E (RP); Supp Fig 14 A (MRS, RP), B (RP); Fig 15 (MRS); Supp Fig 15 (MRS; RP); Fig 16 (SRH)

Additionally, a modified version of Figures 17 and 18 has been published at *Cancer Discovery*:

Kondrashova, O., M. Nguyen, K. Artin-Shield, A.V. Tinker, N.H. Teng, M.I. Harrell, M.J. Kuiper, G.Y. Ho, H. Barker, M. Jasin, R. Prakash, E.M. Kass, M.R. Sullivan, G.J. Brunette, K.A. Bernstein, R.L. Coleman, A. Floquet, M. Friedlander, G. Kichenadasse, D.M. O'Malley, A. Oza, J. Sun, L. Robillard, L. Maloney, D. Bowtell, H. Giordano, M.J. Wakefield, S. Kaufmann, A.D. Simmons, T.C. Harding, M. Raponi, I.A. McNeish, E.M. Swisher, K.K. Lin, C.L. Scott, AOCS Study Group (2017) Secondary somatic mutations restoring *RAD51C* and *RAD51D* associated with acquired resistance to the PARP inhibitor rucaparib in patients with high-grade ovarian carcinoma. *Cancer Discovery*, 7(9):984-998.

Fig 18 A (GJB), B (MRS), C (RP), D (MRS)

We thank David Schild for XRCC3 Y2H plasmids, Jun Huang for the cDNA used to generate *RAD51C* and *RAD51B* plasmids, and Paul Russell for providing *RAD51D* cDNA. We thank Sarah Hengel for producing the RAD51C model from I-TASSER. We thank all of the women who participated in the ARIEL2 study.

4.0 GENERAL DISCUSSION

This research aimed to characterize RAD51 regulatory factors that promote HR to ultimately preserve genome stability. Here, we investigated RAD51 paralog complexes to show that disruption of these complexes through loss or mutation has deleterious consequences on genome stability. This research provides a framework in which to understand the emerging importance of the RAD51 paralog mutations in cancer predisposition.

4.1 A NEW MODEL IN WHICH TO STUDY THE SHU COMPLEX

The conservation of the RAD51 paralogs throughout eukaryotes has enabled us to perform studies in model organisms that inform studies in human systems. Our work on the *C. elegans* Shu complex, a RAD51 paralog-containing complex, will help to guide future studies in cell culture and mouse models to ultimately understand the role of the human Shu complex and why mutations in RAD51 paralogs are associated with cancer predisposition. The lethality and infertility of mouse models has limited study of RAD51 paralogs in a muliticellular organism. Future study of the Shu complex in *C. elegans* provides a viable and fertile model in which to study a RAD51 paralog-containing complex. Discussed here are insights gained and outstanding questions about the *C. elegans* Shu complex and its mammalian counterpart.

4.1.1 Insights provided by the evolutionarily conserved Shu complex in *C. elegans*

C. elegans sws-1 was identified as an *S. cerevisiae* Shu2 ortholog through its evolutionarily conserved zinc-finger binding SWIM domain (Godin et al. 2015). Through our work, we showed that *sws-1* was not only evolutionarily conserved, but also functionally conserved and interacts with RAD-51 paralogs, *rfs-1* and *rip-1*, similar to the yeast and human Shu complexes (Chapter 2). Given the conservation of the Shu complex throughout eukaryotes, our work in *C. elegans* can be used to inform studies of the human Shu complex comprised of *SWS1* and *SWSAP1*. Previously, I had shown that mutations at highly conserved residues of the SWIM domain in human *SWS1* disrupted interaction with *SWSAP1* by Y2H (Godin et al, 2015). It is possible that this loss of interaction between SWS1 and SWSAP1 was due to the loss of zinc binding in SWIM domain mutants. As *SWSAP1* is a highly divergent human RAD51 paralog, this gene will be an interesting candidate in which to investigate cancer-associated mutations as we have done for *RAD51C*. Cancer-associated mutations in *SWSAP1* and *SWS1* have not yet been included in breast and ovarian cancer screening panels. However, it is plausible that mutations in these RAD51 regulators will have similar prevalence in cancers associated with mutations in the canonical RAD51 paralogs. For example, a homozygous *SWS1* mutation has been identified in a colorectal adenomatous polyposis (Spier et al. 2016). The increase of patient screening and more in-depth patient profiling will reveal if the Shu complex RAD51 regulators, *SWS1* and *SWSAP1*, emerge as cancer-predisposition genes as the canonical RAD51 paralogs have in recent years.

4.1.2 Could the Shu complex be a therapeutic target?

The Shu complex has selective sensitivity to genotoxic agents unlike other RAD51 paralogs. In yeast, the Shu complex has been shown to have unique sensitivity to MMS but not to classical DSB-inducing agents, such as IR or etoposide (Godin et al. 2016b). Forthcoming work shows that loss of the Shu complex in human cell lines also show this unique MMS sensitivity (Martino et al, unpublished work). In a base excision repair (BER)-deficient setting, the Shu complex becomes particularly important to respond to repair intermediates during S phase (Godin et al, 2016b). When BER intermediates occur in S phase, they can collide with a replication fork causing stalling or collapse. These lesions can be repaired using HR machinery to promote error-free damage tolerance. The Shu complex is known to bind to replication fork substrates and is thought to play a role in processing these repair intermediates as Shu mutant yeast cells lacking DNA glycosylases are particularly sensitive to MMS (Gaines et al 2015; Godin et al 2016b). Like other RAD51 paralogs, the Shu complex may promote RAD51 activity in these contexts, but unlike other RAD51 paralogs, its activity is highly specialized to a particular substrate (Gaines et al 2015). This selectivity suggests that the Shu complex could be a good therapeutic target in a similar manor to PARPi treatment of HR-deficient tumors. Inhibition of the Shu complex could be a target with few deleterious outcomes in surrounding tissue. Unlike the canonical RAD51 paralogs or other RAD51 regulators, which are essential for survival, loss of *SWS1* or *SWSAP1* is tolerated in mouse models (Abreu et al, 2018). This recent discovery provides a new model in which to study the consequences of loss of the Shu complex and how it could be used as a therapeutic target. The combination of loss of the Shu complex with DSB-inducing agents used in the clinic such as MMC, MMS, or cisplatin could have synthetic lethal effects that could be targeted in Shu complex-deficient tumors or using a Shu complex inhibitor.

4.1.3 Genetic studies of the Shu complex inform biochemical studies

Although biochemical work on the RAD51 paralogs has been extremely limited, recent work using the *C. elegans* Shu complex has provided new data that has implications for RAD51 paralogs throughout eukaryotes (Taylor et al, 2015; Taylor et al, 2016). Single molecule studies observed by TIRF microscopy have revealed a possible new role for the RAD51 paralogs as regulators of homology search and strand invasion HR steps by remodeling RAD51 nucleoprotein filaments (Figure 3B). In Chapter 2, SWIM domain mutants of SWS-1 and Walker A and B mutants of RIP-1 and RFS-1 were critical for protein-protein interactions. These residues were later hypothesized to be critical for maintaining end capping of the RAD51 nucleoprotein filament (Taylor et al, 2016). Testing Walker A and B and SWIM domain mutants in these single molecule studies will provide insight their regulation of RAD51 and could be expanded to other model organisms. This model was extended to the *S. cerevisiae* Shu complex to similarly propose Walker A and B and SWIM domains would be critical to end capping activity. Given that the *S. cerevisiae* Shu complex was also recently crystalized and shown to form a horseshoe-like shape, the *C. elegans* and *S. cerevisiae* Shu complexes may have more similar conformations than previously thought (Zhang et al. 2017b). Future work to uncover if the structure of the human Shu complex has similar conformation and may also have end capping activity.

4.1.4 Can the Shu complex in model organisms reveal new human Shu complex binding partners?

We do not yet know the composition of the human Shu complex. It is minimally composed of SWS1 and SWSAP1, and several other binding partners have been proposed including several

RAD51 paralogs (Martin et al, 2006; Liu et al, 2011). However, the only validated RAD51 paralog binding partner of SWS1 is SWSAP1. Given the composition of *C. elegans* and *S. cerevisiae* Shu complexes have been composed of multiple RAD51 paralogs (two or three respectively), it will be interesting to see if new binding partners of the human Shu complex are also revealed to be RAD51 paralogs.

New evidence suggests a new RAD51 paralog may be conserved in humans and is a good candidate for the human Shu complex. Human FIGNL1 contains a AAA-ATPase domain and was shown to bind RAD51 (Yuan and Chen 2013). Recently, work on the FIGNL1 rice homolog, OsFIGNL1, revealed this AAA-ATPase protein contained Walker A and B motifs and that OsFIGNL1 interacts with rice RAD51 paralogs by Y2H (Zhang et al. 2017a). Together, this evidence supports the conservation of yet another RAD51 paralog throughout species. Because the Shu complex is well conserved among eukaryotes, we recently investigated if the *C. elegans* FIGL-1 interacted with known *C. elegans* RAD51 paralogs by Y2H. We found *C. elegans* RIP-1 interacts with a novel binding partner, FIGL-1, and this interaction was disrupted by the Walker A D131A *RIP-1* mutation (Chelsea Smith, unpublished data, Bernstein lab). RIP-1 is one of two RAD51 paralogs in the *C. elegans* Shu complex. Given the high conservation of *C. elegans* FIGL-1 and human FIGNL1, it will be interesting to determine if FIGNL1 is a human Shu complex member. Furthermore, FIGL-1 and FIGNL1 are putative RAD51 paralogs based on the identification of OsFIGNL1 as a RAD51 paralog (Zhang et al, 2017a). We have proposed RIP-1 to be the equivalent of human SWSAP1 as these RAD51 paralogs interact directly with SWS-1 or SWS1, respectively. Thus the RIP-1 interaction with FIGL-1 may suggest a similar interaction between SWSAP1 and FIGNL1. Using the Y2H system to investigate other Shu complex members, as we did to identify SWS-1 interactions, new Shu complex members could be identified in *C. elegans* as well as

humans. As is needed for the known human RAD51 paralogs, future biochemical work will reveal if FIGNL1 binds or hydrolyzes ATP through its Walker A and B motifs like RAD51.

4.2 RAD51C MUTATIONS AND GENOME STABILITY

The ultimate goal of our work is to link specific *RAD51C* mutations to precision medicine strategies by understanding the basic biology of RAD51C function and how mutations within *RAD51C* disrupt that function. We aimed to use RAD51C mutants that are currently considered to be variants unknown significance (VUSs) and correlate them with specific phenotypes to predict the therapeutic sensitivity of cells expressing RAD51C mutants. Further this analysis would provide a framework to identify specific cancer-associated *RAD51C* mutations that would be sensitive to therapies similar to those currently used in *BRCA1/2*-deficient tumors (Figure 19).

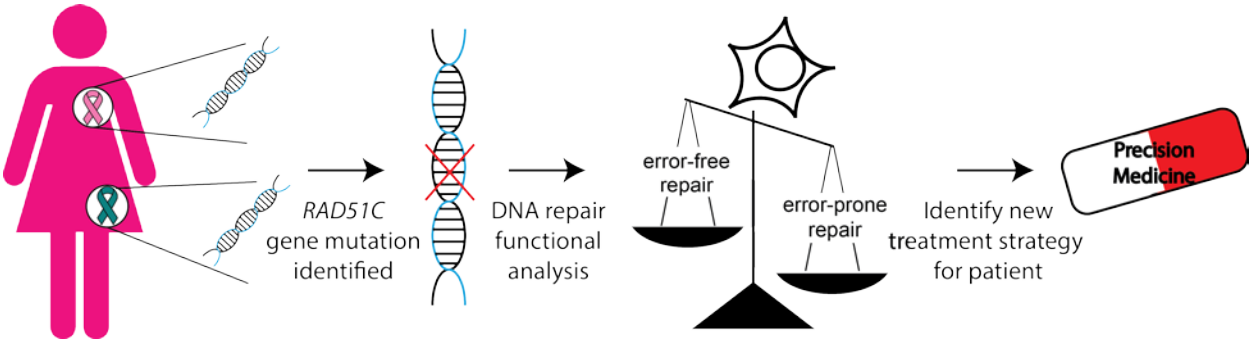

Figure 19. Precision medicine strategy for RAD51C-mutated cancers.

By identifying gene mutations in RAD51C (left) and assessing their DNA repair function (center), we can determine if cells will be competent for homologous recombination or will rely on a more error-prone repair alternative (center) to select the most appropriate therapeutic strategy for that patient (right).

4.2.1 Understanding RAD51C in p53 proficient and deficient contexts

Our studies in MCF10A cells aimed to understand RAD51C function in a normal context expressing functional p53 (Chapter 3). However, this required the use of a conditional knockout model as loss of RAD51C is not tolerated in a p53 proficient background (Garcin et al, submitted). Therefore, most previous work studying RAD51C mutants has used RAD51C mutant hamster cells (CL-V4B) (Somyajit et al. 2015a). In this model, p53 is mutated and tolerates loss of RAD51C through an unknown mechanism. Using this model, emerging evidence suggests that, like BRCA1/2, some RAD51C mutants could be targeted by PARPi (Somyajit et al, 2015a). RAD51C mutants in RAD51C mutant hamster cells are sensitive to PARPi alone and in combination with IR. They showed an increase in chromosomal aberrations and increased NHEJ before cell death (Somyajit et al, 2015a). This compelling evidence underscores the need to determine which *RAD51C* mutations will affect RAD51C function thus sensitizing cells to PARPi strategies.

Alternatively, RAD51C mutant fibroblasts from the FA-like patient (SH20238-F) have been complemented with RAD51C mutants and show decreased RAD51 foci (Meindl et al, 2010). Our work here suggests that RAD51C-R258H could be a dominant negative allele as it was highly enriched in co-immunoprecipitation experiments with RAD51B but did not interact with XRCC3. Therefore, the work in Meindl et al presents a problem, as the presence of RAD51C-R258H in this cell line may be a confounding variable in these experiments. Further implications of RAD51C-R258H are discussed in the following section. RAD51C mutants analyzed in CL-V4B and SH20238-F cells are summarized in Table 7. While these initial studies provided the first insights to the consequences of RAD51 point mutations, we do not know how the loss of p53 or the presence of RAD51C-R258H in these studies influenced their functional analysis. Therefore, our

studies in p53-proficient, RAD51C-deficient background are the first insight into phenotypes of RAD51C mutants without these confounding factors (Chapter 3). We analyzed protein-protein interactions and homologous recombination proficiency, but much future work remains to be done to understand the consequences of *RAD51C* mutations. Future studies using this model can investigate specific steps of HR with more sensitive assays such as RAD51 foci formation as well as the role of RAD51C in the DDR, replication fork protection, and ICL repair. The many nuances of RAD51C function that all cumulatively influence genome stability will clarify how individual RAD51C mutations contribute to cancer predisposition.

Future biochemical assays will be instrumental to understand RAD51C function. Similar to studies performed with purified yeast Rad51 paralogs, Rad55-57 and the Shu complex, future studies with purified human RAD51 paralogs will reveal if they similarly promote Rad51 filament formation and strand exchange activities (Sung 1997b; Gaines et al 2015). Further biochemical studies can also inform which substrates the RAD51 paralogs preferentially bind such as the specificity of the yeast Shu complex for forked DNA substrates (Gaines et al 2015). Importantly, these types of biochemical assays could be used to determine if RAD51C mutants have decreased affinity for binding a particular substrate or fail to promote RAD51 activity.

Mutation	Previous Publications	survival after MMC, HU, MMS, or CPT in CL-V4B cells	RAD51 foci in complemented RAD51C-mutant FA fibroblasts	MMC-induced chromatid breaks and radials in CL-V4B cells	HR by DR-GFP in CL-V4B cells	Interaction with XRCC3 in CL-V4B cells	Sensitivity to PARPi (4-ANI) + IR in CL-V4B cells	Fork protection and restart in CL-V4B cells
R12W								
D108Y								
T121R								
G125S								
G125V	1,3,5	no (3,5)	no foci (1)	high (5)	low (3,5)	reduced (5)	high (3)	
A126T	1,2							
T132P								
C135Y	2		reduced foci (2)					
L138F	1,2,3,4,5	no (3,5)	reduced foci (1)	high (5)	low (3,5)	reduced (5)	high (3)	low (4)
I144T								
G153D								
D159N								
G162E								
L219S	2,3	no (3)	no foci (2)		low (3)		high (3)	
P247L								
R249C								
R258H	4,5	reduced (3,5)			reduced (5)	reduced (5)		low (4)
A279V								
T287A	1,3,5	reduced (3,5)		moderate (5)	reduced (3,5)	reduced (5)	moderate (3)	
A308T								
R312W								
A324T								
P330H								

Table 7. Previous molecular analysis of RAD51C mutations.

RAD51C mutations previously studied are indicated in the first column as listed. The conclusions of each investigation are summarized in subsequent columns from the following studies: 1. Meindl A., et al., 2010 Nature Genetics. 2. Osorio A., et al., 2012 Human Molecular Genetics. 3. Somyajit K., et al., 2015 Carcinogenesis. 4. Somyajit K., et al., 2015 Nucleic Acids Research. 5. Somyajit K., et al., 2012 Journal of Biological Chemistry.

4.2.2 RAD51C/FANCO in Fanconi anemia-like syndromes

The significance of RAD51C in maintaining genome stability has been primarily associated with cancer predisposition but is also underscored by cases of Fanconi anemia-like (FA-like) syndromes in patients with *RAD51C* mutations. It is intriguing that heterozygous *RAD51C* mutations predispose to cancer and only the tumor itself displays LOH, while biallelic germline mutations can lead to FA-like syndromes leading to the classification of RAD51C to receive a FANC

complementation group, FANCO (Vaz et al, 2010; Jacquinet, 2018). Two distinct cases have been reported thus far which have interesting and significant differences. The first case had biallelic point mutations (R258H), whereas the second had two distinct mutant alleles, a point mutation (R312Q) and a RAD51C splice variant (Vaz et al, 2010; Jacquinet, 2018). It remains to be determined if two mutated copies of RAD51C are necessary to confer FA-like syndromes or if dominant negative mutations in RAD51C could also cause FA-like syndromes. Interestingly, our findings suggest that RAD51C-R258H may be a dominant negative mutation as it binds RAD51B two-fold more tightly than does WT RAD51C in co-immunoprecipitations (Chapter 3). This binding could sequester RAD51C within the BCDX2 complex and limit RAD51C binding with XRCC3 in the CX3 complex. Further investigation of this particular mutation in our MCF10A model will be of particular interest. For example, co-infecting cells with wild-type RAD51C and RAD51C-R258H could reveal deleterious phenotypes by titrating different ratios of the two RAD51Cs.

Recently a dominant negative RAD51 mutation within the Walker A motif (T131P) was identified in a FA-like syndrome (Wang et al. 2015). The RAD51 Walker A motif mutant mirrors the phenotypes in our study of RAD51C Walker A mutants (Chapter 3). RAD51-T131P was critical for ATP binding and hydrolysis. While it did not display impaired HR through the DR-GFP assay, these cells were sensitive to genotoxins that produce more complex lesions including MMC and PARPi. We found that RAD51C mutations that exhibit partial protein-protein interactions but are HR proficient can still exhibit sensitivity to cisplatin in combination with Olaparib. These results suggest that it is possible that some RAD51C mutations may have replication fork protection defects independent from RAD51C HR function. RAD51C-R258H could also be used as a separation-of-function mutant as discussed in the following section.

It is interesting to note that all the members of the recently described PALB2-RAD51-RAD51C-BRCA2 complex are FA genes as well as cancer-associated (Park et al, 2013). While the function of this complex is unknown, it is tempting to speculate that perhaps there is a commonality that has yet to be experimentally addressed. Since the RAD51 paralogs interact with each other to function in complexes and their stability is intimately intertwined, it is possible that more FA patients with mutations in the RAD51 mediators may be identified. The emerging role of RAD51C and potentially other RAD51 paralogs in ICL repair is still an emerging field of study, and we have yet to determine if these proteins are playing roles upstream of canonical HR during ICL repair.

4.2.3 Separation of function mutations in *RAD51C*

Analysis of RAD51C mutant protein-protein interactions also provides an opportunity to further separate the distinct roles of the individual RAD51C-associated complexes in repair. We identified several RAD51C mutants that disrupt function with only one or two of the three binding partners. For example, by co-immunoprecipitation, L219S maintains interaction with RAD51B but loses interaction with XRCC3 (Chapter 3). Similarly P247L maintains interaction with RAD51B but partially loses interaction with XRCC3 (Chapter 3). These mutations are nearby the Walker B motif (aa238-242) and may be important for maintaining the integrity of the CX3 complex. We did not have any *RAD51C* mutations closer to the Walker B motif. It will therefore be interesting to see if other cancer-associated mutations fall near or within the Walker B motif. Additionally, mutations introduced into the conserve Walker B residues may disrupt CX3 but maintain BCDX2. These mutations could then be used to identify roles distinct for the CX3 complex. Similarly, the

FA-like RAD51C-R258H mutant which binds RAD51B more tightly than does wild-type RAD51C could be used to identify these functions in future studies.

4.2.4 Structure/function analysis of RAD51C

Although we do not have crystal structures of the RAD51 paralogs, we have used the I-TASSER protein structure prediction server to model the probable physical locations of our RAD51C mutants (Yang and Zhang, 2015; Sarah Hengel unpublished data). This model revealed patterns that were not obvious in our linear RAD51C schematic. While we may have hypothesized that the mutations that disrupt protein-protein interactions would be surface residues, we instead found that mutations that disrupted Y2H interactions clustered around the Walker A and B motifs in 3D space (Figure 20-compare Y2H and Walker A and B motif images). Future RAD51 paralog protein structures will shed more light on regions of RAD51C that correlate with cancer-associated mutations or regions that mediate particular RAD51 paralog interactions.

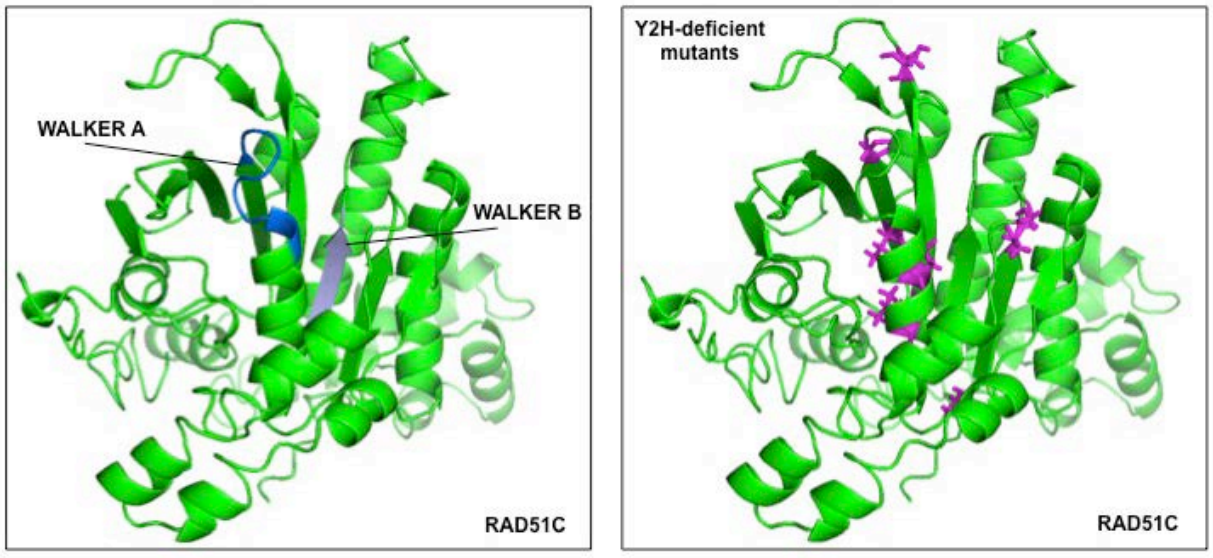

Figure 20. RAD51C modeling reveals mutation clustering.

Left: RAD51C Walker A and B motifs are highlighted in blue and grey respectively. Right: RAD51C mutants deficient for interaction with the BCDX2 or CX3 complexes are highlighted in purple. These mutations cluster primarily around the Walker A motif with a lesser number clustering around the Walker B motif.

4.3 CONCLUDING REMARKS: USING BASIC SCIENCE TO INFORM TRANSLATIONAL MEDICINE

My dissertation research focused on a novel RAD51 paralog-containing complex, the Shu complex, which we defined and characterized in *C. elegans* to show it is functionally conserved from yeast and primed studies for the human Shu complex (Chapter 2). We found that the *C. elegans* Shu complex is composed of the RAD-51 paralogs RFS-1 and RIP-1, which interact with SWS-1, and together are needed to stabilize RAD-51 in response to CPT resolve RAD-51 foci in meiotic HR. I additionally worked to characterize the human RAD51 paralog, RAD51C and its tumor variants. RAD51C point mutations proximal to the Walker A motif are particularly critical

for preserving genome stability and thus for preventing predisposition to breast and ovarian cancer. This work has expanded our knowledge of the RAD51 paralogs in cancer predisposition and therapeutic resistance. Future work will expand on these analyses to understand RAD51 paralog mutations on a larger scale, and if mutations in regions disrupting RAD51C function will be common to all RAD51 paralogs. Through our study of multiple RAD51 paralog-containing complexes, the field is now poised to fully uncover RAD51 paralog function and why their mutations contribute to cancer predisposition (Figure 21).

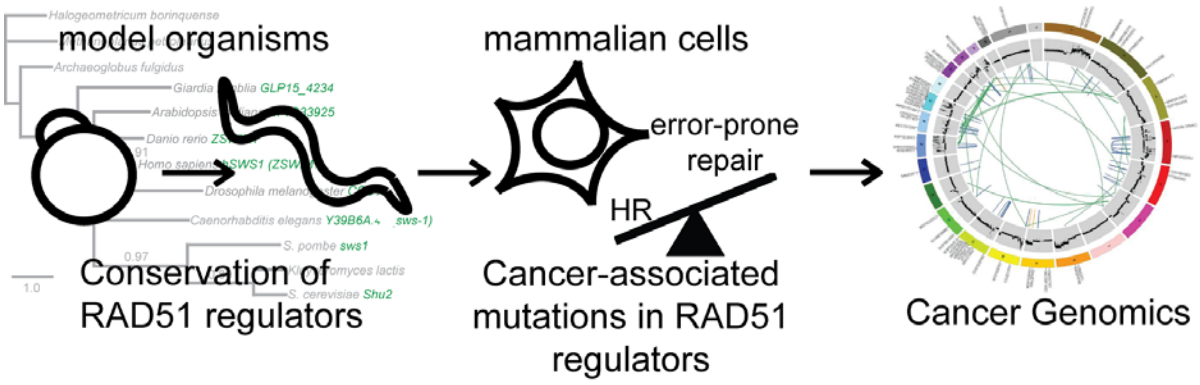

Figure 21. Using basic science to inform translational medicine.

We used classical genetic approaches to understand the underlying mechanisms of genomic instability, an enabling characteristic of cancer in RAD51 paralog mutated tumors. This growing field holds promise in predicting the best treatments for patients and that using new technologies will complement the classical genetic approaches that have been used to define the roles of the RAD51 paralogs

APPENDIX A

CHAPTER 2 SUPPLEMENTARY FIGURES AND TABLES

A.1 SUPPLEMENTAL FIGURES

Supplemental Figure 1.

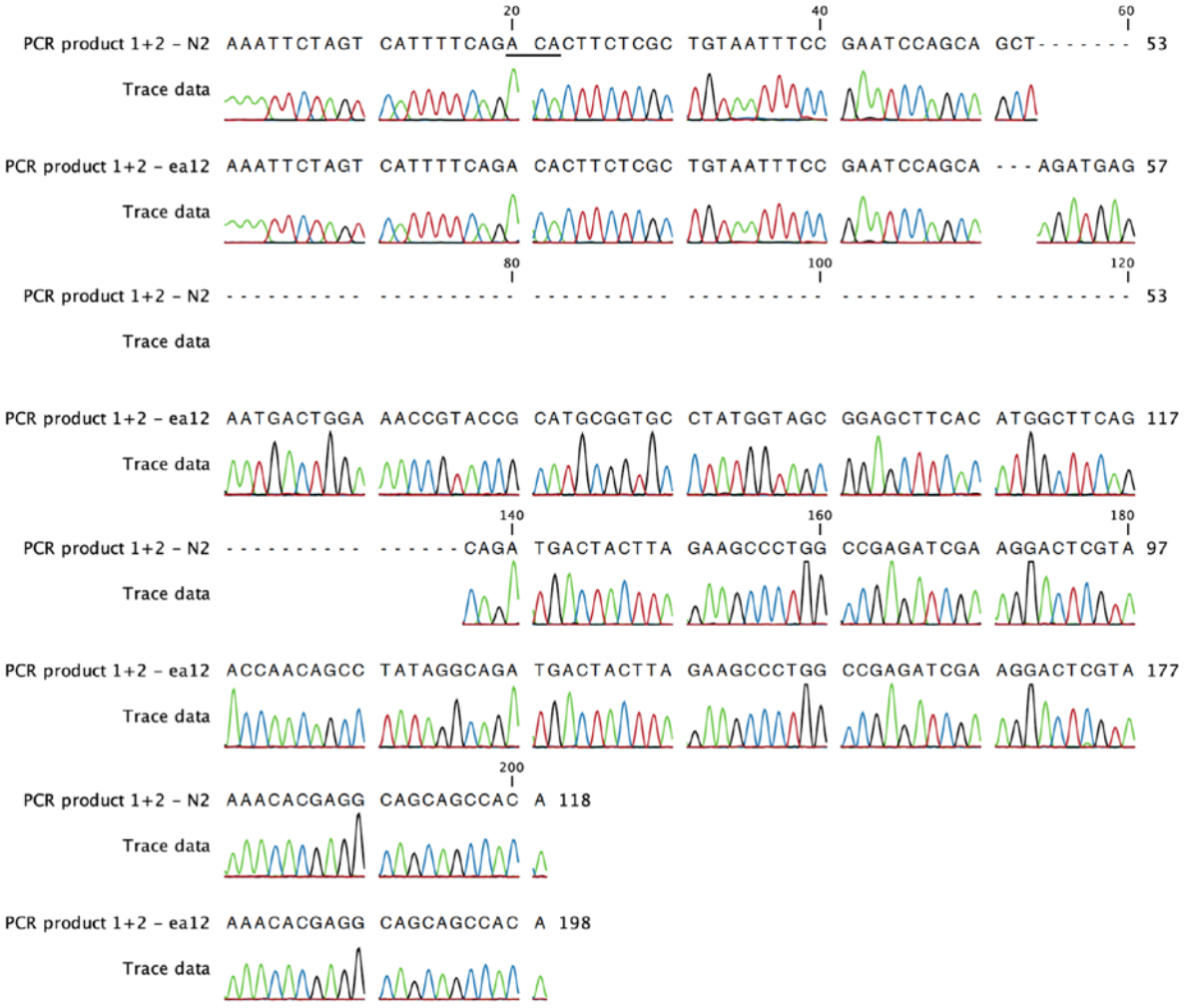

Supplemental Figure 1. Alignment of sws-1 exon 2 in N2 and ea12 Sequencing data for exon 2 of *sws-1* in N2 and *sws-1(ea12)* worms. PCR products were amplified with primers 1 and 2 and purified as described in Section 2.2.2. Line marks both beginning of exon 2 and establishes translation frame.

Supplemental Figure 2.

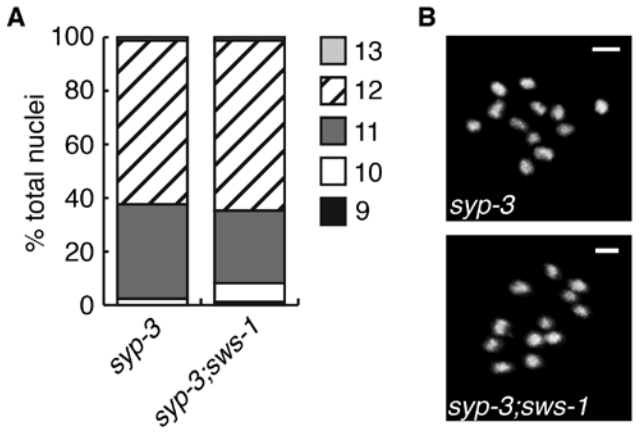

Supplemental Figure 2. sws-1 is competent for intersister HR A. Quantification of the number of DAPI-staining bodies at diakinesis in *syp-3* and *syp-3;sws-1* germ lines. The -1 and -2 oocytes were used for analysis (n=85 nuclei for both *syp-3* and *syp-3;sws-1*). B. Representative images of -1 oocytes showing 12 condensed univalents. Scale bar is 2 µm.

Supplemental Figure 3.

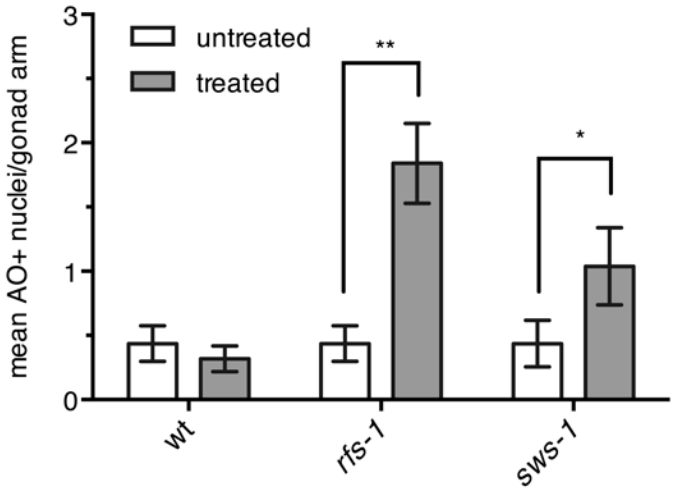

Supplemental Figure 3. Apoptosis increases in response to CPT in rfs-1 and sws-1 germ lines. Apoptosis in wt, *rfs-1*, and *sws-1* germ lines as determined by retention of acridine orange (AO) staining. Young adult hermaphrodites were treated with 0 (untreated) or 500 nM (treated) CPT and stained with AO in the timeframe corresponding to assessment of progeny survival (Figure 8) as described in Materials and Methods. The data are presented as mean AO-positive nuclei per gonad arm ± SEM for 25 hermaphrodites. * $p<0.05$, ** $p<0.001$, Mann-Whitney.

Supplemental Figure 4.

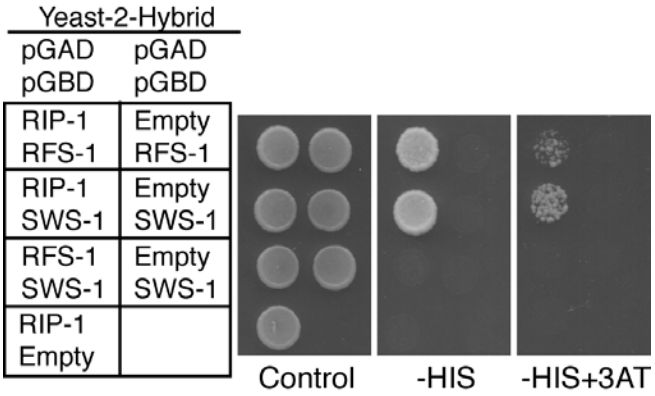

Supplemental Figure 4. SWS-1, RIP-1, RFS-1 Y2H interactions are also observed when the genes are cloned into the opposite pGAD or pGBD vectors shown in Figure 10.

SWS-1 interacts with RIP-1 when RIP-1 is expressed in the pGAD plasmid and SWS-1 is expressed in the pGBD plasmid. SWS-1 does not interact with RFS-1 when RFS-1 is expressed in the pGAD plasmid and SWS-1 is expressed in the pGBD plasmid.

Supplemental Figure 5.

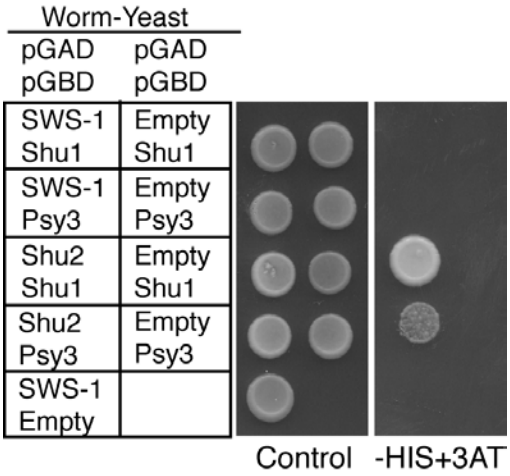

Supplemental Figure 5. Y2H of SWS-1 with yeast Shu complex components.Interactions between worm SWS-1 and yeast Shu1 or Psy3 were not detected. Controls show known interactions between the yeast SWS1 family member, Shu2, and its binding partners Shu1 and Psy3 on -HIS+3AT.

A.2 SUPPLEMENTAL TABLES

Supplemental Table 1.

Supplemental Table 1. Strains generated for Chapter 2.

STRAIN	GENOTYPE	REFERENCE IN TEXT
QP1203	*helq-1(tm2134)* III;*sws-1(ea12)* V	*helq-1;sws-1*
QP1204	*rfs-1(ok1372)* III;*sws-1(ea12)* V	*rfs-1;sws-1*
QP1205	*rip-1(tm2948)* III;*sws-1(ea12)* V	*rip-1;sws-1*
QP1206	*rfs-1(ok1372),rip-1(tm2948)* III;*sws-1(ea12)* V	*rfs-1,rip-1;sws-1*
QP1208	*sws-1(ea12)* V	*sws-1*
QP1179	*sws-1(ea12)* V;*unc-58(e665)* X	*sws-1;unc-58*
QP1234	*dog-1(gk10)* I;*sws-1(ea12)* V	*dog-1;sws-1*
QP1263	*syp-3(ok758)* I;*sws-1(ea12)* V	*syp-3;sws-1*

Supplemental Table 2.

Supplemental Table 2. Primers used in Chapter 2.

PRIMER	SEQUENCE (5'→3')
sws-1 5' gRNA	AAGTAGTCATCTGAGCTGCGTTTTAGAGCTAGAAATAGCAAGT
sws-1 3' gRNA	AGTGTAAATCCGAAATAGTGTTTTAGAGCTAGAAATAGCAAGT
1	AGCGGGAATTTGAAGATG
2	AGCTGGAAACTCTGAAAC
3	CCCATATTTCCAGTCAACC
4	GTGCCTGGAGTTGGAAAA
SWS-1.C133S.F	CATTATTGTACATCTCCATACTTTCAATC
SWS-1.C133S.R	GATTGAAAGTATGGAGATGTACAATAATG
SWS-1.A156T.F	GTGTTCATATTTTAACTTACTATTTTGC
SWS-1.A156T.R	GCAAAATAGTAAGTTAAAATATGAACAC
RIP-1.F	GCGGGATCCATGTCAGAATCGTGCAATTC
RIP-1.R	GCGGTCGACGAAAATTCATTTAATAAAAACC
RIP-1.D131A.F	GGTCGTCGTGATTGCTTTGAGAGATGAT
RIP-1.D131A.R	ATCATCTCTCAAAGCAATCACGACGACC
RFS-1.F	GCGAATTCATGGATCCTTCTGAGAATGTATTC
RFS-1.R	GAAGATCTTCATTCCACTGCTTTGAGTC

Supplemental Table 3.

Supplemental Table 3. One-way ANOVA multiple comparisons of lethality among genetic combinations of sws-1, rfs-1, and rip-1.

COMPARISON	MEAN DIFF.	95% CI OF DIFF.	p<0.05
sws-1 vs. *rip-1;sws-1*	5.867	-1.328 to 13.06	No
sws-1 vs. *rip-1*	2.121	-8.095 to 12.34	No
sws-1 vs. *rfs-1,rip-1*	-0.02070	-8.152 to 8.111	No
sws-1 vs. *rfs-1,rip-1;sws-1*	-3.880	-10.45 to 2.689	No
sws-1 vs. *rfs-1*	-0.9106	-9.319 to 7.498	No
sws-1 vs. *rfs-1;sws-1*	0.6105	-7.074 to 8.295	No
rip-1;sws-1 vs. *rip-1*	3.746	-7.013 to 14.50	No
rip-1;sws-1 vs. *rfs-1,rip-1*	-5.888	-14.69 to 2.915	No
rip-1;sws-1 vs. *rfs-1,rip-1;sws-1*	-9.748	-17.13 to -2.363	Yes**
rip-1;sws-1 vs. *rfs-1*	-6.778	-15.84 to 2.282	No
rip-1;sws-1 vs. *rfs-1;sws-1*	-5.257	-13.65 to 3.135	No
rip-1 vs. *rfs-1,rip-1*	-2.142	-13.55 to 9.264	No
rip-1 vs. *rfs-1,rip-1;sws-1*	-6.002	-16.35 to 4.349	No
rip-1 vs. *rfs-1*	-3.032	-14.64 to 8.574	No
rip-1 vs. *rfs-1;sws-1*	-1.511	-12.60 to 9.581	No
rfs-1,rip-1 vs. *rfs-1,rip-1;sws-1*	-3.860	-12.16 to 4.439	No
rfs-1,rip-1 vs. *rfs-1*	0.8899	-8.930 to 10.71	No
rfs-1,rip-1 vs. *rfs-1;sws-1*	-0.6312	-9.838 to 8.576	No
rfs-1,rip-1;sws-1 vs. *rfs-1*	-2.970	-11.54 to 5.601	No
rfs-1,rip-1;sws-1 vs. *rfs-1;sws-1*	-4.491	-12.35 to 3.371	No
rfs-1 vs. *rfs-1;sws-1*	1.521	-7.932 to 10.97	No

Tukey's test performed simultaneously with one-way ANOVA. Asterisks indicate multiplicity adjusted p values (** p<0.01).

Supplemental Table 4.

Supplemental Table 4. One-way ANOVA multiple comparisons of male frequency among genetic combinations of sws-1, rfs-1, and rip-1.

COMPARISON	MEAN DIFF.	95% CI OF DIFF.	p<0.05
sws-1 vs. *rip-1;sws-1*	-0.2374	-1.177 to 0.7025	No
sws-1 vs. *rip-1*	-1.151	-2.486 to 0.1833	No
sws-1 vs. *rfs-1,rip-1*	-1.568	-2.630 to -0.5058	Yes***
sws-1 vs. *rfs-1,rip-1;sws-1*	-1.798	-2.656 to -0.9398	Yes****
sws-1 vs. *rfs-1*	-1.583	-2.681 to -0.4846	Yes***
sws-1 vs. *rfs-1;sws-1*	-1.152	-2.156 to -0.1480	Yes*
rip-1;sws-1 vs. *rip-1*	-0.914	-2.319 to 0.4914	No
rip-1;sws-1 vs. *rfs-1,rip-1*	-1.331	-2.480 to -0.1808	Yes*
rip-1;sws-1 vs. *rfs-1,rip-1;sws-1*	-1.561	-2.525 to -0.5961	Yes****
rip-1;sws-1 vs. *rfs-1*	-1.346	-2.529 to -0.1622	Yes*
rip-1;sws-1 vs. *rfs-1;sws-1*	-0.9145	-2.011 to 0.1817	No
rip-1 vs. *rfs-1,rip-1*	-0.4167	-1.907 to 1.073	No
rip-1 vs. *rfs-1,rip-1;sws-1*	-0.6467	-1.999 to 0.7054	No
rip-1 vs. *rfs-1*	-0.4317	-1.948 to 1.084	No
rip-1 vs. *rfs-1;sws-1*	-0.0005128	-1.449 to 1.448	No
rfs-1,rip-1 vs. *rfs-1,rip-1;sws-1*	-0.23	-1.314 to 0.8541	No
rfs-1,rip-1 vs. *rfs-1*	-0.015	-1.298 to 1.268	No
rfs-1,rip-1 vs. *rfs-1;sws-1*	0.4162	-0.7865 to 1.619	No
rfs-1,rip-1;sws-1 vs. *rfs-1*	0.215	-0.9046 to 1.335	No
rfs-1,rip-1;sws-1 vs. *rfs-1;sws-1*	0.6462	-0.3808 to 1.673	No
rfs-1 vs. *rfs-1;sws-1*	0.4312	-0.8037 to 1.666	No

Tukey's test performed simultaneously with one-way ANOVA. Asterisks indicate multiplicity adjusted p values (* p<0.05, ** p<0.01, *** p<0.001, ****p<0.0001).

APPENDIX B

CHAPTER 3 SUPPLEMENTARY FIGURES AND TABLES

B.1 SUPPLEMENTAL FIGURES

Supplemental Figure 6.

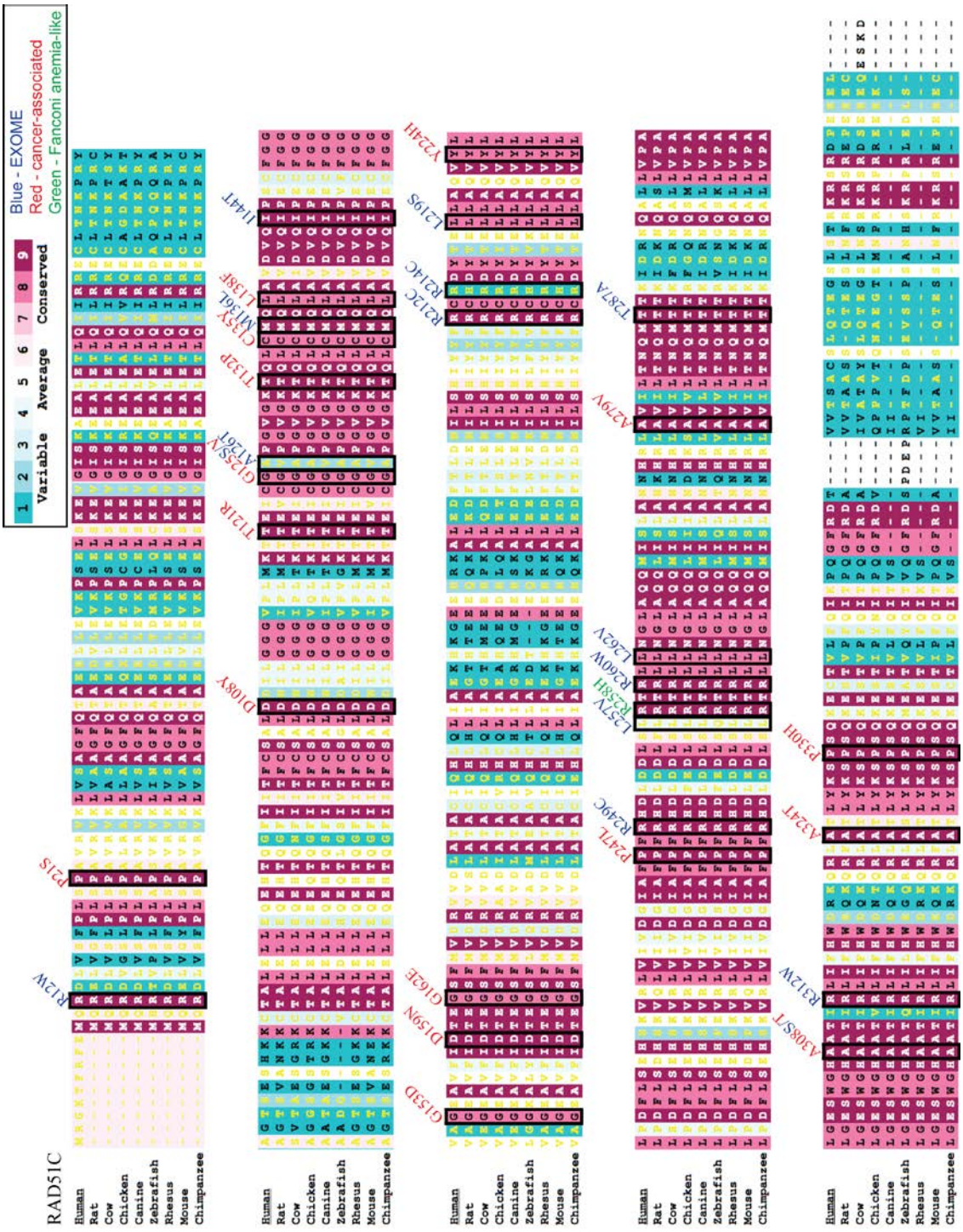

Supplemental Figure 6. ConSurf alignment of vertebrate RAD51C residues. ConSurf software was used to align 9 vertebrate species and indicates protein conservation based on primary amino acid sequence. Least conserved residues are indicated in blue and highly conserved residues are indicated in magenta as indicated

by the key. Human RAD51C mutations reported in this study are indicated along the top of each aligned row. SNPs are indicated in blue, cancer-associated mutations in red, and the Fanconi anemia-like mutation in green.

Supplemental Figure 7.

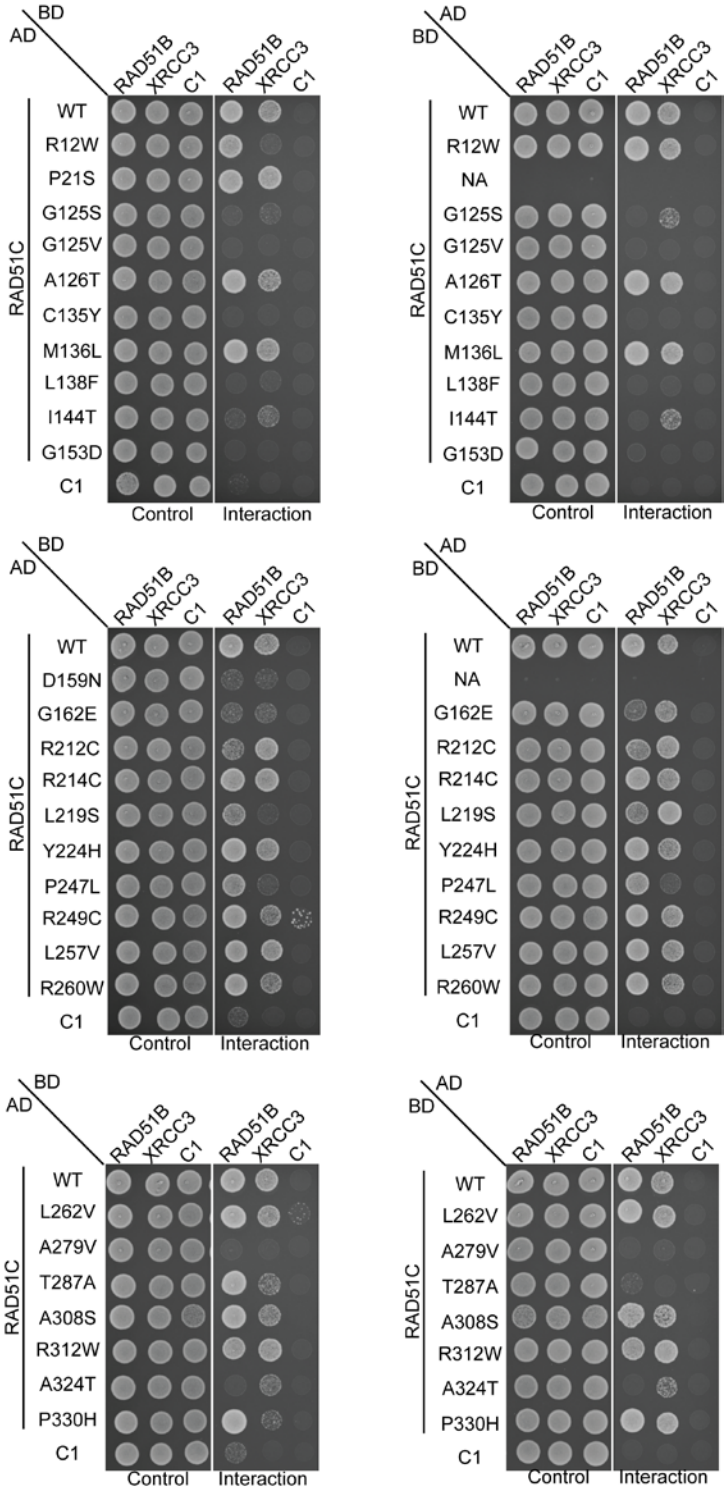

Supplemental Figure 7. Complete Y2H analysis of RAD51C mutant interactions.Physical interactions between RAD51C mutants and either RAD51B or XRCC3 were queried. Data on the left indicates RAD51C expressed in the pGAD plasmid and RAD51B or XRCC3 expressed in the pGBD plasmid, and data on the right indicates RAD51C expressed in the pGBD plasmid and RAD51B or XRCC3 expressed in the pGAD plasmid. C1 indicates an empty vector negative control. The control plates contain SC-LEU-TRP media to select for expression of each plasmid. The interaction plates indicate SC-LEU-TRP-HIS media for the expression of the reporter histidine indicating a direct interaction between the indicated RAD51 paralogs.

Supplemental Figure 8.

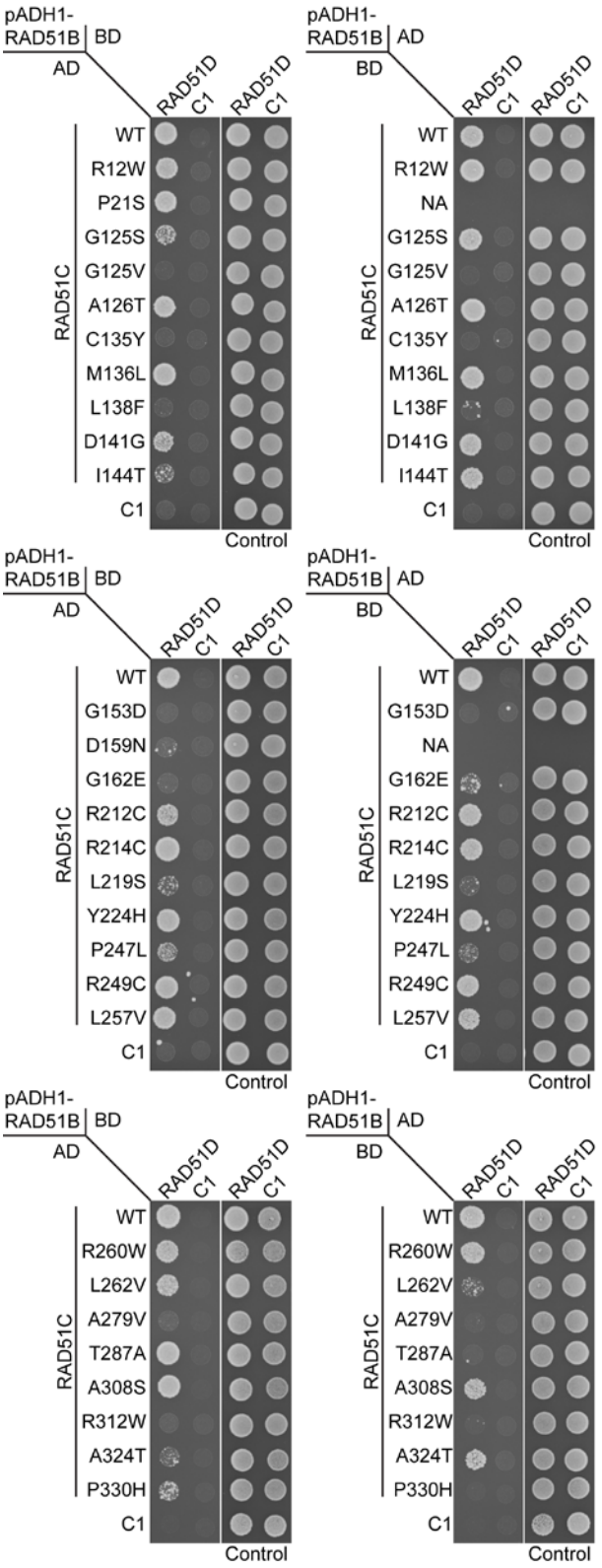

Supplemental Figure 8. Complete Y3H analysis of RAD51C mutant interactions. Physical interactions between RAD51C mutants and RAD51D were queried. Data on the left indicates RAD51C expressed in the pGAD plasmid and RAD51D expressed in the pGBD plasmid, and data on the right indicates RAD51C expressed in the pGBD plasmid and RAD51D expressed in the pGAD plasmid. pADH1-RAD51B is constitutively expressed RAD51B to stabilize RAD51C expression. C1 indicates an empty vector negative control. The control plates contain SC-LEU-TRP-URA media to select for expression of each plasmid. The interaction plates indicate SC-LEU-TRP-URA-HIS media for the expression of the reporter histidine indicating an interaction between the indicated RAD51 paralogs.

Supplemental Figure 9.

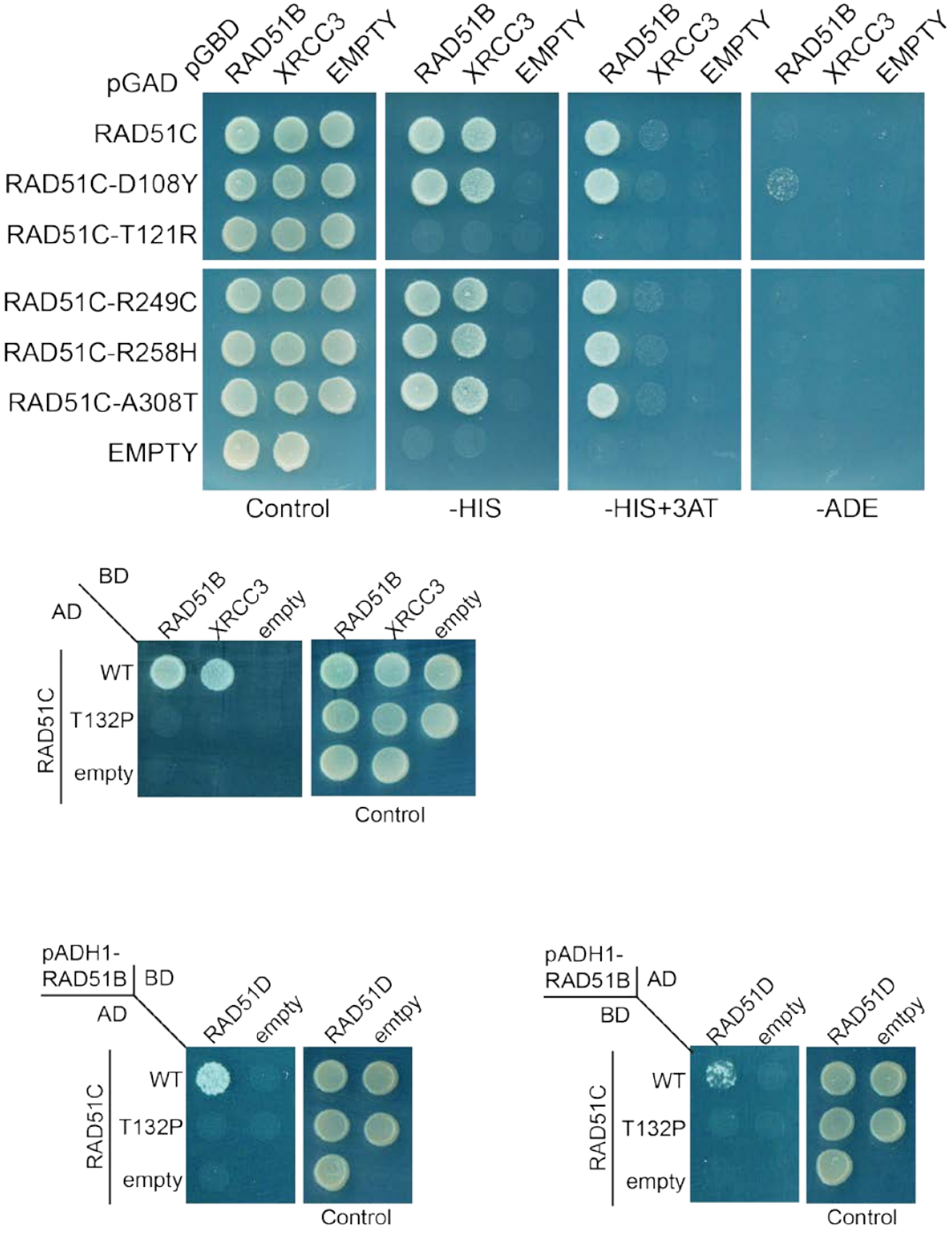

Supplemental Figure 9. Y2H and Y3H of RAD51C mutants from Memorial Sloan Kettering Database and Stand Up To Cancer Database.

Y2H interactions sourced from Memorial Sloan Kettering databases and the Stand Up to Cancer dream team were queried separately from initial screening but the same methodology was used for these experiments.

Supplemental Figure 10.

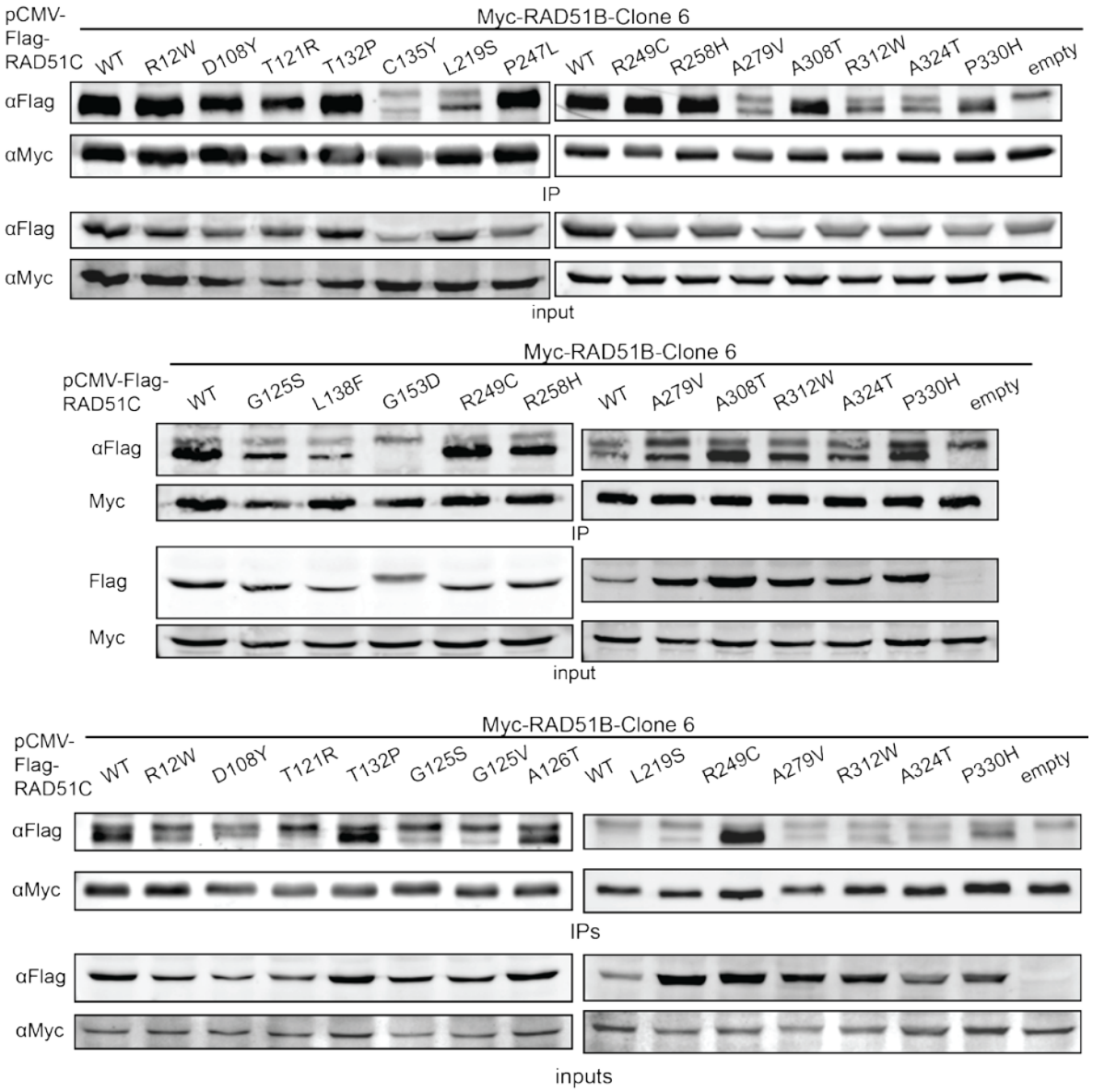

Supplemental Figure 10. Complete RAD51B IPs with RAD51C mutants. Complete set of representative U2OS co-immunoprecipitations are shown for RAD51C and RAD51C point mutations with RAD51B (In addition to Figure 12). IP indicates immunoprecipitations of Myc-RAD51B. co-IP indicates Flag-RAD51C or Flag-RAD51C point mutations bound to the IP. Inputs are 10% of the total sample. IPs were performed in triplicate, and a sample set are shown here.

Supplemental Figure 11.

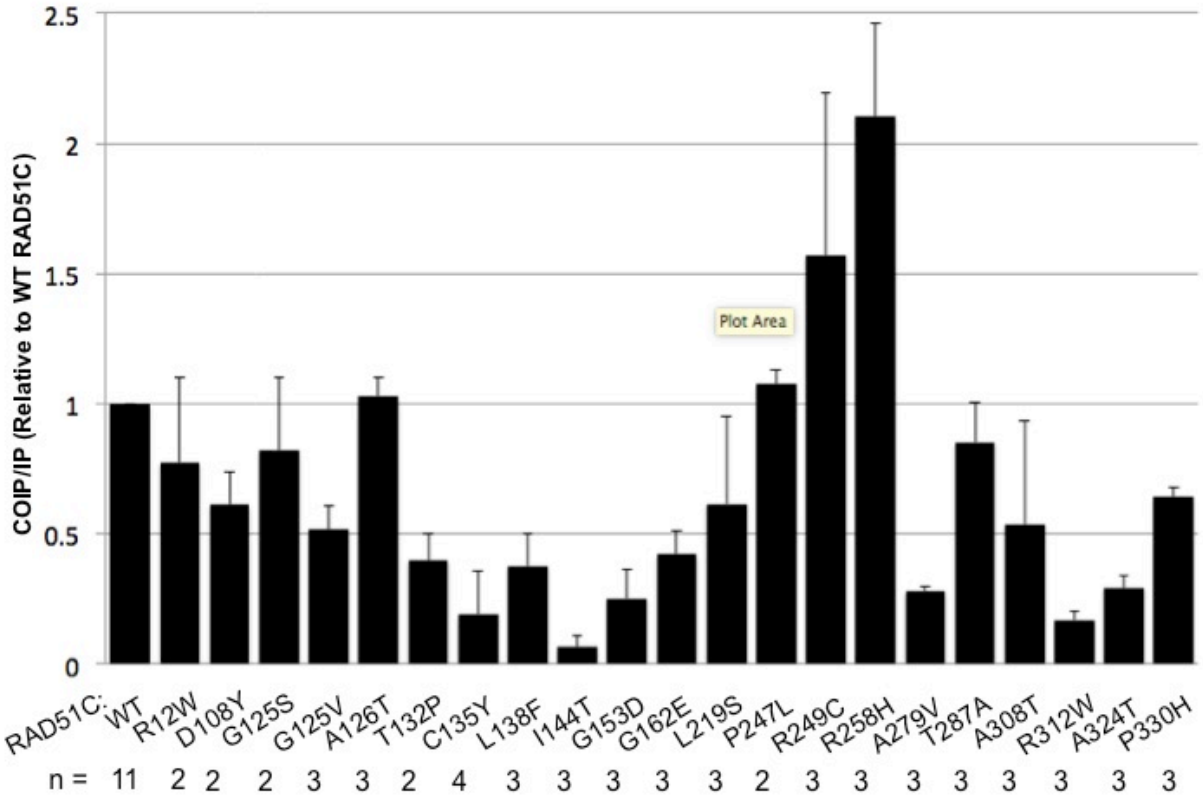

Supplemental Figure 11. Quantification of RAD51B IPs with RAD51C mutants.coIPs with RAD51B were quantified using LiCor imaging software, normalizing each mutant to the relative input (controlling for transfection efficiency) and then shown here as a ratio of coIP/IP (RAD51C/RAD51B) relative to wild type RAD51C. n represents the number of times each experiment was performed. Error bars are standard error of the mean.

Supplemental Figure 12.

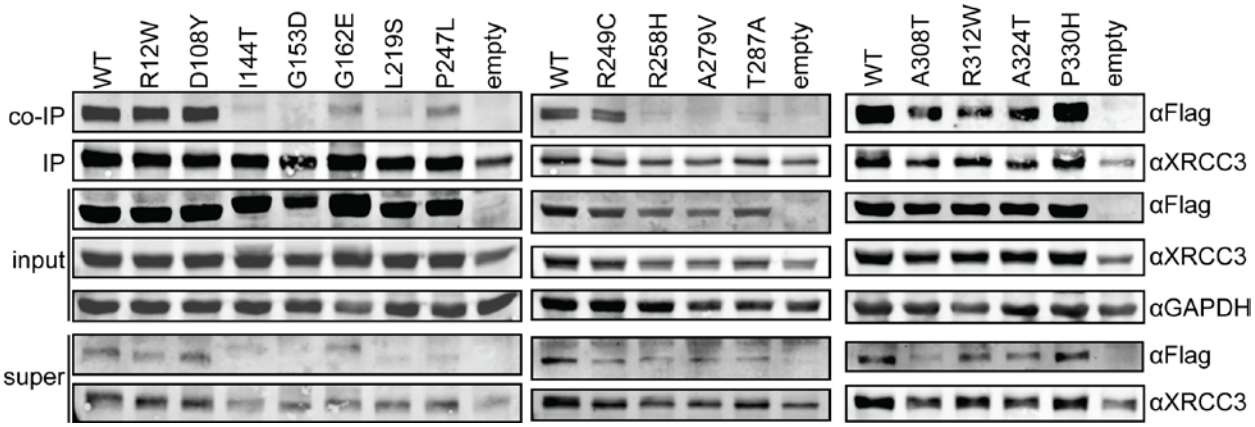

Supplemental Figure 12. Complete XRCC3 IPs with RAD51C mutants.Complete set of U2OS co-immunoprecipitations are shown for RAD51C and RAD51C point mutations with XRCC3 (In addition to Figure 12). IP indicates immunoprecipitations of XRCC3. co-IP indicates Flag-RAD51C or Flag-RAD51C point mutations bound to the IP. Inputs are 10% of the total sample.

Supplemental Figure 13.

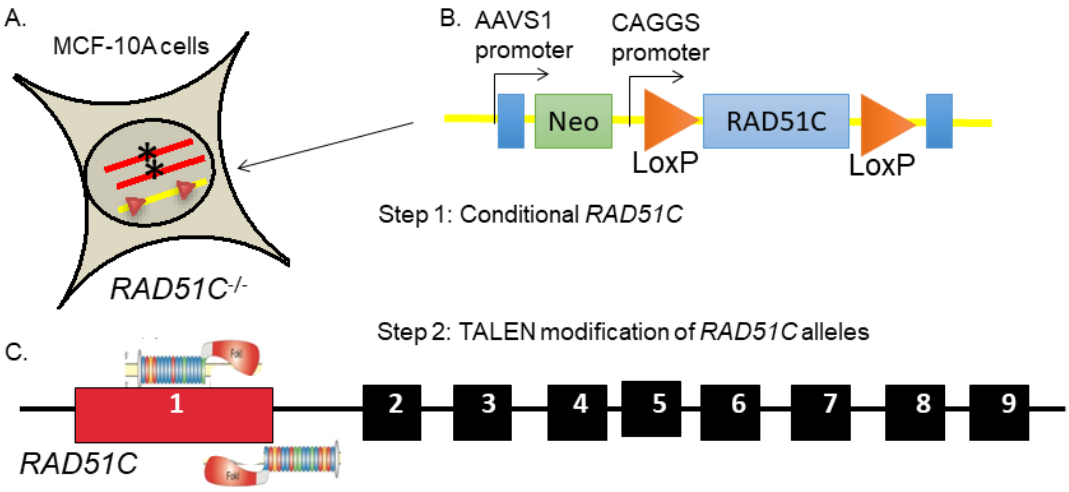

Supplemental Figure 13. MCF10A RAD51C cell line generation schematic. RAD51C conditional knockout cell line construction. A. MCF-10A cells containing the DR-GFP reporter construct were used to create the conditional RAD51C knockouts. B. Due to the lethality of RAD51C loss, first a conditional copy of wild type RAD51C flanked by LoxP sites was integrated at the AAVS1 locus. The AAVS1 (adeno-associated virus site 1) locus is a safe harbor locus on chromosome 19 (19q13.42). TALEN-resistant RAD51C cDNA was targeted to the AAVS1 locus using zinc finger nucleases. C. Subsequently, the endogenous copies of RAD51C were disrupted via TALENS targeting the first exon of RAD51C through two consecutive rounds of targeting. This produced a cell line in which RAD51C expression could be controlled through CRE expression.

Supplemental Figure 14.

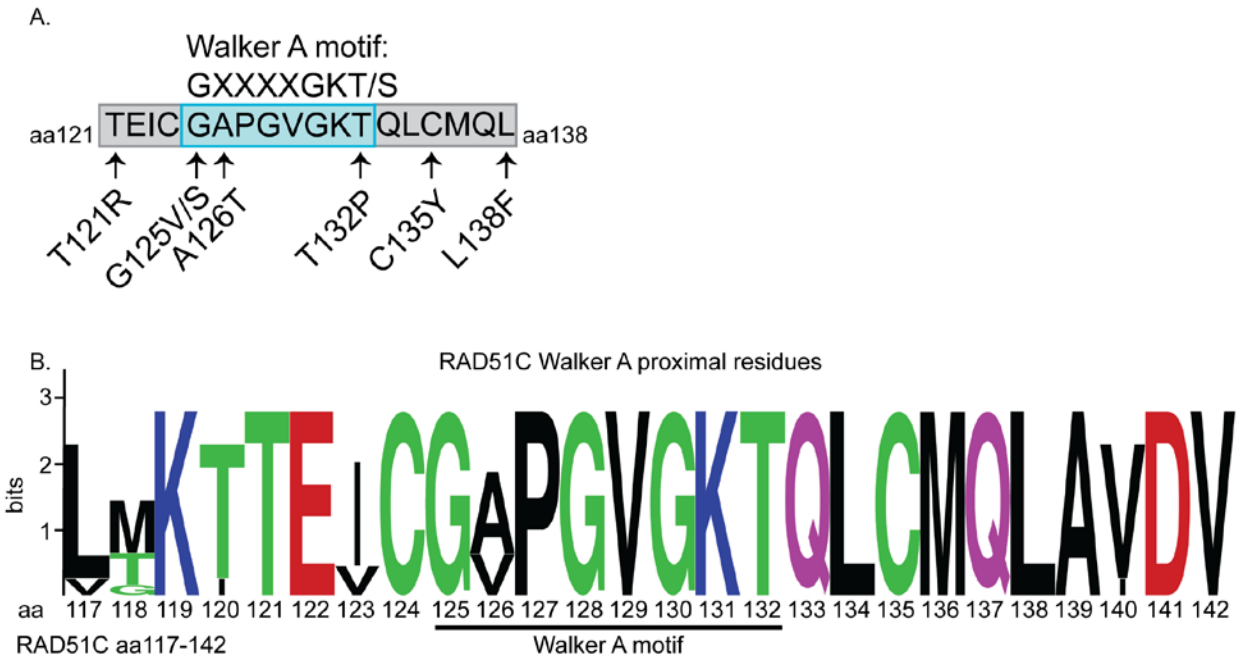

Supplemental Figure 14. RAD51C mutants are proximal to the Walker A motif. Seven *RAD51C* mutations around the Walker A motif are indicated with arrows underneath the amino acid sequence of aa121-38. The Walker A motif is highlighted in blue from aa125-132. The conserved residues of the Walker A motif are indicated above the amino acid sequence. B. WebLogo was used to generate a graphical representation of region of RAD51C containing the Walker A motif depicted in A. The amino acid sequences of 9 vertebrate species are represented. The total stack height represents the conservation of that residue, and the height of each letter within the stack represents the frequency of that amino acid. Polar amino acids are green, neutral amino acids are purple, basic amino acids are blue, acidic amino acids are red, and hydrophobic amino acids are black.

Supplemental Figure 15.

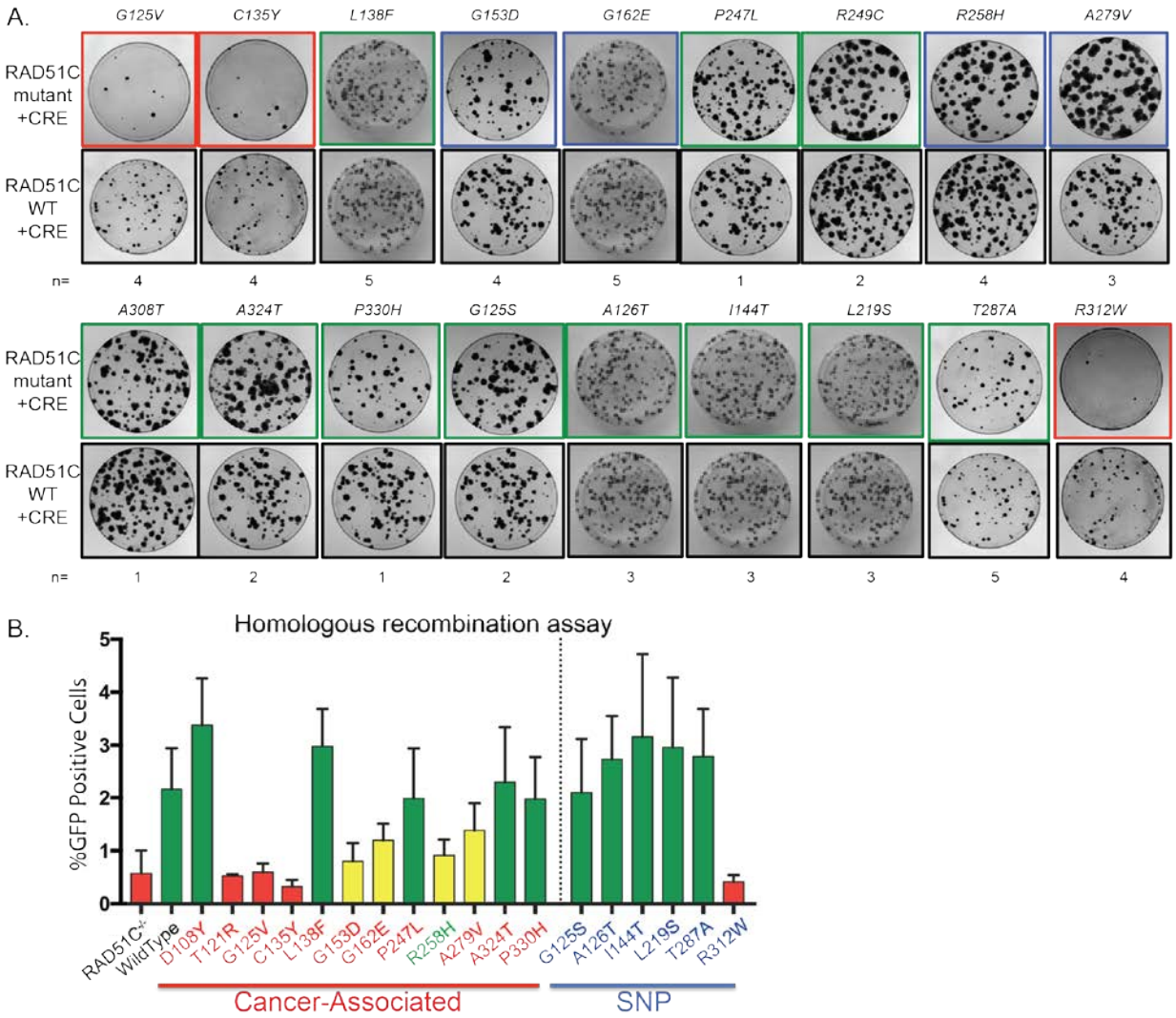

Supplemental Figure 15. RAD51C mutant viability and HR proficiency.A. RAD51C mutant viability post CRE compared to wild type (WT) RAD51C viability. RAD51C mutants that did not complement viability are indicated with red boxes. RAD51C mutants that did complement viability are indicated by blue or green boxes. Green boxes indicate the RAD51C mutant was also proficient for HR (shown in B). Blue boxes indicate the RAD51C mutant had a partial impairment for HR (shown in B). B. HR proficiency was analyzed using the DR-GFP reporter assay. RAD51C mutants that were deficient for HR are indicated by red bars. RAD51C mutants that were intermediate for HR proficiency are indicated by yellow bars. RAD51C mutants proficient for HR

are indicated by green bars. RAD51C mutants are cluster by cancer-associated (including the FA-like R258H) with red labels or SNPs with blue labels.

Supplemental Figure 16.

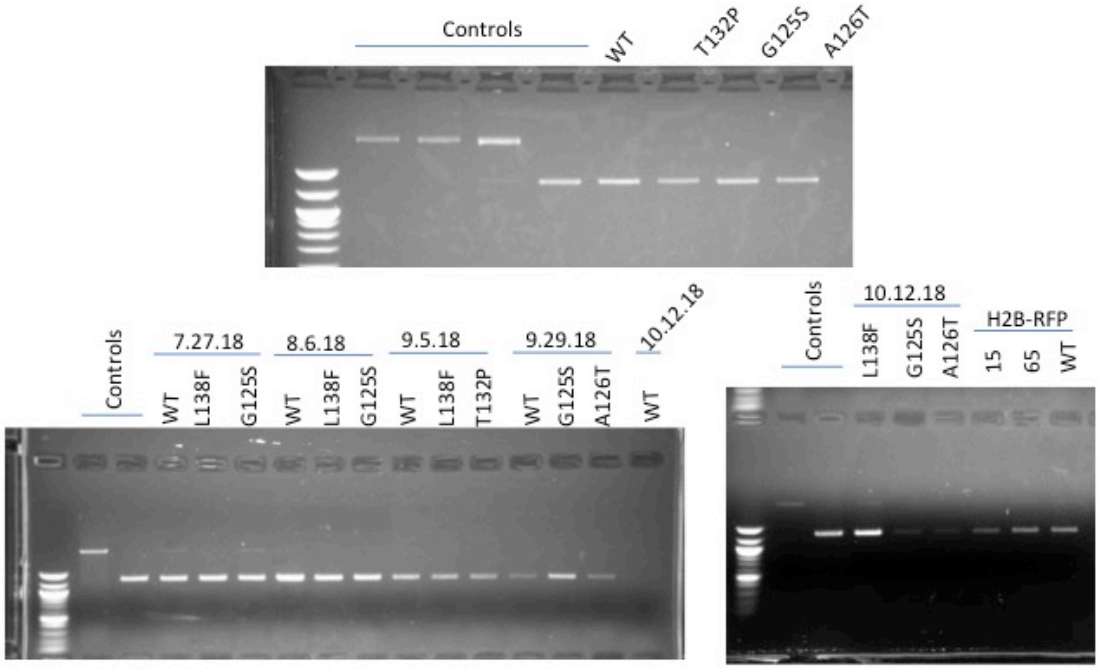

Supplemental Figure 16. RAD51C Cre excision in MCF-10A cells.PCR was used to determine Cre efficiency in clonogenic survival experiments. Predicted band sizes: ~2.5kb corresponds to pre-cre and ~1.3kb corresponds to post cre. For all experiments, Cre efficiency was verified to be efficient based on controls at corresponding sizes.

BIBLIOGRAPHY

Abreu CM, Prakash R, Romanienko PJ, Roig I, Keeney S, Jasin M. 2018. Shu complex SWS1-SWSAP1 promotes early steps in mouse meiotic recombination. *Nat Commun* **9**: 3961.

Adam J, Deans B, Thacker J. 2007. A role for Xrcc2 in the early stages of mouse development. *DNA Repair (Amst)* **6**: 224-234.

Adzhubei IA, Schmidt S, Peshkin L, Ramensky VE, Gerasimova A, Bork P, Kondrashov AS, Sunyaev SR. 2010. A method and server for predicting damaging missense mutations. *Nature methods* **7**: 248-249.

Alexeev A, Mazin A, Kowalczykowski SC. 2003. Rad54 protein possesses chromatin-remodeling activity stimulated by the Rad51-ssDNA nucleoprotein filament. *Nat Struct Biol* **10**: 182-186.

Alpi A, Pasierbek P, Gartner A, Loidl J. 2003. Genetic and cytological characterization of the recombination protein RAD-51 in Caenorhabditis elegans. *Chromosoma* **112**: 6-16.

Arribere JA, Bell RT, Fu BX, Artiles KL, Hartman PS, Fire AZ. 2014. Efficient Marker-Free Recovery of Custom Genetic Modifications with CRISPR/Cas9 in Caenorhabditis elegans. *Genetics*.

Aten JA, Stap J, Krawczyk PM, van Oven CH, Hoebe RA, Essers J, Kanaar R. 2004. Dynamics of DNA double-strand breaks revealed by clustering of damaged chromosome domains. *Science* **303**: 92-95.

Baldock RA, CA Pressimone, JM Baird, A Khodakov, CM Smith, Y Karpenshif, DS Bratton-Palmer, EB Garcin, S Gon, M Modesti, and KA Bernstein. RAD51D splice variants and cancer-associated mutations reveal XRCC2 interaction to be critical for homologous recombination. *DNA Repair*, In revision.

Ball LG, Zhang K, Cobb JA, Boone C, Xiao W. 2009. The yeast Shu complex couples error-free post-replication repair to homologous recombination. *Molecular microbiology* **73**: 89-102.

Barnes TM, Kohara Y, Coulson A, Hekimi S. 1995. Meiotic recombination, noncoding DNA and genomic organization in Caenorhabditis elegans. *Genetics* **141**: 159-179.

Bennett CB, Lewis AL, Baldwin KK, Resnick MA. 1993. Lethality induced by a single site-specific double-strand break in a dispensable yeast plasmid. *Proc Natl Acad Sci U S A* **90**: 5613-5617.

Bernards SS, Pennington KP, Harrell MI, Agnew KJ, Garcia RL, Norquist BM, Swisher EM. 2018. Clinical characteristics and outcomes of patients with BRCA1 or RAD51C methylated versus mutated ovarian carcinoma. *Gynecol Oncol* **148**: 281-285.

Bernstein KA, Rothstein R. 2009. At loose ends: resecting a double-strand break. *Cell* **137**: 807-810.

Bhattacharjee S, Nandi S. 2017. DNA damage response and cancer therapeutics through the lens of the Fanconi Anemia DNA repair pathway. *Cell Commun Signal* **15**: 41.

Bishop DK, Ear U, Bhattacharyya A, Calderone C, Beckett M, Weichselbaum RR, Shinohara A. 1998. Xrcc3 is required for assembly of Rad51 complexes in vivo. *The Journal of biological chemistry* **273**: 21482-21488.

Blanco A, Gutierrez-Enriquez S, Santamarina M, Montalban G, Bonache S, Balmana J, Carracedo A, Diez O, Vega A. 2014. RAD51C germline mutations found in Spanish site-specific breast cancer and breast-ovarian cancer families. *Breast Cancer Res Treat* **147**: 133-143.

Bouwman P, Aly A, Escandell JM, Pieterse M, Bartkova J, van der Gulden H, Hiddingh S, Thanasoula M, Kulkarni A, Yang Q et al. 2010. 53BP1 loss rescues BRCA1 deficiency and is associated with triple-negative and BRCA-mutated breast cancers. *Nat Struct Mol Biol* **17**: 688-695.

Braybrooke JP, Spink KG, Thacker J, Hickson ID. 2000. The RAD51 family member, RAD51L3, is a DNA-stimulated ATPase that forms a complex with XRCC2. *The Journal of biological chemistry* **275**: 29100-29106.

Brenner S. 1974. The genetics of Caenorhabditis elegans. *Genetics* **77**: 71-94.

Bryant HE, Schultz N, Thomas HD, Parker KM, Flower D, Lopez E, Kyle S, Meuth M, Curtin NJ, Helleday T. 2005. Specific killing of BRCA2-deficient tumours with inhibitors of poly(ADP-ribose) polymerase. *Nature* **434**: 913-917.

Bunting SF, Callen E, Wong N, Chen HT, Polato F, Gunn A, Bothmer A, Feldhahn N, Fernandez-Capetillo O, Cao L et al. 2010. 53BP1 inhibits homologous recombination in Brca1-deficient cells by blocking resection of DNA breaks. *Cell* **141**: 243-254.

Carreira A, Hilario J, Amitani I, Baskin RJ, Shivji MK, Venkitaraman AR, Kowalczykowski SC. 2009. The BRC repeats of BRCA2 modulate the DNA-binding selectivity of RAD51. *Cell* **136**: 1032-1043.

Cartwright R, Tambini CE, Simpson PJ, Thacker J. 1998. The XRCC2 DNA repair gene from human and mouse encodes a novel member of the recA/RAD51 family. *Nucleic acids research* **26**: 3084-3089.

Chapman JR, Sossick AJ, Boulton SJ, Jackson SP. 2012. BRCA1-associated exclusion of 53BP1 from DNA damage sites underlies temporal control of DNA repair. *J Cell Sci* **125**: 3529-3534.

Chen PL, Chen CF, Chen Y, Xiao J, Sharp ZD, Lee WH. 1998. The BRC repeats in BRCA2 are critical for RAD51 binding and resistance to methyl methanesulfonate treatment. *Proc Natl Acad Sci U S A* **95**: 5287-5292.

Chen R, Wold MS. 2014. Replication protein A: single-stranded DNA's first responder: dynamic DNA-interactions allow replication protein A to direct single-strand DNA intermediates into different pathways for synthesis or repair. *Bioessays* **36**: 1156-1161.

Cheung I, Schertzer M, Rose A, Lansdorp PM. 2002. Disruption of dog-1 in Caenorhabditis elegans triggers deletions upstream of guanine-rich DNA. *Nature genetics* **31**: 405-409.

Cho NW, Dilley RL, Lampson MA, Greenberg RA. 2014. Interchromosomal homology searches drive directional ALT telomere movement and synapsis. *Cell* **159**: 108-121.

Chun J, Buechelmaier ES, Powell SN. 2013. Rad51 paralog complexes BCDX2 and CX3 act at different stages in the BRCA1-BRCA2-dependent homologous recombination pathway. *Mol Cell Biol* **33**: 387-395.

Ciccia A, Elledge SJ. 2010. The DNA damage response: making it safe to play with knives. *Molecular cell* **40**: 179-204.

Clague J, Wilhoite G, Adamson A, Bailis A, Weitzel JN, Neuhausen SL. 2011. RAD51C germline mutations in breast and ovarian cancer cases from high-risk families. *PLoS One* **6**: e25632.

Cole F, Keeney S, Jasin M. 2010. Evolutionary conservation of meiotic DSB proteins: more than just Spo11. *Genes & development* **24**: 1201-1207.

Couch FJ, Shimelis H, Hu C, Hart SN, Polley EC, Na J, Hallberg E, Moore R, Thomas A, Lilyquist J et al. 2017. Associations Between Cancer Predisposition Testing Panel Genes and Breast Cancer. *JAMA Oncol* **3**: 1190-1196.

Craig AL, Moser SC, Bailly AP, Gartner A. 2012. Methods for studying the DNA damage response in the Caenorhabdatis elegans germ line. *Methods in cell biology* **107**: 321-352.

Crooks GE, Hon G, Chandonia JM, Brenner SE. 2004. WebLogo: a sequence logo generator. *Genome Res* **14**: 1188-1190.

Deans AJ, West SC. 2009. FANCM connects the genome instability disorders Bloom's Syndrome and Fanconi Anemia. *Molecular cell* **36**: 943-953.

-. 2011. DNA interstrand crosslink repair and cancer. *Nat Rev Cancer* **11**: 467-480.

Deans B, Griffin CS, Maconochie M, Thacker J. 2000. Xrcc2 is required for genetic stability, embryonic neurogenesis and viability in mice. *EMBO J* **19**: 6675-6685.

Deans B, Griffin CS, O'Regan P, Jasin M, Thacker J. 2003. Homologous recombination deficiency leads to profound genetic instability in cells derived from Xrcc2-knockout mice. *Cancer research* **63**: 8181-8187.

Densham RM, Garvin AJ, Stone HR, Strachan J, Baldock RA, Daza-Martin M, Fletcher A, Blair-Reid S, Beesley J, Johal B et al. 2016. Human BRCA1-BARD1 ubiquitin ligase activity counteracts chromatin barriers to DNA resection. *Nat Struct Mol Biol* **23**: 647-655.

Dickinson DJ, Ward JD, Reiner DJ, Goldstein B. 2013. Engineering the Caenorhabditis elegans genome using Cas9-triggered homologous recombination. *Nature methods* **10**: 1028-1034.

Ding YC, AW Adamson, L Steele, AM Bailis, EM John, G Tomlinson, SL Neuhausen. 2018. Discovery of mutations in homologous recombination genes in African-American women with breast cancer. *Fam Cancer* **17**:187-195.

Dion V, Kalck V, Horigome C, Towbin BD, Gasser SM. 2012. Increased mobility of double-strand breaks requires Mec1, Rad9 and the homologous recombination machinery. *Nat Cell Biol* **14**: 502-509.

Esashi F, Galkin VE, Yu X, Egelman EH, West SC. 2007. Stabilization of RAD51 nucleoprotein filaments by the C-terminal region of BRCA2. *Nat Struct Mol Biol* **14**: 468-474.

Feng W, Jasin M. 2017. BRCA2 suppresses replication stress-induced mitotic and G1 abnormalities through homologous recombination. *Nat Commun* **8**: 525.

Fong PC, Boss DS, Yap TA, Tutt A, Wu P, Mergui-Roelvink M, Mortimer P, Swaisland H, Lau A, O'Connor MJ et al. 2009. Inhibition of poly(ADP-ribose) polymerase in tumors from BRCA mutation carriers. *N Engl J Med* **361**: 123-134.

Forbes SA, Beare D, Boutselakis H, Bamford S, Bindal N, Tate J, Cole CG, Ward S, Dawson E, Ponting L et al. 2017. COSMIC: somatic cancer genetics at high-resolution. *Nucleic acids research* **45**: D777-D783.

Fukushige T, Krause M. 2012. Myogenic conversion and transcriptional profiling of embryonic blastomeres in Caenorhabditis elegans. *Methods* **56**: 50-54.

Fuller LF, Painter RB. 1988. A Chinese hamster ovary cell line hypersensitive to ionizing radiation and deficient in repair replication. *Mutat Res* **193**: 109-121.

Gaines WA, Godin SK, Kabbinavar FF, Rao T, VanDemark AP, Sung P, Bernstein KA. 2015. Promotion of presynaptic filament assembly by the ensemble of S. cerevisiae Rad51 paralogues with Rad52. *Nat Commun* **6**: 7834.

Garcin E.B. S Gon, R Prakash, MR Sullivan, KA Bernstein, M Jasin, and M Modesti. 2018. The five classical RAD51 paralogs are dispensable fo viability in human cancer cells but are equied for homologous recombination. *Molecular cell* **Submitted**.

Gayther SA, Mangion J, Russell P, Seal S, Barfoot R, Ponder BA, Stratton MR, Easton D. 1997. Variation of risks of breast and ovarian cancer associated with different germline mutations of the BRCA2 gene. *Nature genetics* **15**: 103-105.

Ghezraoui H, Oliveira C, Becker JR, Bilham K, Moralli D, Anzilotti C, Fischer R, Deobagkar-Lele M, Sanchiz-Calvo M, Fueyo-Marcos E et al. 2018. 53BP1 cooperation with the REV7-shieldin complex underpins DNA structure-specific NHEJ. *Nature* **560**: 122-127.

Glaser F, Pupko T, Paz I, Bell RE, Bechor-Shental D, Martz E, Ben-Tal N. 2003. ConSurf: identification of functional regions in proteins by surface-mapping of phylogenetic information. *Bioinformatics* **19**: 163-164.

Godin S, Wier A, Kabbinavar F, Bratton-Palmer DS, Ghodke H, Van Houten B, VanDemark AP, Bernstein KA. 2013. The Shu complex interacts with Rad51 through the Rad51 paralogues Rad55-Rad57 to mediate error-free recombination. *Nucleic acids research* **41**: 4525-4534.

Godin SK, Meslin C, Kabbinavar F, Bratton-Palmer DS, Hornack C, Mihalevic MJ, Yoshida K, Sullivan M, Clark NL, Bernstein KA. 2015. Evolutionary and functional analysis of the invariant SWIM domain in the conserved Shu2/SWS1 protein family from Saccharomyces cerevisiae to Homo sapiens. *Genetics* **199**: 1023-1033.

Godin SK, Sullivan MR, Bernstein KA. 2016a. Novel insights into RAD51 activity and regulation during homologous recombination and DNA replication. *Biochem Cell Biol* **94**: 407-418.

Godin SK, Zhang Z, Herken BW, Westmoreland JW, Lee AG, Mihalevic MJ, Yu Z, Sobol RW, Resnick MA, Bernstein KA. 2016b. The Shu complex promotes error-free tolerance of alkylation-induced base excision repair products. *Nucleic acids research* **44**: 8199-8215.

Gupta R, Somyajit K, Narita T, Maskey E, Stanlie A, Kremer M, Typas D, Lammers M, Mailand N, Nussenzweig A et al. 2018. DNA Repair Network Analysis Reveals Shieldin as a Key Regulator of NHEJ and PARP Inhibitor Sensitivity. *Cell* **173**: 972-988 e923.

Hakem R, de la Pompa JL, Mak TW. 1998. Developmental studies of Brca1 and Brca2 knock-out mice. *J Mammary Gland Biol Neoplasia* **3**: 431-445.

Hanahan D, Weinberg RA. 2011. Hallmarks of cancer: the next generation. *Cell* **144**: 646-674.

Hanzlikova H, I Kalasova, AA Demin, LE Pennicott, Z Cihlarova, and KW Caldecott. 2018. The importance of Poly(ADP-Ribose) Polymerase as a sensor of unligated Okazaki fragments during DNA replication. *Mol Cell* **71**:319-331.

Harris J, Lowden M, Clejan I, Tzoneva M, Thomas JH, Hodgkin J, Ahmed S. 2006. Mutator phenotype of Caenorhabditis elegans DNA damage checkpoint mutants. *Genetics* **174**: 601-616.

Hashimoto Y, Ray Chaudhuri A, Lopes M, Costanzo V. 2010. Rad51 protects nascent DNA from Mre11-dependent degradation and promotes continuous DNA synthesis. *Nat Struct Mol Biol* **17**: 1305-1311.

Heyer WD. 2015. Regulation of recombination and genomic maintenance. *Cold Spring Harbor perspectives in biology* **7**: a016501.

Hillers KJ, Villeneuve AM. 2003. Chromosome-wide control of meiotic crossing over in C. elegans. *Curr Biol* **13**: 1641-1647.

Hodgkin J, Horvitz HR, Brenner S. 1979. Nondisjunction Mutants of the Nematode CAENORHABDITIS ELEGANS. *Genetics* **91**: 67-94.

Hong S, Kim KP. 2013. Shu1 promotes homolog bias of meiotic recombination in Saccharomyces cerevisiae. *Mol Cells* **36**: 446-454.

Hong S, Sung Y, Yu M, Lee M, Kleckner N, Kim KP. 2013. The logic and mechanism of homologous recombination partner choice. *Molecular cell* **51**: 440-453.

Hoogewijs D, Houthoofd K, Matthijssens F, Vandesompele J, Vanfleteren JR. 2008. Selection and validation of a set of reliable reference genes for quantitative sod gene expression analysis in C. elegans. *BMC molecular biology* **9**: 9.

Hu T, Miller CM, Ridder GM, Aardema MJ. 1999. Characterization of p53 in Chinese hamster cell lines CHO-K1, CHO-WBL, and CHL: implications for genotoxicity testing. *Mutat Res* **426**: 51-62.

Jackson SP, Bartek J. 2009. The DNA-damage response in human biology and disease. *Nature* **461**: 1071-1078.

Jacquinet A, Brown L, Sawkins J, Liu P, Pugash D, Van Allen MI, Patel MS. 2018. Expanding the FANCO/RAD51C associated phenotype: Cleft lip and palate and lobar holoprosencephaly, two rare findings in Fanconi anemia. *Eur J Med Genet* **61**: 257-261.

James P, Halladay J, Craig EA. 1996. Genomic libraries and a host strain designed for highly efficient two-hybrid selection in yeast. *Genetics* **144**: 1425-1436.

Jaramillo-Lambert A, Ellefson M, Villeneuve AM, Engebrecht J. 2007. Differential timing of S phases, X chromosome replication, and meiotic prophase in the C. elegans germ line. *Dev Biol* **308**: 206-221.

Jasin M, Rothstein R. 2013. Repair of strand breaks by homologous recombination. *Cold Spring Harbor perspectives in biology* **5**: a012740.

Jensen RB, Carreira A, Kowalczykowski SC. 2010. Purified human BRCA2 stimulates RAD51-mediated recombination. *Nature* **467**: 678-683.

Johnson RD, Liu N, Jasin M. 1999. Mammalian XRCC2 promotes the repair of DNA double-strand breaks by homologous recombination. *Nature* **401**: 397-399.

Jones NJ, Cox R, Thacker J. 1987. Isolation and cross-sensitivity of X-ray-sensitive mutants of V79-4 hamster cells. *Mutat Res* **183**: 279-286.

Jonkers J, Meuwissen R, van der Gulden H, Peterse H, van der Valk M, Berns A. 2001. Synergistic tumor suppressor activity of BRCA2 and p53 in a conditional mouse model for breast cancer. *Nature genetics* **29**: 418-425.

Karpenshif Y, Bernstein KA. 2012. From yeast to mammals: recent advances in genetic control of homologous recombination. *DNA Repair (Amst)* **11**: 781-788.

Keeney S, Giroux CN, Kleckner N. 1997. Meiosis-specific DNA double-strand breaks are catalyzed by Spo11, a member of a widely conserved protein family. *Cell* **88**: 375-384.

Kessler Z, Yanowitz J. 2014. Methodological considerations for mutagen exposure in C. elegans. *Methods* **68**: 441-449.

Knies K, S Inano, MJ Ramirez, M Ishiai, J Surralles, M Takata, and D Schindler. 2017. Biallelic mutations in the ubiquitin ligase RFWD3 cause Fanconi anemia. *J Clin Invest* **127**:3013-3027.

Kondrashova O, Nguyen M, Shield-Artin K, Tinker AV, Teng NNH, Harrell MI, Kuiper MJ, Ho GY, Barker H, Jasin M et al. 2017. Secondary Somatic Mutations Restoring RAD51C and RAD51D Associated with Acquired Resistance to the PARP Inhibitor Rucaparib in High-Grade Ovarian Carcinoma. *Cancer Discov* **7**: 984-998.

Krawczyk PM, Borovski T, Stap J, Cijsouw T, ten Cate R, Medema JP, Kanaar R, Franken NA, Aten JA. 2012. Chromatin mobility is increased at sites of DNA double-strand breaks. *J Cell Sci* **125**: 2127-2133.

Krejci L, Altmannova V, Spirek M, Zhao X. 2012. Homologous recombination and its regulation. *Nucleic acids research* **40**: 5795-5818.

Kristeleit RS, Miller RE, Kohn EC. 2016. Gynecologic Cancers: Emerging Novel Strategies for Targeting DNA Repair Deficiency. *Am Soc Clin Oncol Educ Book* **35**: e259-268.

Kurumizaka H, Ikawa S, Nakada M, Eda K, Kagawa W, Takata M, Takeda S, Yokoyama S, Shibata T. 2001. Homologous-pairing activity of the human DNA-repair proteins Xrcc3.Rad51C. *Proc Natl Acad Sci U S A* **98**: 5538-5543.

Kurumizaka H, Ikawa S, Nakada M, Enomoto R, Kagawa W, Kinebuchi T, Yamazoe M, Yokoyama S, Shibata T. 2002. Homologous pairing and ring and filament structure formation activities of the human Xrcc2*Rad51D complex. *The Journal of biological chemistry* **277**: 14315-14320.

Kuznetsov S, Pellegrini M, Shuda K, Fernandez-Capetillo O, Liu Y, Martin BK, Burkett S, Southon E, Pati D, Tessarollo L et al. 2007. RAD51C deficiency in mice results in early prophase I arrest in males and sister chromatid separation at metaphase II in females. *J Cell Biol* **176**: 581-592.

Kuznetsov SG, Haines DC, Martin BK, Sharan SK. 2009. Loss of Rad51c leads to embryonic lethality and modulation of Trp53-dependent tumorigenesis in mice. *Cancer research* **69**: 863-872.

Landau M, Mayrose I, Rosenberg Y, Glaser F, Martz E, Pupko T, Ben-Tal N. 2005. ConSurf 2005: the projection of evolutionary conservation scores of residues on protein structures. *Nucleic acids research* **33**: W299-302.

Lant B, Derry WB. 2014. Fluorescent visualization of germline apoptosis in living Caenorhabditis elegans. *Cold Spring Harbor protocols* **2014**: 420-427.

Lee JY, Terakawa T, Qi Z, Steinfeld JB, Redding S, Kwon Y, Gaines WA, Zhao W, Sung P, Greene EC. 2015. DNA RECOMBINATION. Base triplet stepping by the Rad51/RecA family of recombinases. *Science* **349**: 977-981.

Lim DS, Hasty P. 1996. A mutation in mouse rad51 results in an early embryonic lethal that is suppressed by a mutation in p53. *Mol Cell Biol* **16**: 7133-7143.

Lin Z, Kong H, Nei M, Ma H. 2006. Origins and evolution of the recA/RAD51 gene family: evidence for ancient gene duplication and endosymbiotic gene transfer. *Proc Natl Acad Sci U S A* **103**: 10328-10333.

Lio YC, Schild D, Brenneman MA, Redpath JL, Chen DJ. 2004. Human Rad51C deficiency destabilizes XRCC3, impairs recombination, and radiosensitizes S/G2-phase cells. *The Journal of biological chemistry* **279**: 42313-42320.

Lisby M, Rothstein R. 2015. Cell biology of mitotic recombination. *Cold Spring Harbor perspectives in biology* **7**: a016535.

Liu T, Wan L, Wu Y, Chen J, Huang J. 2011. hSWS1.SWSAP1 is an evolutionarily conserved complex required for efficient homologous recombination repair. *The Journal of biological chemistry* **286**: 41758-41766.

Ma CJ, Gibb B, Kwon Y, Sung P, Greene EC. 2017. Protein dynamics of human RPA and RAD51 on ssDNA during assembly and disassembly of the RAD51 filament. *Nucleic acids research* **45**: 749-761.

Makarova KS, Aravind L, Koonin EV. 2002. SWIM, a novel Zn-chelating domain present in bacteria, archaea and eukaryotes. *Trends in biochemical sciences* **27**: 384-386.

Mankouri HW, Ngo HP, Hickson ID. 2007. Shu proteins promote the formation of homologous recombination intermediates that are processed by Sgs1-Rmi1-Top3. *Molecular biology of the cell* **18**: 4062-4073.

Martin V, Chahwan C, Gao H, Blais V, Wohlschlegel J, Yates JR, 3rd, McGowan CH, Russell P. 2006. Sws1 is a conserved regulator of homologous recombination in eukaryotic cells. *EMBO J* **25**: 2564-2574.

Martino J, Bernstein KA. 2016. The Shu complex is a conserved regulator of homologous recombination. *FEMS Yeast Res* **16**.

Masson JY, Stasiak AZ, Stasiak A, Benson FE, West SC. 2001a. Complex formation by the human RAD51C and XRCC3 recombination repair proteins. *Proc Natl Acad Sci U S A* **98**: 8440-8446.

Masson JY, Tarsounas MC, Stasiak AZ, Stasiak A, Shah R, McIlwraith MJ, Benson FE, West SC. 2001b. Identification and purification of two distinct complexes containing the five RAD51 paralogs. *Genes & development* **15**: 3296-3307.

Matondo A, Jo YH, Shahid M, Choi TG, Nguyen MN, Nguyen NNY, Akter S, Kang I, Ha J, Maeng CH et al. 2017. The Prognostic 97 Chemoresponse Gene Signature in Ovarian Cancer. *Sci Rep* **7**: 9689.

Maxwell KN, Wubbenhorst B, Wenz BM, De Sloover D, Pluta J, Emery L, Barrett A, Kraya AA, Anastopoulos IN, Yu S et al. 2017. BRCA locus-specific loss of heterozygosity in germline BRCA1 and BRCA2 carriers. *Nat Commun* **8**: 319.

McClendon TB, Sullivan MR, Bernstein KA, Yanowitz JL. 2016. Promotion of Homologous Recombination by SWS-1 in Complex with RAD-51 Paralogs in Caenorhabditis elegans. *Genetics* **203**: 133-145.

Meindl A, Hellebrand H, Wiek C, Erven V, Wappenschmidt B, Niederacher D, Freund M, Lichtner P, Hartmann L, Schaal H et al. 2010. Germline mutations in breast and ovarian cancer pedigrees establish RAD51C as a human cancer susceptibility gene. *Nature genetics* **42**: 410-414.

Meneely PM, Farago AF, Kauffman TM. 2002. Crossover distribution and high interference for both the X chromosome and an autosome during oogenesis and spermatogenesis in Caenorhabditis elegans. *Genetics* **162**: 1169-1177.

Miller KA, Sawicka D, Barsky D, Albala JS. 2004. Domain mapping of the Rad51 paralog protein complexes. *Nucleic acids research* **32**: 169-178.

Miller KA, Yoshikawa DM, McConnell IR, Clark R, Schild D, Albala JS. 2002. RAD51C interacts with RAD51B and is central to a larger protein complex in vivo exclusive of RAD51. *The Journal of biological chemistry* **277**: 8406-8411.

Mine-Hattab J, Rothstein R. 2012. Increased chromosome mobility facilitates homology search during recombination. *Nat Cell Biol* **14**: 510-517.

Mirman Z, Lottersberger F, Takai H, Kibe T, Gong Y, Takai K, Bianchi A, Zimmermann M, Durocher D, de Lange T. 2018. 53BP1-RIF1-shieldin counteracts DSB resection through CST- and Polalpha-dependent fill-in. *Nature* **560**: 112-116.

Moldovan GL, D'Andrea AD. 2009. How the fanconi anemia pathway guards the genome. *Annu Rev Genet* **43**: 223-249.

Murai J, Y Zhang, J Morris, J Ji, S Takeda, JH Doroshow, and Y Pommier. 2014. Rationale for Poly(ADP-ribose) Polymerase (PARP) Inhibitors in Combination Therapy with Camptothecins or Temozolomide Based on PARP Trapping versus Catalytic Inhibition. *J Pharmacol Exp Ther* **349**: 408-416.

Muzzini DM, Plevani P, Boulton SJ, Cassata G, Marini F. 2008. Caenorhabditis elegans POLQ-1 and HEL-308 function in two distinct DNA interstrand cross-link repair pathways. *DNA Repair (Amst)* **7**: 941-950.

Nalepa G, Clapp DW. 2018. Fanconi anaemia and cancer: an intricate relationship. *Nat Rev Cancer* **18**: 168-185.

Nepal M, Che R, Zhang J, Ma C, Fei P. 2017. Fanconi Anemia Signaling and Cancer. *Trends Cancer* **3**: 840-856.

Nik-Zainal S, Morganella S. 2017. Mutational Signatures in Breast Cancer: The Problem at the DNA Level. *Clin Cancer Res* **23**: 2617-2629.

Noordermeer SM, Adam S, Setiaputra D, Barazas M, Pettitt SJ, Ling AK, Olivieri M, Alvarez-Quilon A, Moatti N, Zimmermann M et al. 2018. The shieldin complex mediates 53BP1-dependent DNA repair. *Nature* **560**: 117-121.

O'Connor MJ. 2015. Targeting the DNA Damage Response in Cancer. *Molecular cell* **60**: 547-560.

Ollier M, Radosevic-Robin N, Kwiatkowski F, Ponelle F, Viala S, Privat M, Uhrhammer N, Bernard-Gallon D, Penault-Llorca F, Bignon YJ et al. 2015. DNA repair genes implicated in triple negative familial non-BRCA1/2 breast cancer predisposition. *Am J Cancer Res* **5**: 2113-2126.

Orthwein A, SM Noordermeer, MD Wilson, S Landry, RI Enchev, A Sherker, M Munro, J Pinder, J Salsman, G Dellaire, B Xia, M Peter, and D Durocher. 2015. A mechanism for the suppression of homologous recombination in G1 cells. *Nature* **528**:422-426.

Osorio A, Endt D, Fernandez F, Eirich K, de la Hoya M, Schmutzler R, Caldes T, Meindl A, Schindler D, Benitez J. 2012. Predominance of pathogenic missense variants in the RAD51C gene occurring in breast and ovarian cancer families. *Hum Mol Genet* **21**: 2889-2898.

Paix A, Wang Y, Smith HE, Lee CY, Calidas D, Lu T, Smith J, Schmidt H, Krause MW, Seydoux G. 2014. Scalable and versatile genome editing using linear DNAs with microhomology to Cas9 Sites in Caenorhabditis elegans. *Genetics* **198**: 1347-1356.

Park JY, Singh TR, Nassar N, Zhang F, Freund M, Hanenberg H, Meetei AR, Andreassen PR. 2014. Breast cancer-associated missense mutants of the PALB2 WD40 domain, which directly binds RAD51C, RAD51 and BRCA2, disrupt DNA repair. *Oncogene* **33**: 4803-4812.

Pellegrini L, Yu DS, Lo T, Anand S, Lee M, Blundell TL, Venkitaraman AR. 2002. Insights into DNA recombination from the structure of a RAD51-BRCA2 complex. *Nature* **420**: 287-293.

Pelttari LM, Nurminen R, Gylfe A, Aaltonen LA, Schleutker J, Nevanlinna H. 2012. Screening of Finnish RAD51C founder mutations in prostate and colorectal cancer patients. *BMC Cancer* **12**: 552.

Pennington KP, Walsh T, Harrell MI, Lee MK, Pennil CC, Rendi MH, Thornton A, Norquist BM, Casadei S, Nord AS et al. 2014. Germline and somatic mutations in homologous recombination genes predict platinum response and survival in ovarian, fallopian tube, and peritoneal carcinomas. *Clin Cancer Res* **20**: 764-775.

Pierce AJ, Johnson RD, Thompson LH, Jasin M. 1999. XRCC3 promotes homology-directed repair of DNA damage in mammalian cells. *Genes & development* **13**: 2633-2638.

Pittman DL, Schimenti JC. 2000. Midgestation lethality in mice deficient for the RecA-related gene, Rad51d/Rad51l3. *Genesis* **26**: 167-173.

Prakash R, Zhang Y, Feng W, Jasin M. 2015. Homologous recombination and human health: the roles of BRCA1, BRCA2, and associated proteins. *Cold Spring Harbor perspectives in biology* **7**: a016600.

Qi Z, Redding S, Lee JY, Gibb B, Kwon Y, Niu H, Gaines WA, Sung P, Greene EC. 2015. DNA sequence alignment by microhomology sampling during homologous recombination. *Cell* **160**: 856-869.

Rodgers K, McVey M. 2016. Error-Prone Repair of DNA Double-Strand Breaks. *J Cell Physiol* **231**: 15-24.

Sanchez H, Paul MW, Grosbart M, van Rossum-Fikkert SE, Lebbink JHG, Kanaar R, Houtsmuller AB, Wyman C. 2017. Architectural plasticity of human BRCA2-RAD51 complexes in DNA break repair. *Nucleic acids research* **45**: 4507-4518.

Sarek G, JB Vannier, S Panier, JHJ Petrini, and SJ Boulton. 2015. TRF2 recruits RTEL1 to telomeres in S phase to promote t-loop unwinding. *Mol Cell* **57**:622-635.

Sartori AA, Lukas C, Coates J, Mistrik M, Fu S, Bartek J, Baer R, Lukas J, Jackson SP. 2007. Human CtIP promotes DNA end resection. *Nature* **450**: 509-514.

Sasanuma H, Tawaramoto MS, Lao JP, Hosaka H, Sanda E, Suzuki M, Yamashita E, Hunter N, Shinohara M, Nakagawa A et al. 2013. A new protein complex promoting the assembly of Rad51 filaments. *Nat Commun* **4**: 1676.

Schild D, Lio YC, Collins DW, Tsomondo T, Chen DJ. 2000. Evidence for simultaneous protein interactions between human Rad51 paralogs. *The Journal of biological chemistry* **275**: 16443-16449.

Schlacher K, Christ N, Siaud N, Egashira A, Wu H, Jasin M. 2011. Double-strand break repair-independent role for BRCA2 in blocking stalled replication fork degradation by MRE11. *Cell* **145**: 529-542.

Schlacher K, Wu H, Jasin M. 2012. A distinct replication fork protection pathway connects Fanconi anemia tumor suppressors to RAD51-BRCA1/2. *Cancer Cell* **22**: 106-116.

Schmittgen TD, Livak KJ. 2008. Analyzing real-time PCR data by the comparative C(T) method. *Nature protocols* **3**: 1101-1108.

Schneider TD, Stephens RM. 1990. Sequence logos: a new way to display consensus sequences. *Nucleic acids research* **18**: 6097-6100.

Shamseldin HE, Elfaki M, Alkuraya FS. 2012. Exome sequencing reveals a novel Fanconi group defined by XRCC2 mutation. *J Med Genet* **49**: 184-186.

She Z, Gao ZQ, Liu Y, Wang WJ, Liu GF, Shtykova EV, Xu JH, Dong YH. 2012. Structural and SAXS analysis of the budding yeast SHU-complex proteins. *FEBS letters* **586**: 2306-2312.

Shibata A, Jeggo PA. 2014. DNA double-strand break repair in a cellular context. *Clin Oncol (R Coll Radiol)* **26**: 243-249.

Shor E, Weinstein J, Rothstein R. 2005. A genetic screen for top3 suppressors in Saccharomyces cerevisiae identifies SHU1, SHU2, PSY3 and CSM2: four genes involved in error-free DNA repair. *Genetics* **169**: 1275-1289.

Shu Z, Smith S, Wang L, Rice MC, Kmiec EB. 1999. Disruption of muREC2/RAD51L1 in mice results in early embryonic lethality which can Be partially rescued in a p53(-/-) background. *Mol Cell Biol* **19**: 8686-8693.

Sigurdsson S, Van Komen S, Bussen W, Schild D, Albala JS, Sung P. 2001. Mediator function of the human Rad51B-Rad51C complex in Rad51/RPA-catalyzed DNA strand exchange. *Genes & development* **15**: 3308-3318.

Simandlova J, Zagelbaum J, Payne MJ, Chu WK, Shevelev I, Hanada K, Chatterjee S, Reid DA, Liu Y, Janscak P et al. 2013. FBH1 helicase disrupts RAD51 filaments in vitro and modulates homologous recombination in mammalian cells. *The Journal of biological chemistry* **288**: 34168-34180.

Smiraldo PG, Gruver AM, Osborn JC, Pittman DL. 2005. Extensive chromosomal instability in Rad51d-deficient mouse cells. *Cancer research* **65**: 2089-2096.

Smith MJ, Rothstein R. 2017. Poetry in motion: Increased chromosomal mobility after DNA damage. *DNA Repair (Amst)* **56**: 102-108.

Smolikov S, Eizinger A, Hurlburt A, Rogers E, Villeneuve AM, Colaiacovo MP. 2007a. Synapsis-defective mutants reveal a correlation between chromosome conformation and the mode

of double-strand break repair during Caenorhabditis elegans meiosis. *Genetics* **176**: 2027-2033.

Smolikov S, Eizinger A, Schild-Prufert K, Hurlburt A, McDonald K, Engebrecht J, Villeneuve AM, Colaiacovo MP. 2007b. SYP-3 restricts synaptonemal complex assembly to bridge paired chromosome axes during meiosis in Caenorhabditis elegans. *Genetics* **176**: 2015-2025.

Somyajit K, Mishra A, Jameei A, Nagaraju G. 2015a. Enhanced non-homologous end joining contributes toward synthetic lethality of pathological RAD51C mutants with poly (ADP-ribose) polymerase. *Carcinogenesis* **36**: 13-24.

Somyajit K, Saxena S, Babu S, Mishra A, Nagaraju G. 2015b. Mammalian RAD51 paralogs protect nascent DNA at stalled forks and mediate replication restart. *Nucleic acids research* **43**: 9835-9855.

Soutoglou E, Dorn JF, Sengupta K, Jasin M, Nussenzweig A, Ried T, Danuser G, Misteli T. 2007. Positional stability of single double-strand breaks in mammalian cells. *Nat Cell Biol* **9**: 675-682.

Soutoglou E, Misteli T. 2007. Mobility and immobility of chromatin in transcription and genome stability. *Curr Opin Genet Dev* **17**: 435-442.

Spier I, Kerick M, Drichel D, Horpaopan S, Altmuller J, Laner A, Holzapfel S, Peters S, Adam R, Zhao B et al. 2016. Exome sequencing identifies potential novel candidate genes in patients with unexplained colorectal adenomatous polyposis. *Fam Cancer* **15**: 281-288.

Stark JM, AJ Pierce, J Oh, A Pastink, and M Jasin. 2004. Genetic steps of mammalian homologous repair with distinct mutagenic consequences. *Mol Cell Biol* **24**:9305-9316.

Stover EH, Konstantinopoulos PA, Matulonis UA, Swisher EM. 2016. Biomarkers of Response and Resistance to DNA Repair Targeted Therapies. *Clin Cancer Res* **22**: 5651-5660.

Sullivan MR and KA Bernstein. 2018. RAD-ical new insights into RAD51 regulation. *Genes*. In Press.

Sung P. and SA Stratton. 1996. Yeast Rad51 recombinase mediates polar DNA strand exchange in the absence of ATP hydrolysis. *J Biol Chem* **271**:27983-27986.

Sung P. 1997a. Function of yeast Rad52 protein as a mediator between replication protein A and the Rad51 recombinase. *The Journal of biological chemistry* **272**: 28194-28197.

-. 1997b. Yeast Rad55 and Rad57 proteins form a heterodimer that functions with replication protein A to promote DNA strand exchange by Rad51 recombinase. *Genes & development* **11**: 1111-1121.

Suwaki N, Klare K, Tarsounas M. 2011. RAD51 paralogs: roles in DNA damage signalling, recombinational repair and tumorigenesis. *Seminars in cell & developmental biology* **22**: 898-905.

Swisher EM, Lin KK, Oza AM, Scott CL, Giordano H, Sun J, Konecny GE, Coleman RL, Tinker AV, O'Malley DM et al. 2017. Rucaparib in relapsed, platinum-sensitive high-grade ovarian carcinoma (ARIEL2 Part 1): an international, multicentre, open-label, phase 2 trial. *Lancet Oncol* **18**: 75-87.

Symington LS, Gautier J. 2011. Double-strand break end resection and repair pathway choice. *Annu Rev Genet* **45**: 247-271.

Takata M, Sasaki MS, Sonoda E, Fukushima T, Morrison C, Albala JS, Swagemakers SM, Kanaar R, Thompson LH, Takeda S. 2000. The Rad51 paralog Rad51B promotes homologous recombinational repair. *Mol Cell Biol* **20**: 6476-6482.

Takata M, Sasaki MS, Tachiiri S, Fukushima T, Sonoda E, Schild D, Thompson LH, Takeda S. 2001. Chromosome instability and defective recombinational repair in knockout mutants of the five Rad51 paralogs. *Mol Cell Biol* **21**: 2858-2866.

Tao Y, Li X, Liu Y, Ruan J, Qi S, Niu L, Teng M. 2012. Structural analysis of Shu proteins reveals a DNA binding role essential for resisting damage. *The Journal of biological chemistry* **287**: 20231-20239.

Tate JG, Bamford S, Jubb HC, Sondka Z, Beare DM, Bindal N, Boutselakis H, Cole CG, Creatore C, Dawson E et al. 2018. COSMIC: the Catalogue Of Somatic Mutations In Cancer. *Nucleic acids research*.

Taylor MR, Spirek M, Chaurasiya KR, Ward JD, Carzaniga R, Yu X, Egelman EH, Collinson LM, Rueda D, Krejci L et al. 2015. Rad51 Paralogs Remodel Pre-synaptic Rad51 Filaments to Stimulate Homologous Recombination. *Cell* **162**: 271-286.

Taylor MRG, Spirek M, Jian Ma C, Carzaniga R, Takaki T, Collinson LM, Greene EC, Krejci L, Boulton SJ. 2016. A Polar and Nucleotide-Dependent Mechanism of Action for RAD51 Paralogs in RAD51 Filament Remodeling. *Molecular cell* **64**: 926-939.

Tercero JA, Diffley JF. 2001. Regulation of DNA replication fork progression through damaged DNA by the Mec1/Rad53 checkpoint. *Nature* **412**: 553-557.

Thacker J. 1999. A surfeit of RAD51-like genes? *Trends Genet* **15**: 166-168.

-. 2005. The RAD51 gene family, genetic instability and cancer. *Cancer letters* **219**: 125-135.

Thompson ER, Boyle SE, Johnson J, Ryland GL, Sawyer S, Choong DY, kConFab, Chenevix-Trench G, Trainer AH, Lindeman GJ et al. 2012. Analysis of RAD51C germline mutations in high-risk breast and ovarian cancer families and ovarian cancer patients. *Hum Mutat* **33**: 95-99.

Thompson LH, Schild D. 1999. The contribution of homologous recombination in preserving genome integrity in mammalian cells. *Biochimie* **81**: 87-105.

-. 2002. Recombinational DNA repair and human disease. *Mutat Res* **509**: 49-78.

Tsuzuki T, Fujii Y, Sakumi K, Tominaga Y, Nakao K, Sekiguchi M, Matsushiro A, Yoshimura Y, MoritaT. 1996. Targeted disruption of the Rad51 gene leads to lethality in embryonic mice. *Proc Natl Acad Sci U S A* **93**: 6236-6240.

Tung N, Lin NU, Kidd J, Allen BA, Singh N, Wenstrup RJ, Hartman AR, Winer EP, Garber JE. 2016. Frequency of Germline Mutations in 25 Cancer Susceptibility Genes in a Sequential Series of Patients With Breast Cancer. *J Clin Oncol* **34**: 1460-1468.

Vaz F, Hanenberg H, Schuster B, Barker K, Wiek C, Erven V, Neveling K, Endt D, Kesterton I, Autore F et al. 2010. Mutation of the RAD51C gene in a Fanconi anemia-like disorder. *Nature genetics* **42**: 406-409.

Vencken PM, Kriege M, Hoogwerf D, Beugelink S, van der Burg ME, Hooning MJ, Berns EM, Jager A, Collee M, Burger CW et al. 2011. Chemosensitivity and outcome of BRCA1- and BRCA2-associated ovarian cancer patients after first-line chemotherapy compared with sporadic ovarian cancer patients. *Ann Oncol* **22**: 1346-1352.

Verma P, Greenberg RA. 2016. Noncanonical views of homology-directed DNA repair. *Genes & development* **30**: 1138-1154.

Wagner CR, Kuervers L, Baillie DL, Yanowitz JL. 2010. xnd-1 regulates the global recombination landscape in Caenorhabditis elegans. *Nature* **467**: 839-843.

Wang AT, Kim T, Wagner JE, Conti BA, Lach FP, Huang AL, Molina H, Sanborn EM, Zierhut H, Cornes BK et al. 2015. A Dominant Mutation in Human RAD51 Reveals Its Function in DNA Interstrand Crosslink Repair Independent of Homologous Recombination. *Molecular cell* **59**: 478-490.

Ward JD, Barber LJ, Petalcorin MI, Yanowitz J, Boulton SJ. 2007. Replication blocking lesions present a unique substrate for homologous recombination. *EMBO J* **26**: 3384-3396.

Ward JD, Muzzini DM, Petalcorin MI, Martinez-Perez E, Martin JS, Plevani P, Cassata G, Marini F, Boulton SJ. 2010. Overlapping mechanisms promote postsynaptic RAD-51 filament disassembly during meiotic double-strand break repair. *Molecular cell* **37**: 259-272.

Wesoly J, Agarwal S, Sigurdsson S, Bussen W, Van Komen S, Qin J, van Steeg H, van Benthem J, Wassenaar E, Baarends WM et al. 2006. Differential contributions of mammalian Rad54 paralogs to recombination, DNA damage repair, and meiosis. *Mol Cell Biol* **26**: 976-989.

Wiese C, Collins DW, Albala JS, Thompson LH, Kronenberg A, Schild D. 2002. Interactions involving the Rad51 paralogs Rad51C and XRCC3 in human cells. *Nucleic acids research* **30**: 1001-1008.

Witkiewicz AK, McMillan EA, Balaji U, Baek G, Lin WC, Mansour J, Mollaee M, Wagner KU, Koduru P, Yopp A et al. 2015. Whole-exome sequencing of pancreatic cancer defines genetic diversity and therapeutic targets. *Nat Commun* **6**: 6744.

Wong AK, Pero R, Ormonde PA, Tavtigian SV, Bartel PL. 1997. RAD51 interacts with the evolutionarily conserved BRC motifs in the human breast cancer susceptibility gene brca2. *The Journal of biological chemistry* **272**: 31941-31944.

Xia B, Sheng Q, Nakanishi K, Ohashi A, Wu J, Christ N, Liu X, Jasin M, Couch FJ, Livingston DM. 2006. Control of BRCA2 cellular and clinical functions by a nuclear partner, PALB2. *Molecular cell* **22**: 719-729.

Yang J, Yan R, Roy A, Xu D, Poisson J, Zhang Y. 2015. The I-TASSER Suite: protein structure and function prediction. *Nature methods* **12**: 7-8.

Yang J, Zhang Y. 2015. I-TASSER server: new development for protein structure and function predictions. *Nucleic acids research* **43**: W174-181.

Yanowitz JL. 2008. Genome integrity is regulated by the Caenorhabditis elegans Rad51D homolog rfs-1. *Genetics* **179**: 249-262.

Youds JL, O'Neil NJ, Rose AM. 2006. Homologous recombination is required for genome stability in the absence of DOG-1 in Caenorhabditis elegans. *Genetics* **173**: 697-708.

Yu X, Fu S, Lai M, Baer R, Chen J. 2006. BRCA1 ubiquitinates its phosphorylation-dependent binding partner CtIP. *Genes & development* **20**: 1721-1726.

Yuan J, Chen J. 2013. FIGNL1-containing protein complex is required for efficient homologous recombination repair. *Proc Natl Acad Sci U S A* **110**: 10640-10645.

Zhang P, Zhang Y, Sun L, Sinumporn S, Yang Z, Sun B, Xuan D, Li Z, Yu P, Wu W et al. 2017a. The Rice AAA-ATPase OsFIGNL1 Is Essential for Male Meiosis. *Front Plant Sci* **8**: 1639.

Zhang S, Wang L, Tao Y, Bai T, Lu R, Zhang T, Chen J, Ding J. 2017b. Structural basis for the functional role of the Shu complex in homologous recombination. *Nucleic acids research* **45**: 13068-13079.